



EDITORIAL BOARD

E.O. Paton Electric Welding Institute, Kyiv, Ukraine:

B.E. Paton (*Editor-in-Chief*),

S.I. Kuchuk-Yatsenko (*Deputy Editor-in-Chief*),

V.M. Lipodaev (*Deputy Editor-in-Chief*),

O.M. Berdnikova, Yu.S. Borisov,

V.V. Knysh, V.M. Korbyk, I.V. Krivtsun,

Yu.M. Lankin, L.M. Lobanov, S.Yu. Maksimov,

M.O. Pashchin, V.D. Poznyakov,

I.O. Ryabtsev, K.A. Yushchenko;

V.V. Dmitrik, NTUU

«Kharkiv Polytechnic Institute», Kharkiv, Ukraine;

E.P. Chvertko, V.V. Kvasnitsky, NTUU

«Igor Sikorsky Kyiv Polytechnic Institute»,

Kyiv, Ukraine;

M.M. Student, Karpenko Physico-Mechanical

Institute, Lviv, Ukraine;

M. Zinigrad, Ariel University, Israel;

Ya. Pilarczyk, Welding Institute, Gliwice, Poland;

U. Reisgen, Welding and Joining Institute,

Aachen, Germany

Founders

E.O. Paton Electric Welding Institute

International Association «Welding»

Publisher

International Association «Welding»

Translators

A.O. Fomin, I.M. Kutianova

Editor

N.G. Khomenko

Electron galley

D.I. Sereda, T.Yu. Snegiryova

Address

E.O. Paton Electric Welding Institute,

International Association «Welding»

11 Kazymyr Malevych Str. (former Bohlenko),

03150, Kyiv, Ukraine

Tel./Fax: (38044) 200 82 77

E-mail: journal@paton.kiev.ua

www.patonpublishinghouse.com/eng/journals/tpwj

State Registration Certificate

KV 4790 of 09.01.2001

ISSN 0957-798X

DOI: <http://dx.doi.org/10.37434/tpwj>

Subscriptions

12 issues per year, back issues available.

\$384, subscriptions for the printed (hard copy) version,
air postage and packaging included.

\$312, subscriptions for the electronic version
(sending issues of Journal in pdf format
or providing access to IP addresses).

Institutions with current subscriptions on printed version
can purchase online access to the electronic versions
of any back issues that they have not subscribed to.

Issues of the Journal (more than two years old)
are available at a substantially reduced price.

All rights reserved.

This publication and each of the articles contained
herein are protected by copyright.

Permission to reproduce material contained in this
journal must be obtained in writing from the Publisher.

CONTENTS

SCIENTIFIC AND TECHNICAL

Kuchuk-Yatsenko S.I., Antipin E.V., Didkovskiy O.V., Shvets V.I.

and *Kavunichenko O.V.* Evaluation of quality of welded joints
of high-strength railway rails of modern production taking
into account the requirements of Ukrainian and European
standards 2

Babych O.A., Korzhyk V.M., Grynyuk A.A., Khaskin V.Yu.,

Chunlin Dong and Shanguo Han. Hybrid welding of aluminium
1561 and 5083 alloys using plasma-arc and consumable
electrode arc (Plasma-MIG) 11

Labur T.M., Yavorska M.R. and Koval V.A. Effect of heat

treatment on the structure and mechanical properties of sheet
aluminium alloy V1341 and its welded joints produced by TIG
welding 23

Borysov Yu.S., Borysova A.L., Vigilyanska N.V.,

Gryshchenko O.P. and Kolomytsev M.V. Coatings based
on Fe–Al intermetallics produced by the methods of plasma and
supersonic plasma gas-air spraying 29

INDUSTRIAL

Ostash O.P., Kulyk V.V., Shipitsyn S.Ya., Haivoronskyi O.A. and

Chepil R.V. Influence of content of alloying elements and heat
treatment on life characteristics of high-strength wheel steels
during manufacture of railroad wheels and their repair
surfacing 38

EVALUATION OF QUALITY OF WELDED JOINTS OF HIGH-STRENGTH RAILWAY RAILS OF MODERN PRODUCTION TAKING INTO ACCOUNT THE REQUIREMENTS OF UKRAINIAN AND EUROPEAN STANDARDS

SI .K uchuk-Ya senko, E .V. Antipin, O.V. Didkovskiy, V.I. Shvets and O.V. Kavunichenko

E.O. Paton Electric Welding Institute of the NAS of Ukraine

11 Kazymyr Malevych Str., 03150, Kyiv, Ukraine. E-mail: office@paton.kiev.ua

In most heavy-duty railways of Ukraine, flash-butt welding is the dominant process for joining rails. Welding is performed in special shops and in field conditions during the construction of new main lines and repair of existing railways. Technologies and equipment are constantly being improved in connection with the use in the railways of Ukraine and other countries of the world, of new generations of high-strength rails with an increased wear resistance, in accordance with the requirements to high-speed main lines. In the last decade, the developed countries of the world are revising the basic standards governing the quality of rail steels and requirements to mechanical properties of rail welded joints, taking into account their use on heavy-duty and high-speed main lines. One of the specified tasks is the adaptation of the Ukrainian standard TU U 24.1-40075815-002: 2016 (for stationary and mobile welding machines), which determines the requirements to the quality of welded joints of high-strength rails, to the valid European standard EN 14587-1 2007 (for stationary welding machines) and EN 14587-2 2009 (for mobile welding machines). 9 Ref., 4 Tables, 12 Figures.

Key words : flash-butt welding, railway rails, high-strength rail steels, pulsed flashing, heat-affected zone, temperature fields, rail defects, quality control, seamless track

In the majority of heavy-duty main railways of Ukraine, flash-butt welding is the dominant process for joining rails. Welding is performed in special shops and in the field conditions during construction of new main lines and repair of railway tracks in service. Here, stationary machines of K1000 type and mobile machines of K922-1 type are used, which were developed by PWI and manufactured by PJSC KZESO. The mentioned machines are also used in many countries of the world (RF, PRC, USA, Poland, Malaysia, Baltic countries, etc.). They were supplied by license agreements with PWI. The design of the main components of these machines and control systems is based on application of the technology of continuous flash (CF) butt and pulsed flash (PF) butt welding [1, 2].

Technologies and equipment are being continuously improved in connection with application in the railways of Ukraine and other countries of the world of new generations of high-strength rails with increased wear resistance, in keeping with the requirements to high-speed main lines. In the last decade, the developed countries of the world are revising the main standards regulating the quality of rail steels and requirements to mechanical properties of rail welded

joints, taking into account their use in heavy-duty and high-speed main lines. PWI, together with the enterprises of JSC «Ukrzaliznytsa», takes part in this work. One of the posed tasks is adaptation of Ukrainian standard TU U 24.1-40075815-002:2016 (for stationary and mobile welding machines) that determines the requirements to the quality of welded joints of high-strength rails, to the valid European standard EN 14587-1 2007 (for stationary welding machines) and EN 14587-2009 (for mobile welding machines) [3].

At present high-strength rails of both domestic and foreign origin are used in the railways of Ukraine. Higher requirements are made to wear resistance, mechanical properties and structure of the welded joints. These requirements are described in the standards of different countries.

Table 1 gives the main requirements, which should be followed at evaluation of the quality of welded joints produced by flash-butt welding, in keeping with Ukrainian (TU U 24.1-40075815-002:2016) [4] and European (EN 14587-1 2007 and EN 14587-2009) standards.

All the investigations mentioned in the standard, are performed in full scope at certification of weld-

S.I. Kuchuk-Yatsenko — <https://orcid.org/0000-0002-1166-0253>, E.V. Antipin — <https://orcid.org/0000-0003-3297-5382>,
O.V. Didkovskiy — <https://orcid.org/0000-0001-5268-5599>, V.I. Shvets — <https://orcid.org/0000-0003-4653-7453>,
O.V. Kavunichenko — <https://orcid.org/0000-0002-5164-9796>

© S.I. Kuchuk-Yatsenko, E.V. Antipin, O.V. Didkovskiy, V.I. Shvets and O.V. Kavunichenko, 2020

Tb le 1 Comparison of the Ukrainian and European standards for welding the railway rails

Controlled parameter	EN 14587-1:2007	EN 14587-2:2009	TY Y 24.1-40075815-002:2016
Mechanical testing			
Breaking load on the head, kN	1600	1600	1650
Breaking load on the foot, kN	Not tested	Not tested	1400
Deflection, mm	20	20	30
Macrostructure			
Minimum HAZ width, mm	25	20	Not controlled
Maximum HAZ width, mm	45	45	Same
Admissible difference between HAZ max and HAZ min, mm	10	20	»
Macrostructure			
Presence of martensite and bainite structure	Not allowed	Not allowed	Not controlled
Hardness distribution			
Unhardened rails (R260, R220, R260Mn, M76), <i>HV30</i>	min <i>P</i> = <i>HV30</i> –30 max <i>P</i> = <i>HV30</i> –60	min <i>P</i> = <i>HV30</i> –30 max <i>P</i> = <i>HV30</i> –60	min <i>P</i> = 10 % <i>HV30</i>
Heat-hardened rails (R350HT, K76F, E76F, K76T)), <i>HV30</i>	min <i>P</i> = <i>HV30</i> –325 max <i>P</i> = <i>HV30</i> –410	min <i>P</i> = <i>HV30</i> –30–325 max <i>P</i> = <i>HV30</i> –410	min <i>P</i> = 15 % <i>HV30</i>
Fatigue testing			
Cycle number, mln	5	5	Not controlled
Loading, kN	190	190	Same
*Data are given for rails of R65 and 60E1 (UIC60) type from steel grades R260, R220, R260Mn, M76, R350HT, K76F, E76F, K76T.			

ing technology, welding equipment, as well as when training the welding machine operators.

Comparison of the standards shows that they differ not only by the characteristics that belong to mechanical testing of the welded joints, but also by analysis of the features of the HAZ microstructure and dimensions.

For comprehensive evaluation of the quality of welded joints of high-strength rails, as well as rails used in the railways of Ukraine, of M76, K76F type, produced by PJSC MW «Azovstal» (Mariupol, Ukraine) and rails from imported steels R260 and R350HT (British Standard French rail), PWI employees, together with specialists of JSC «Ukrzaliznytsa» and PJSC «KZESO» welded control batches of rails from different steel grades (in the quantity of 10 butt

joints) in the mobile machine of K922-1 type with their further investigation, in keeping with the given standards (see Table 1).

Chemical composition and mechanical properties of control batches of rails, which were used for the investigations, are given in Table 2.

Practically all the rails in the railways of Ukraine are welded using the technology of pulsed flash-butt welding (PF) [5], which was developed at PWI. That is why, it was exactly the technology used for welding control batches of rails.

A typical program of the change of parameters in PF welding in shown in Figure 1.

Modes of welding different rails batches are different. It should be noted that in welding high-strength

Tb le 2 Chemical composition and mechanical properties of control batches of rails

Steel grade	Chemical composition, %				Hardness, <i>HB</i>	Strength limit, σ_v , MPa	Yield limit, σ_y , MPa	Operating life, gross t	Manu- facturing plant
	C	Mn	Si	V					
M76	0.71–0.82	0.80–1.30	0.25–0.45	–	260–280	800–1100	500–700	0.45	PJSC MW «Azovstal» (Ukraine)
K76F	0.71–0.82	0.80–1.30	0.25–0.45	0.05	341–388	1300–1380	950–1050	0.5	
R260	0.62–0.82	0.70–1.20	0.15–0.58	0.03	250–270	942–980	498–540	0.9	Huta Katowice (Poland)
R350HT	0.72–0.82	0.15–0.60	0.65–0.75	0.03	350–370	1240–1300	840	0.9	British Standard French Rail (France)

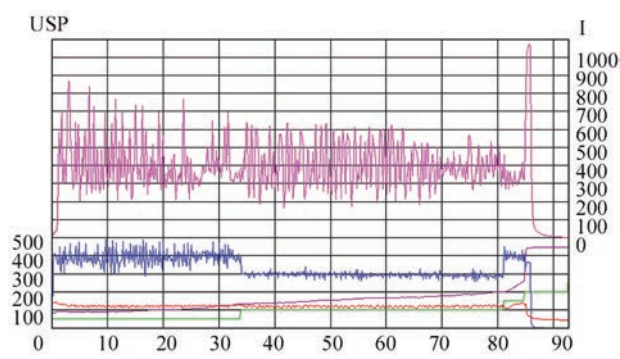


Fig re 1 Program of variation of the main parameters of pulsed flash-butt welding (PF)

rails of steel grades K76F and R350HT, the modes with limited heat input were used, in order to obtain the required mechanical properties. In welding M76 and R260 rails, having a lower hardness, modes with a larger welding heat input range can be used, with preservation of stable results in keeping with TU U 24.1-40075815-002:2016.

The main parameters that determine PF welding modes are given in Table 3.

Mechanich testing Mechanical testing of welded joints of control batches of rails were conducted in TRM press with the measurement limit of 500 tf; testing was conducted with tension of the head and foot. Testing procedure is the same for the above standards. The difference of the European standard consists only in that testing is conducted only with foot tension. Test scheme is given in Figure 2.

The main welding quality characteristics, regulated by both the standards (see Table 1), which were obtained during welding of control batches of rails in the optimum welding modes, are given in Table 4.

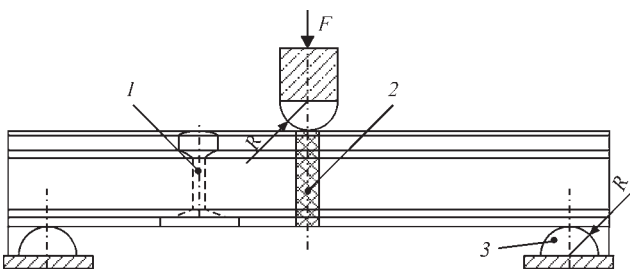


Fig re 2 Scheme of testing the welded butt joint for static mechanical bending (F — force; 1 — side view; 2 — weld; 3 — support)

Results of mechanical testing (see Table 4) showed that in order to obtain the necessary values of mechanical properties of welded joints of high-strength rails, it is necessary to limit and control the heat input in welding and to ensure heating with a higher temperature field gradient.

The values at bend testing in Ukrainian standard TU U 24.1-40075815-002:2016 are higher than the requirements of the European standard EN 14587-2:2009, both as to the deflection, and as to breaking load. Mechanical characteristics at testing the control batches are 1.5 to 2 times higher than the normative values of the European standard and satisfy the requirements of the Ukrainian standard. It should be noted that fine sulphide inclusions not exceeding the requirements admissible by the Ukrainian and European standards, were found in the fractures of some of the studied rails.

Comparison of the controlled characteristics (see Table 1) shows that alongside control of mechanical characteristics for static mechanical bending of welded joints of rails, there is a number of differences, envisaged by the European standard that concern the procedure of quality studies, in particular, met-

Tb le 3 Main parameters of the studied rail batches

Parameter	Rail type			
Steel grade	K76F	R260	R350HT	M76
Welding time, s	70–90	70–100	7–095	80–110
Welding current, A	370–390	350–370	360–390	340–370
Flashing allowance, mm	9–13	12–17	10–14	13–19
Upsetting value, mm	11–14	11–14	11–14	11–14

Tb le 4 Results of studying the quality of welded joints of control batches of rails

Steel grade	Bend testing		HAZ size, mm	Hardness distribution in the HAZ, HV	
	Breaking load, kN	Deflection, mm		min	max
K76F	<u>2100–2400</u> 2250	<u>32–50</u> 36	24–29	305	385
R350HT	<u>2150–2400</u> 2200	<u>34–55</u> 40	24–32	320	380
R260	<u>2000–2350</u> 2100	<u>32–55</u> 40	25–35	245	320
M76	<u>1900–2350</u> 2200	<u>32–57</u> 40	25–38	245	308

allographic, hardness measurements, as well as fatigue testing, not envisaged by the Ukrainian standard. Therefore, comprehensive studies of the control batches were conducted, taking into account the requirements of the two above-mentioned standards.

In PF welding of test batches in the optimum modes, the temperature fields were studied, at which sound joints were produced. Investigations were conducted using mathematical modeling of the process of rail heating by the method of flash-butt welding [6, 7], and modeling results are given in Figure 3.

Figure 3 gives the temperature fields in welding the control batches of rails in the optimum modes, and dot-dash lines show the temperature fields, corresponding to limit values of the HAZ width, admissible by European standard EN 14587-2:2009.

All the control batches of high-strength rails of R350HT, K76F steel grade (see Figure 3), differ by a narrower HAZ, and are within the limits, admissible by the European standard. In order to obtain the optimum metal structure in the HAZ, it is necessary to considerably limit the energy input. The temperature field in welding of high-strength rails differs by a higher gradient and smaller HAZ. More stable bending characteristics can be obtained at strict monitoring of the energy input.

High values of mechanical properties were achieved in welding in the optimum modes, which is due to formation in the HAZ metal of a finer structure of pearlite with ferrite precipitates on the grain boundaries, than in welding with a larger heat input. Performed investigations revealed that lowering of energy input in welding due to shortening of the flashing process duration and increase of welding current, allows improvement of the metal structure in the HAZ, while considerably reducing its width.

Ine stig in s 6 the HAZ width. The standard of Ukraine TU U 24.1-40075815-002:2016 does not have any requirements to HAZ width. In keeping with the European standard, the HAZ width is determined visually by macrosections, as well as by lines of hardness distribution. In these areas, the temperature reaches that of high temperature tempering. Here, the welded joint macrostructure should meet the following EN 14587-2:2009 requirements:

1. The visible HAZ zone of the welded macrosection should have a symmetrical shape within the tolerance around the weld line and it should be within 20–45 mm for mobile machines. The admissible deviation between the HAZ minimum and maximum dimensions should not exceed 20 mm. This requirement should be applied equally to vertical axial sections along the entire rail depth and to the edges of the rail foot.

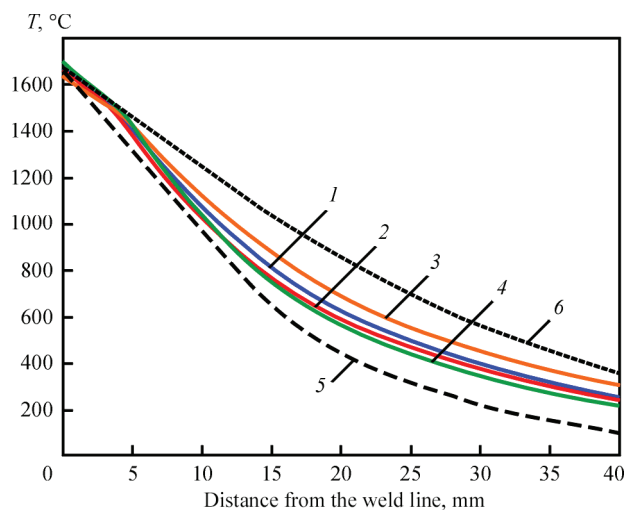


Fig re 3 Temperature fields in welding the test batch of rails in the optimum modes: 1 — R260; 2 — R350HT; 3 — M76; 4 — K76F; 5 — min; 6 — max

2. There should be no indications of the joint absence, inclusions, cracks or shrinkage deformation.

3. Two flat spots are allowed on the weld line, which meet the following requirements:

- maximum vertical size of 10 mm and maximum thickness of 0.7 mm in the case, if the flat spots look like the densification of the weld line, and do not have a lens like shape;

- maximum vertical size of 4 mm and maximum thickness of 0.7 mm in the case, if the flat spot is lens-shaped;

- there should be no embrittlement as a result of welding, cooling or heat treatment.

Figure 4 shows the macrosections of welded joints of control batches.

HAZ width (Figures 3, 4) in welding high-strength and high-alloyed rails changes within 26–32 mm that is by 4–6 mm smaller than in welding rails of M76 type with lower strength and smaller content of such alloying elements as C, Mn.

It should be noted that welding of all control batches of rails was performed without post-weld heat treatment, which is used at contact welding of rails in foreign practice to improve the values of mechanical properties of the welded joints.

As one can see from the results, in order to obtain high mechanical properties, it is necessary to reduce the heating zone width to a greater extent for high-strength rails, than for rails with a lower hardness. The required HAZ can be determined by the temperature field obtained after welding in the optimum mode. It is also possible to determine the maximum admissible deviations of the HAZ from the optimum one, as in keeping with the European standard the deviation field is quite broad.

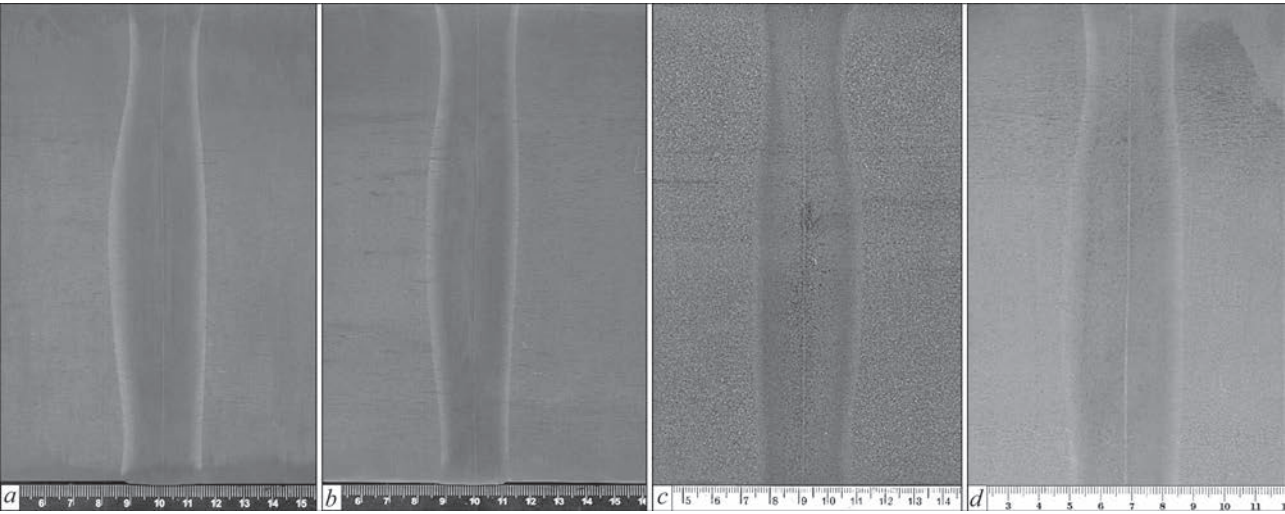


Fig re 4 Macrosections of rails of different steel grades in pulsed flash-butt welding in the optimum modes *a* — R350HT (HAZ — 28 mm); *b* — K76F (HAZ — 27 mm); *c* — R260 (HAZ — 31 mm); *d* — M76F (HAZ — 37 mm)

One can see from the macrosections that HAZ width of the studied rail batches corresponds to the temperature fields obtained at modeling the process of flash-butt welding in the optimum modes. It should be also noted that in all the rail batches the deviation of the HAZ width across the entire cross-section is insignificant and does not exceed 10 mm that satisfies the requirements of the European standard (maximum admissible deviation of the HAZ width over the rail cross-section is 20 mm for mobile machines).

Hardness studies. Hardness studies were performed in batches of welded rails, which are shown in Figure 5. Investigations were conducted by the procedure which is specified by the European standard.

Hardness measurements were performed over the entire near-weld zone of each of the two welded samples, directly from their joint line, using the method of Vickers hardness testing, in keeping with EN ISO 6507-1 and with subsequent parameters:

- *HV* 30;
- measurements should be taken 3–5 mm below the working rolling surface of the rail. Distance between the measurements should be 2 mm;
- width measurement is taken at not less than 20 mm distance from the weld through the HAZ into the base metal of the welded rails.

Here, in keeping with the European standard, different deviations of hardness distribution are allowed for different steel grades.

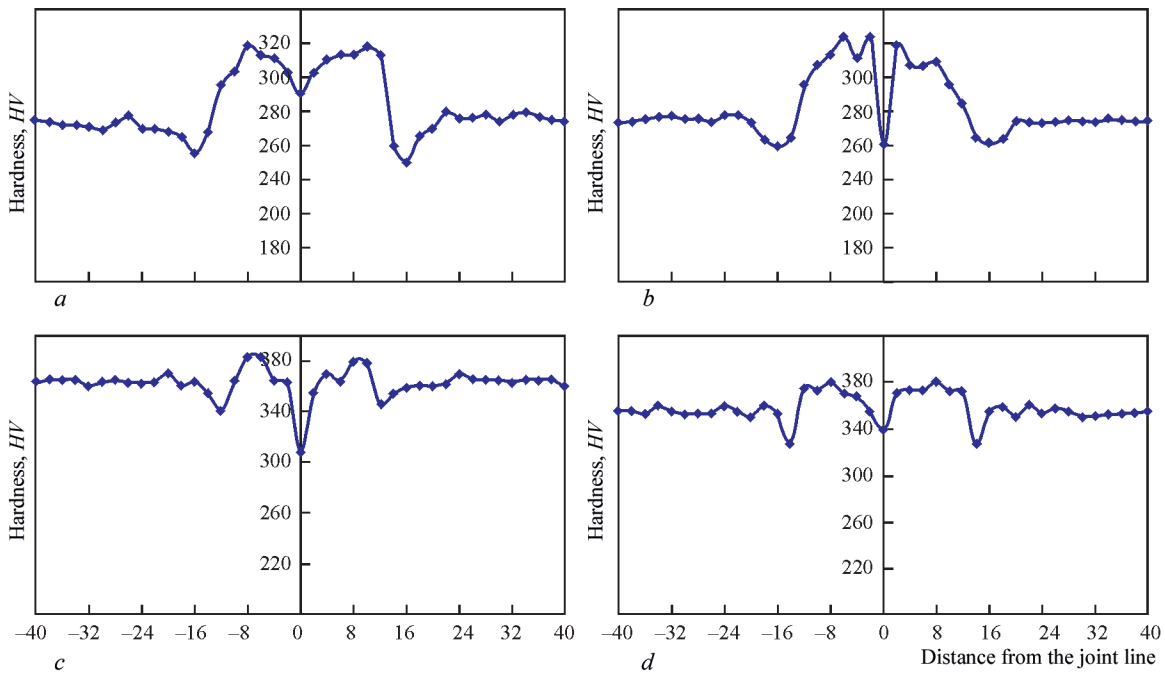


Fig re 5 Hardness distribution in welded rail batches: R260 (*a*); M76 (*b*); K76F (*c*); R350HT (*d*)

Rails 6 steels grades R220, R260 and R260Mn. For R220, R260, and R260Mn rails the obtained values of minimum and maximum strength should meet the following requirements:

- a) minimum strength P should not be smaller than $HV30 — 30$;
- b) maximum strength P should not exceed $HV30 — 60$, where P is the average strength of the initial rail, measured in hardened rail traverse.

In particular, the hardness value that goes beyond the limits of the above minimum and maximum values should be allowed, if such a hardness value is within the limits of two adjacent values that correspond to the requirements.

Rails 6 R350HT steel grade. For R350HT rails the values of minimum and maximum strength, obtained within 10 mm on each side from the weld line, should meet the following requirements:

- minimum hardness should not exceed $HV30 — 325$;
- maximum hardness should not exceed $HV30 — 410$.

In particular, the hardness value that exceeds the above minimum and maximum values should be allowed only in the case, when it is on the weld line.

Hardness decreases in the weld center, where a structure of sorbite-pearlite and areas of the ferrite phase form. In the weld central part, where the sorbite structure prevails, the hardness value is maximal. Hardness lowering is observed also along the HAZ boundaries, where presence of high-temperature tempering structure, which forms at temperatures of 580–620 °C, is observed. Temperature rise in the areas, adjacent to the weld center, depends on the temperature field gradient and temperature of the HAZ region.

Heat input determines the cooling rate of the butt joint – the lower the heat input, the higher the cooling rate. In its turn, the cooling rate determines the temperature of austenite decomposition. Lowering of decomposition temperature is the cause for reduction of interplate distance in sorbite and, consequently, hardness increase.

Heat-hardened rails of K76F and R350HT steel grades feature a high hardness, unlike M76 and R260 rails. That is why these rails require different energy input in welding. In welding of high-strength rails, it is necessary to avoid large hardness dips in the HAZ, and in welding rails with a low hardness, the large increase of hardness in the near-weld zone should be avoided. Maximum hardness deviations in the HAZ metal are regulated by the European standard.

As one can see (Figure 5), investigation results correspond to the requirements of the European standard.

Metallographic investigations. In the Ukrainian standard, metallographic examination of welded joints is not envisaged. Microstructural studies of rail steels R260 and R350HT, as well as of the microstructure of welded joints of control batches of rails (Figure 6), were conducted, in accordance with the European standard. The welded joints should have no indications of martensite or bainite at 100fold magnification of the visible zone due to heating impact. Microstudies are conducted on samples 15 mm high and 25 mm wide. Here, the sample should be cut out of the rail head 3 mm below the rolling surface. The sample should include 2 mm on one side of the weld, the joint line and 23 mm on the other side of the weld.

Base metal of R260 and R350HT rails has the structure of sorbite-pearlite. The microstructure of rails of R350HT grade, compared with that of rails of R260 grade, is characterized by a smaller size of sorbite colonies, and a small number of pearlite colonies. The grain size of the metal of R260 grade rails corresponds to numbers 2–3, and that of rails of R350HT grade — to numbers 4–5 by ASTM scale. The above enumerated structural factors determine the strength properties of heat-hardened rails.

In welded joints of R260 (Figure 7) and R350HT (Figure 8) rails in the areas of the joint line and coarse grain, the microstructure is that of sorbite-pearlite. Precipitation of hypoeutectoid ferrite is observed along the joint line, on the boundaries of primary austenite grains.

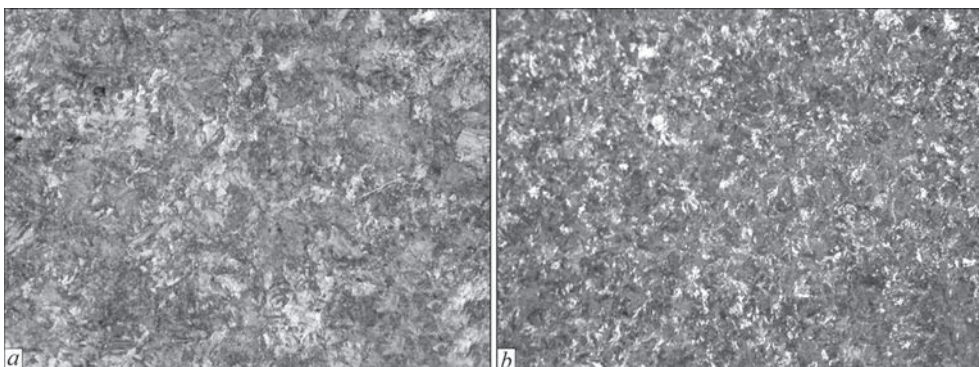


Figure 6 Microstructure ($\times 100$) of rail steel of the following grades: *a* — R260; *b* — R350HT

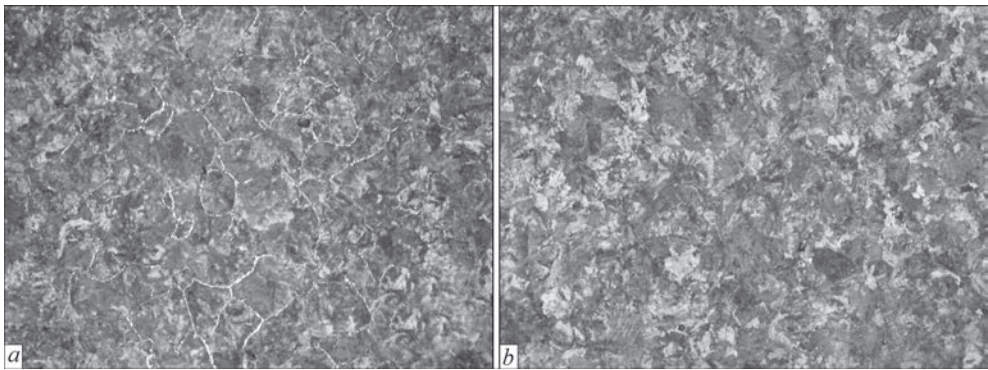


Fig re 7 Microstructure ($\times 100$) of a welded joint of R260 rails in the head zone: *a* — joint line; *b* — coarse grain region

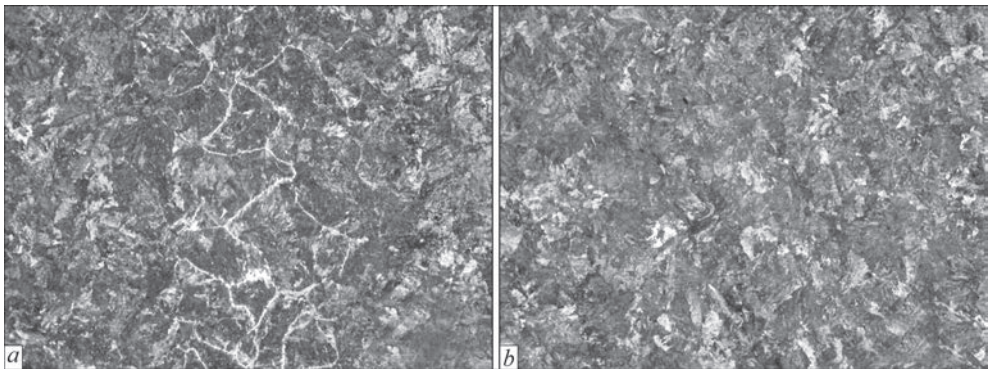


Fig re 8 Microstructure ($\times 100$) of a welded joint of R350HT rails in the head zone; *a* — joint line; *b* — coarse grain region

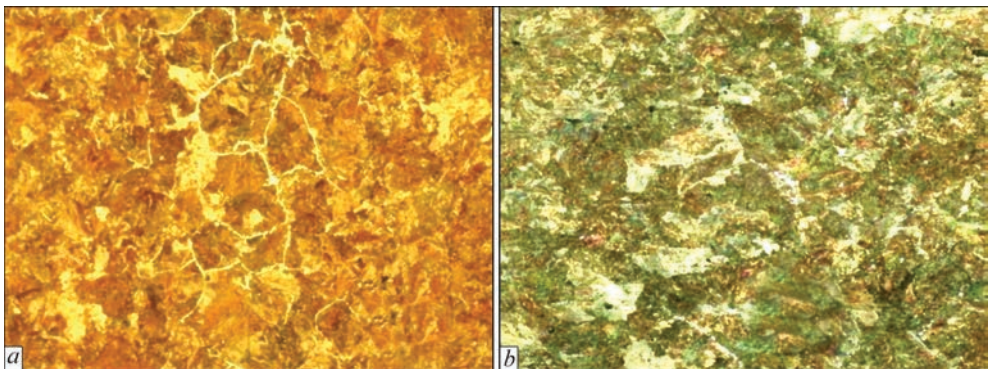


Fig re 9 Microstructure ($\times 100$) of a weld of rail of the following grade: *a* — M76 and *b* — K76F along the joint line

Ferrite precipitation in a much smaller amount is observed in the coarse grain areas, adjacent to the joint line. Characteristically, in rails of R260 grade the fraction of ferrite is greater, both along the joint line, and in the coarse grain regions.

Base metal of rails of K76F and M76 grade has sorbite-pearlite structure. The microstructure of the

joint line of rails from steels of M76 and K76F grade was also studied in pulsed flash-butt welding (Figure 9). The welded joints of K76F rails have more visible ferrite than those of R350HT and R260 rails.

As a result of comparison, it can be noted that no traces of bainite or martensite structures were revealed in welded joints of the studied rail batches, produced in the optimum modes. Moreover, the welded samples of rails of the control batches were tested by UT means and by dye-penetrant method, in keeping with the European standard procedures. No defects were found in the welded joints.

Fa ig e streng h testing. Also in accordance with the requirements of the European standard, all the butt joints were subjected to fatigue strength testing (Figure 10). Fatigue testing of samples of rails of R260 and R350HT steel grades were conducted, in

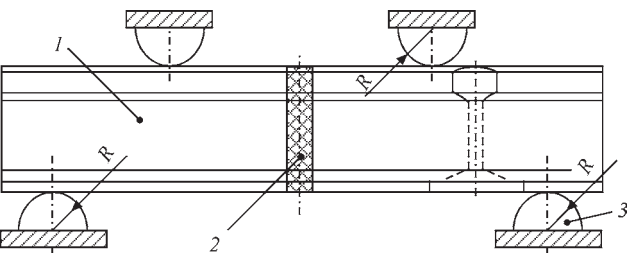


Fig re 10 Fatigue strength testing of a welded joint: *1* — side view; *2* — weld; *3* — support

keeping with EN 14587-2:2009E normative document in ZDM-200Pu testing machine, certified by the appropriate state services. Test welded butt joints of rails from control batches 1.2 m long were tested by pure bending by cyclic loading with maximum cycle stresses of 190 MPa, and loading cycle asymmetry of 0.1. Test base was 5.0 mln. cycles, and loading frequency was 5 Hz. Samples withstood 5 mln cycles without fracture.

It was found that in the case of application of PF technology the mechanical, and strength properties and the structure of the joints, required in keeping with the European and Ukrainian standards, are ensured.

Analysis of results of studying the mechanical properties and structure of welded joints shows the high stability of properties at mechanical testing and evaluation of structural changes in the welded joints. The HAZ width is in the lower value range. This is due to the fact, according to the Ukrainian standard, the deflection should be not less than 30 mm, compared to the deflection of 20 mm, specified by the European standard. In order to obtain higher ductility properties according to the standard of Ukraine, the modes of welding with controlled energy input were developed. It allows producing a finer structure in the weld central part at admissible hardness deviation. Therefore, the HAZ width in the control batches of welded samples of rails is equal to 27–31 mm, that is within the tolerance field of this parameter, but in the region close to the minimum admissible one (20 mm), hardness remaining within the limits admissible by the European standard.

Optimum values of the characteristics, satisfying the requirements of the considered standards, were determined on the base of the conducted experimental studies of the mechanical properties and structure of metal of the control batches of rails.

No inclusions of martensite and bainite type were found in the structure of the HAZ metal of all the rail batches. A mathematical model of temperature field calculation at flash-butt welding of railway rails was used to

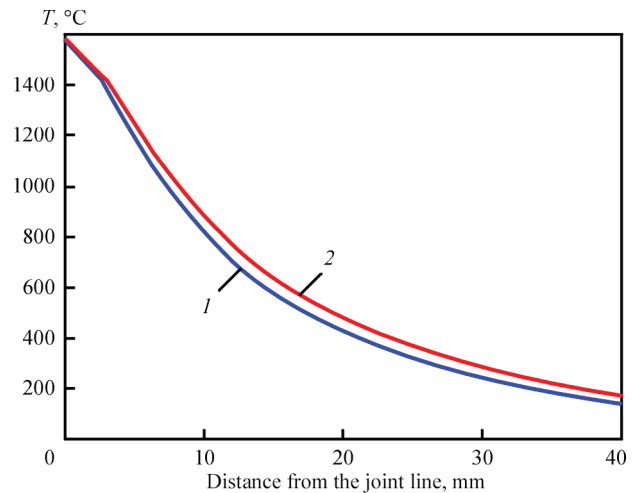


Fig re 11. Welding of rails of R350HT (1) and R260 steel grades with lower energy input

predict the probable appearance of such structures, at the possible determined welding modes [6, 7].

As is known, HAZ width and its admissible deviations in keeping with the European standard are given in Table 1. Taking into account the performed calculations, mathematical modeling should be used to determine the minimal admissible width of the HAZ for the studied rail steels. It was also established that heating and total heat input should be reduced within reasonable limits, as it is accompanied by increase of the cooling rate, metal grain refinement in the HAZ, as here the probability of formation of defects of oxide spot type in the joint plane becomes higher [8]. In addition, there arises the need for appearance of hardening structures, such as martensite and bainite, in the HAZ metal.

The developed mathematical model, as well as the conducted experiments, was used to establish that appearance of bainitic and martensitic structures in the HAZ metal in welding high-alloyed and high-strength rails of E260 and R350HT type can be expected at formation of temperature fields with HAZ width of approximately 17–20 mm, given in Figure 11. Lowering of heating and reduction of the HAZ size affects the structure of rails of R260 type to a greater extend,

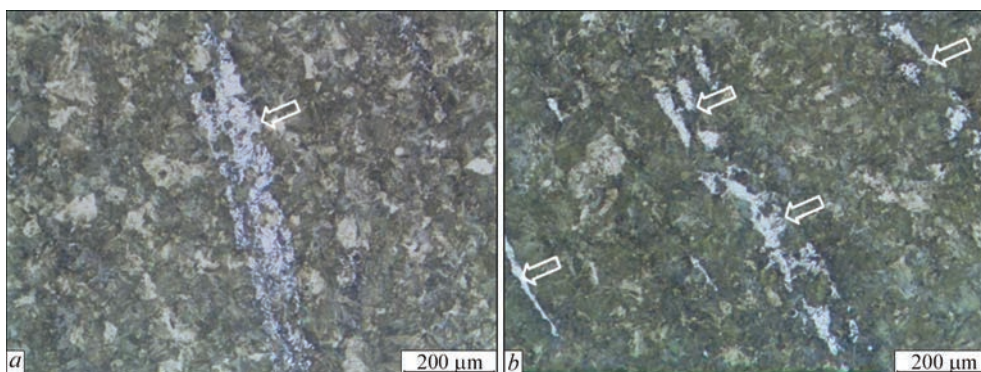


Fig re 2 Martensite structures in the near-weld zone of welded joints of R350HT (a) and R260 (b) rails in welding with lower energy input

and proneness of this steel to appearance of hardening structures, such as martensite and bainite, is high due to their high alloying with Mn.

HAZ width in this case is equal to 17–20 mm. It is experimentally confirmed that at such a heating, martensite structures are present in the welded joint of R260 rails at HAZ width reduction below 20 mm, as shown in Figure 12. Martensite-austenite structures are located both along the rolling lines, and in an arbitrary volume of metal [9]. In welding rails of R350HT and K76F grades appearance of martensite structures was observed at lowering of heating and producing HAZ smaller than 18 mm that is below the value allowed by the European standard.

The highest values of mechanical and strength properties, as well as absence of hardening structures, were achieved in welding high-strength rails with formation of the next region of the temperature fields, which are presented in Figure 3.

At determination of welding modes of high-strength and high-alloyed rail steels of the mentioned types, formation of temperature fields (Figure 11), corresponding to minimum admissible width of the HAZ, specified by the European standard, should be avoided. This requires application of control systems, which allow monitoring the energy input in welding.

Conclusion

Control batches of rails of M76 and K76F grades, made in Ukraine, as well as rails of R260 and R350HT grade, made in Europe, which were welded in the optimum modes in keeping with the standard of Ukraine TU U 27.1-40081293:2016 fully meet the requirements of European standard EN 14587-2 2009.

It was established that development of the technology of welding high-strength rails should take into account the HAZ width as a controlled parameter that significantly affects the welded joint quality.

The effect of the possible deviations from the main welding parameters, which are regulated by the valid Ukrainian standard, on formation of the temperature fields and joint quality in different pulsed flash-butt welding modes was determined experimentally, as well as using the developed procedure of mathematical modeling of the process of metal heating in flash-butt welding.

It was established that in order to obtain high mechanical values in welding high-strength rails of K76F, R260 and R350HT steel grades, it is necessary to apply technologies, which ensure highly concentrated heating with limited energy input. Such heating is provided by pulsed flash-butt welding technology. Here, formation of HAZ of smaller than 20 mm width, which is specified by the European standard as the minimum admissible one, should be avoided.

The optimum programs for controlling the main welding parameters that ensure the required values of strength and structure of high-alloyed and high-strength rails of the studied batches, were determined within the considered standards. All the mentioned rail batches were welded using the main welding parameters that correspond to the Ukrainian standard, allowing for their correction within the admissible limits.

It is recommended to introduce into the Ukrainian standard the definition and control of the HAZ width after welding, taking into account the properties of rail steel, used in Ukraine.

1. Kuchuk-Yatsenko, S.I. (1992) *Continuous flash-butt welding*. Kiev, Naukova Dumka [in Russian].
2. Kuchuk-Yatsenko, S.I., Didkovsky, A.V., Shvets, V.I. (2008) Technology and equipment for flash-butt welding of high-strength rails. *The Paton Welding J.*, **11**, 111–120.
3. TU U 27.1-40081293-002:2016: New welded rails for railways: Dnipropetrovske NKTB, NDKTI PJSC Ukrzaliznytsya [in Ukrainian].
4. (2009) *Eurostandard EN 14587-1*, –2.
5. Kuchuk-Yatsenko, S.I., Didkovsky, O.V., Bogorsky, M.V. et al. (2002) *Flash-butt welding method*. Pat. 46820, Ukraine, Int. Cl. 6B23K11/04, C2; Pat. 2222415, RF (2003); Pat. 6.294.752, USA (20.06.01); Pat. ZL001016772/5 (2004), PRC.
6. Weingrill, L., Enzinger, N. (2017) Temperature fields evolution during flash-butt welding of railway rails. *Mat. Sci. Forum*, **9**, 2088–2093.
7. Kuchuk-Yatsenko, S.I., Milenin, A.S., Velikoivanenko, E.A. et al. (2018) Mathematical modeling of the process of metal heating in continuous flash-butt welding. *The Paton Welding J.*, **0**, 2–8.
8. Kuchuk-Yatsenko, S.I., Shvets, V.I., Didkovsky, A.V. et al. (2013) Defects of joints of high-strength rails produced using flash-butt welding. *Ibid.*, **9**, 2–8.
9. Zabilsky, V.V., Nikonova, R.M. (2005) Ductile-brittle transition in steels at near-solidus temperatures. Mechanism of embrittlement of grain boundaries. *Fizika Metallov i Metallovedenie*, 99(3), 19 [in Russian].

Received 24.06.2020



Zaporozhye Industrial Forum

08–10 September, 2020, Zaporozhye, Ukraine

26th International Specialized Exhibition of Industrial Solutions

<https://expo.zp.ua/zpf/>

HYBRID WELDING OF ALUMINIUM 1561 AND 5083 ALLOYS USING PLASMA-ARC AND CONSUMABLE ELECTRODE ARC (PLASMA-MIG)

OA .B b y h¹, V.M. K o r z h y k^{1,2}, A.A. Grynyuk², VY u. Kha kin^{1,2}, C hunlin D o n g¹ and Sha g d i a n¹

¹Guangdong Institute of Welding (China-Ukraine E.O. Paton Institute of Welding)

363 Chiansin Str., 510650, Guangzhou, Tianhe

²E.O. Paton Electric Welding Institute of the NAS of Ukraine

11 Kazymyr Malevych Str., 03150, Kyiv, Ukraine. E-mail: office@paton.kiev.ua

In the article it is shown that to improve mechanical properties and decrease indices of stress-strain state of welded joints of alloyed aluminium 1561 and 5083 alloys it is rational to apply hybrid plasma-arc welding using arc of the consumable electrode, which as compared to traditional welding using arc of the consumable electrode allows reducing the electrode wire consumption by 10–30 %, input energy — up to 25 %, residual deformations — by 2–3 times, residual stresses — by about 20 % according to the absolute values, as well as reducing burnout of such alloying element as Mg by 15–20 %. 19 Ref., 6 Tables, 9 Figures.

Key words: hybrid plasma-arc welding using consumable electrode (Plasma-MIG), pulsed-arc welding using consumable electrode (MIG), surfacing welds, butt welds, strength, burnout of alloying elements, stress-strain state

The intensive development of land, air and sea high-speed transport necessitates the use of innovative high-performance technologies for producing welded joints of aluminium alloys. This is associated with a number of drawbacks inherent in traditional welding processes. Thus, in the case of using consumable electrode arc welding (MIG welding) a significant overheating of the electrode metal occurs, which leads to a partial burnout of alloying elements of aluminium alloys and, as the consequence, a decrease in the strength of the produced joints. In addition, during MIG welding fairly wide welds are formed and significant residual deformations occur. In the case of welding using nonconsumable electrode arc (TIG welding), the efficiency is reduced and significant residual deformations also occur. Producing welded joints is complicated by the fact that the processes of MIG and TIG welding require a preliminary preparation of edges to be welded.

One of the ways to eliminate the mentioned problems is the use of plasma welding. However, this process also has some drawbacks. First, the melting of the filler wire requires additional energy, the consumption of which leads to an increase in the input energy of welding. This can lead to the formation of certain residual stresses (deformations). Secondly, the increased energy intensity and axial concentration of pressure (phenomenon of keyhole formation) lead to

the defects of welds formation (in particular, undercuts, root defects, nonuniform formation of upper reinforcement bead) and the presence of inner porosity.

In the last decade, traditional problems of welding and related technologies are solved through the use of hybrid technologies [1]. Difficulties in producing joints of alloyed high-strength aluminium alloys are also solved by a hybrid combination of the advantages of plasma and arc welding methods. For this purpose in one welding pool the energy of the constricted arc with nonconsumable and an arc with the consumable electrode is concentrated. Such an approach allows narrowing the weld and reducing (or completely eliminate) the need in preparation of edges to be welded. It also increases the efficiency of welding by stabilizing the action of the arc of the consumable electrode by influencing the plasma-arc, which covers the first outside. All this makes the application of the technology of hybrid plasma-arc welding using the consumable electrode, better known in the world as Plasma-MIG, relevant.

The process of plasma-arc welding with the consumable electrode including for joining of aluminium alloys was developed in the 1970s by a group of researchers from the laboratory of the Philips Company [2]. Due to certain difficulties in creating the optimal design of the torch and power sources adapted namely for this process, hybrid Plasma-MIG welding still has some limita-

O.A. Babych — <https://orcid.org/0000-0001-5633-5721>, V.M. Korzhyk — <https://orcid.org/0000-0001-9106-8593>,

A.A. Grynyuk — <https://orcid.org/0000-0002-6088-7980>, V.Yu. Khaskin — <https://orcid.org/0000-0003-3072-6761>,

Chunlin Dong — <https://orcid.org/0000-0003-2672-5985>, Shanguo Han — <https://orcid.org/0000-0002-4299-9786>

© O.A. Babych, V.M. Korzhyk, A.A. Grynyuk, V.Yu. Khaskin, Chunlin Dong and Shanguo Han, 2020

tions in industrial application. For example, it should be taken into account that in this type of hybrid process the arc of the consumable electrode exists in the environment of ionized argon plasma generated by the arc of the nonconsumable electrode, which radically changes the conditions of its burning as compared to GMAW/MIG process. In [3], it was shown that electrical conductivity of the external arc is significantly higher than that of the inner arc due to the higher density of electrons. Respectively, most of the current between the consumable electrode and the base metal flows through the outer arc, and to the inner arc about 5 % of the current goes. This is also confirmed by the higher glow of the outer arc in the area below the end of the consumable electrode. The higher intensity of glow of the inner arc as compared to the outer one, which is noted by most researchers, is predetermined not by the high glow density of current flowing through it, but by a higher glow intensity of the elements that are a part of the gas phase in this area.

At present, active investigations of the process of hybrid plasma-arc welding using consumable electrode continue. Such investigations are carried out at a number of universities, in particular, at the Chemnitz University of Technology and in SLV Muenchen (Germany) [4, 5]. The similar investigations are carried out at the Perm State University (Russia) [6, 7]. The peculiarities of the process of plasma-arc welding using consumable electrode were also studied in China, Japan, and Brazil [8, 9]. In Ukraine, the issues of plasma-arc welding using consumable electrode were undertaken at the Pre-Azov State Technical University and the E.O. Paton Electric Welding Institute of the NASU [10].

The investigations carried out in the last decade were aimed at a thorough study of separate components of the process and its behavior in general. In [11], it was shown that during welding of aluminium alloys with an increased electrode wire feed rate, the size of undercuts decreases as the amount of welding wire in the welding pool increases. Increasing the diameter of the plasma-forming nozzle also facilitates the elimination of undercuts because of a low electromagnetic stirring force caused by a low density of plasma current. However, the increase in the wire feed rate and, accordingly, the arc current of the consumable electrode, shifts the process towards the traditional MIG welding, which eliminates the advantages of the hybrid method. Reduction in the plasma current density can contribute to arising spattering of the metal by the arc of the consumable electrode. In [10, 12] the peculiarities of the behavior of both electric arcs, their influence on each other, on the formation

of a liquid metal drop and the process of mass transfer were studied quite deeply.

The model of heating the electrode wire in the process of hybrid plasma-arc welding using consumable electrode (Plasma-MIG) proposed in [12] allowed carrying out a preliminary evaluation of the plasma temperature of an integrated gas discharge. During welding of aluminium alloys with a thickness of 5–12 mm, it can be about 7300–7400 K. This indicates the danger of burnout low-melting alloying elements that are a part of the electrode wire and the base metal, which can lead to weakening of the produced joints. In addition, in [12] a tendency of increasing the voltage on the arc of the nonconsumable electrode with an increased flow rate of the plasma-forming gas and its temperature is observed. Such a feature of the hybrid process should be taken into account when selecting welding modes, in particular, optimizing the power ratio of plasma and arc components.

In contrast to the previously published works, this paper pays attention to the influence of the hybrid Plasma-MIG process modes on the geometry and stress-strain state of the produced joints, as well as its comparison with a traditional pulsed-arc welding process. In this case, producing high-quality joints is planned due to a concomitant preheating of welded metal by a plasma-arc and reducing the arc voltage of the consumable electrode with a simultaneous increase in its penetration into the metal. It is expected that the mutual influence of the components of the hybrid welding process can contribute to the reduction of input energy and the share of burnout of alloying elements.

The aim of the investigation is to improve the mechanical properties and reduce the stress-strain state of welded joints of alloyed aluminium alloys by reducing the amount of the used electrode wire, input energy and burnout of alloying elements due to the use of hybrid plasma-arc welding.

Achieving this aim was carried out according to the following procedure. At first, on the basis of the literature data, the intervals of varying parameters of the modes of hybrid plasma-arc (Plasma-MIG) welding were selected. Then, applying mathematical modeling, the influence of these parameters on the penetration depth and welding speed was analyzed, and then the most promising parameters from the standpoint of minimizing heat input and energy input were selected. The reliability of the calculations was checked and on the selected modes welding of the test specimens was performed. Moreover, the mutual influence of the plasma-arc and the arc of the consumable electrode on each other, as well as their joint influence on the hybrid welding process were analyzed. To compare

Tb le 1 Chemical composition of aluminium 5083 and 1561 alloys and electrode wire ER5356, wt.%

Grade of alloy	Fe	Si	Mn	Cr	Ti	Al	Cu	Be	Mg	Zn	Impurities
5083	≤0.4	≤0.4	0.4–1.0	0.05–0.25	≤0.15	Base	≤0.1	≤0.005	4.0–4.9	≤0.25	≤0.15
1561	≤0.4	≤0.4	0.7–1.1	–	–	Same	≤0.1	0.0001–0.003	5.5–6.5	≤0.2	≤0.1
ER5356	0.1–0.2	0.08	0.12	0.13	0.13	»	0.02	–	4.95	≤0.02	–

Tb le 2 Generalized thermophysical characteristics of aluminium alloys under normal conditions

Density ρ , kg/m ³	Specific heat capacitance, J/(kg °C)	Coefficient of thermal conductivity λ , W/(m·°C)	Coefficient of thermal conductivity a , m ² /s	Specific heat of melting L , kJ/kg	Specific heat of evaporation E , kJ/kg	Melting point, T_m , K	Temperature of beginning of phase transitions, K
2640	922	122	$5.0122 \cdot 10^{-5}$	390	10530	660	460

the obtained results, traditional pulsed-arc welding of similar specimens was performed at the same speed or as close as possible to the input energy. Mechanical tests of the produced specimens were conducted. The burnout of one of the most volatile alloying elements (magnesium) in welding processes was investigated. The stress-strain state of the welded specimens was investigated. Based on the obtained results, the appropriate conclusions were made.

To perform preliminary technological calculations in terms of the widest application in industrial welded structures, the aluminium alloys 5083 and 1561 were selected, during welding of which the electrode wire ER5356 is used (Table 1). To simplify the evaluation calculations, the generalized thermophysical characteristics of these alloys were used, given in Table 2.

To model the heat source operating during Plasma-MIG welding in the aluminium plate, the model of J. Goldak [13] was used (Figure 1). According to this model, the heat source was represented as a double ellipsoid. The calculation of the considered thermal welding processes was performed using finite element modeling. As a basic assumption, it was assumed that an unlimited plate of aluminium alloy with a thickness δ (for example, $\delta = 10$ mm) is welded by a surfacing weld. In this case, the volume of the metal introduced by the consumable electrode was taken into account as the volume of the metal of the plate to be welded, remelted by the arc of this electrode. To increase the accuracy of calculations in the area of the heat source, a grid with a smaller step was used, and in other areas — with a relatively large step.

The finite element method used in the calculations is based on the assumption that a body can be represented as a set of elements connected to each other only in nodes. The relationship of nodal changes in temperature over time is set by the temperature matrix of the element. Combining the temperature matrices of separate elements into a global temperature matrix

of a body allows recording the conditions of a thermal equilibrium of a body as follows:

$$C(T)\rho(T)\frac{\partial T}{\partial t} = \frac{\partial}{\partial x}\left(\lambda(T)\frac{\partial T}{\partial x}\right) + \frac{\partial}{\partial y}\left(\lambda(T)\frac{\partial T}{\partial y}\right) + \frac{\partial}{\partial z}\left(\lambda(T)\frac{\partial T}{\partial z}\right), \quad 0 < z < \delta, \quad t > 0, \quad (1)$$

where $C(T)$, $\rho(T)$, $\lambda(T)$ is the effective heat capacity of the metal (taking into account the latent heat of fusion), density and thermal conductivity coefficient, respectively; x, y, z are the Cartesian coordinates (heat source moves along the coordinate x at a speed V); δ is the thickness of the metal plate to be welded; t is the time coordinate.

At set temperatures, the action of which changes over time, and at a known global temperature matrix, the solution of the system of equations of thermal equilibrium (balance) allows finding all the nodal values of temperature depending on the time of the heat source, and using the latter — temporary temperature changes within each element. This is how the spatial-temporal distribution of body temperatures was determined [14].

On the surface of the plate, which is heated by a hybrid plasma-arc heat flux $q(t)$ over time t , a volumetric heat source with a radius R_{pl} is formed, which contains a second heat source with a slightly smaller

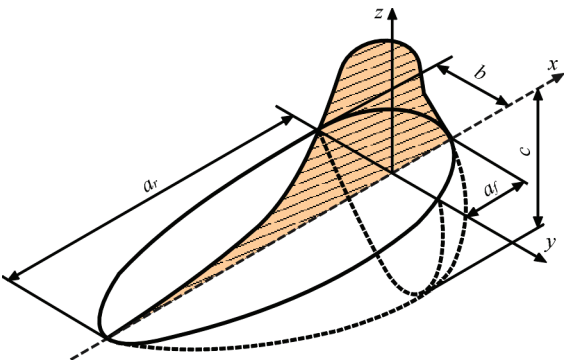


Fig re 1 Scheme of model of distributed volumetric heat source, which has a shape of a double ellipsoid [13]

radius R_{MIG} . In the process of Plasma-MIG welding, at the set point on the surface, at first it will be heated by the plasma source and then by the sum of the arc (MIG) and plasma sources, and finally by the plasma source again. The constant of time (time of influence of the heat source) in each of these three cases will be:

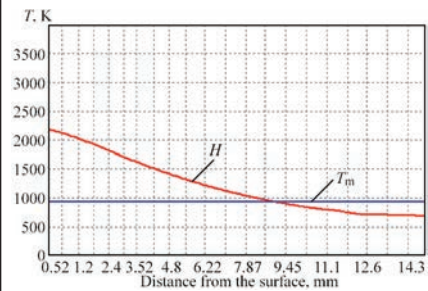
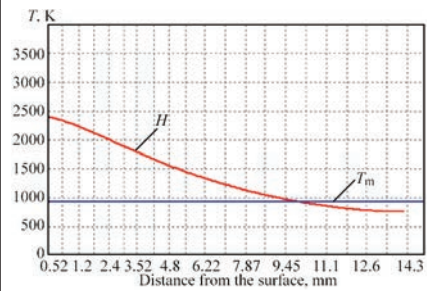
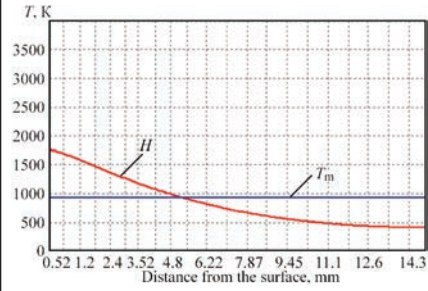
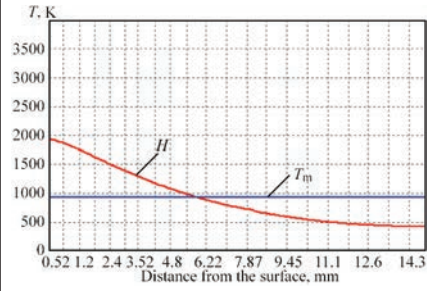
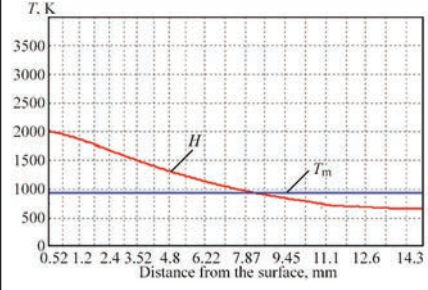
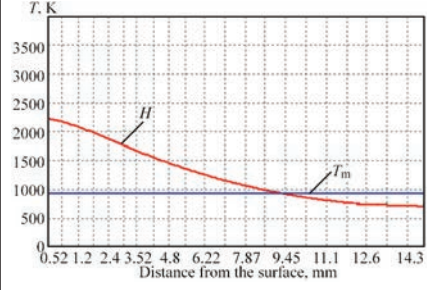
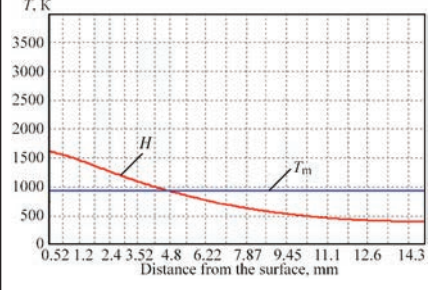
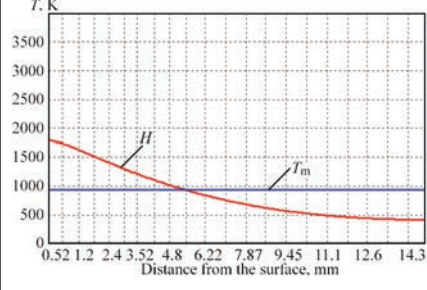
$$t_1 = \frac{R_{PL} - R_{MIG}}{V} ; t_2 = t_1 + \frac{2R_{MIG}}{V} ; t_3 = t_2 + t_1.$$
 (2)

Then on the plate to be welded a heat flux will act

$$q_{\Sigma}(t) \begin{cases} q_{PL}, & 0 < t < t_1 \\ q_{PL} + q_{MIG}, & t_1 < t < t_2 \\ q_{PL}, & t_2 < t < t_3 \end{cases} ;$$
 (3)

where $q_{MIG} = A(T) \frac{P_{MIG}}{\pi R_{MIG}^2}$ is the heat flux introduced by the arc of the consumable electrode (MIG), $q_{PL} = A(T) \frac{P_{PL}}{\pi R_{PL}^2}$ is the heat flux introduced by the arc plasma. Such heat fluxes are created in the plate to

Table 3 Results of calculated determination of height of welds H and constant of time τ , which are obtained during Plasma-MIG welding of aluminium 5083 and 1561 alloys

Mode parameters	Results			
	Welding speed 10.0 mm/s		Welding speed 16.7 mm/s	
	Dependence $H = f(T)$	H , mm/ τ , s	Dependence $H = f(T)$	H , mm/ τ , s
$P_{MIG} \approx 4000$ W, $P_{PL} \approx 5000$ W, $d_{MIG} = 10.0$ mm, $d_{PL} = 11.5$ mm		$H = 9.0$ mm/ $\tau = 1.18$ s		$H = 5.2$ mm/ $\tau = 0.694$ s
$P_{MIG} \approx 4000$ W, $P_{PL} \approx 4000$ W, $d_{MIG} = 10.0$ mm, $d_{PL} = 11.5$ mm		$H = 8.2$ mm/ $\tau = 1.18$ s		$H = 4.7$ mm/ $\tau = 0.694$ s
$P_{MIG} \approx 5000$ W, $P_{PL} \approx 5000$ W, $d_{MIG} = 10.0$ mm, $d_{PL} = 11.5$ mm		$H = 9.9$ mm/ $\tau = 1.18$ s		$H = 5.8$ mm/ $\tau = 0.694$ s
$P_{MIG} \approx 5000$ W, $P_{PL} \approx 4000$ W, $d_{MIG} = 10.0$ mm, $d_{PL} = 11.5$ mm		$H = 9.3$ mm/ $\tau = 1.18$ s		$H = 5.4$ mm/ $\tau = 0.694$ s

be welded by a volumetric heat source, the shape of which is shown in Figure 1.

In the course of the computer modeling, in accordance with the recommendations of [8–12], the modes of Plasma-MIG welding processes were selected, according to which using the method of finite-element modeling, the temperature distribution in the depth in the plate to be welded was determined. By means of the time constant (τ , s) and the size of the heat source (d_{PL} , mm), the welding speed (V , mm/s) was determined. Depending on the evaluation of the temperature distribution in the depth of the plate (depending on the powers of the components of the sources P_{PL} and P_{MIG} , W), this allowed selecting the approximate parameters of the modes in which it is rational to perform welding of butt joints (Table 3).

When choosing the parameters of the Plasma-MIG welding modes, both the depth of penetration H as well as the width of the formed weld were taken into account, approximately corresponding to the parameter d_{MIG} . For welding plates with a thickness of $\delta = 10$ mm, between the edges to be butt-joined a gap was left approximately equal to the diameter of the electrode wire (i.e. ~ 1.6 mm), which allowed narrowing the weld and increase the speed of the process. Welding of plates $\delta = 5$ mm was carried out with a tight joining of edges. In all cases, welding was performed on a substrate to avoid leakage of the pool. Such technological methods in combination with calculated forecasts allow choosing the welding speed of 16.7 mm/s (60 m/h). In this case, in order to avoid an excessive amount of molten metal in the welding pool, the parameters of power variation should approach the ratio $P_{MIG}:P_{PL} \sim 4000:5000$ W. For example, the arc current of the consumable electrode may be $I_{MIG} = 200$ A at an arc voltage of $U_{MIG} = 20$ V, and the current of the plasma-arc $I_{PL} = 160\text{--}180$ A at $U_{PL} = 30$ V.

For experimental verification of the proposed modes, as well as for studying the technological features of Plasma-MIG welding, a laboratory model of the technological complex was designed (Figures 2, 3). When designing the equipment, the specialists focused on welding sheets of aluminium alloys with a thickness from 5 to 10 mm. According to the calculations, the total current load for this purpose should not exceed 500 A. To obtain equal opportunities to study the impact on the process of both the plasma-arc as well as the arc of the consumable electrode, the current load should be divided approximately equally. Based on this assumption, the welding power sources were selected (Tetrix 421 AC/DC of the EWM Company for the arc of the nonconsumable electrode and of FRONIUS TPS 450 for the arc of the consumable electrode) and the plasmatron was designed and integrated capable of withstanding currents

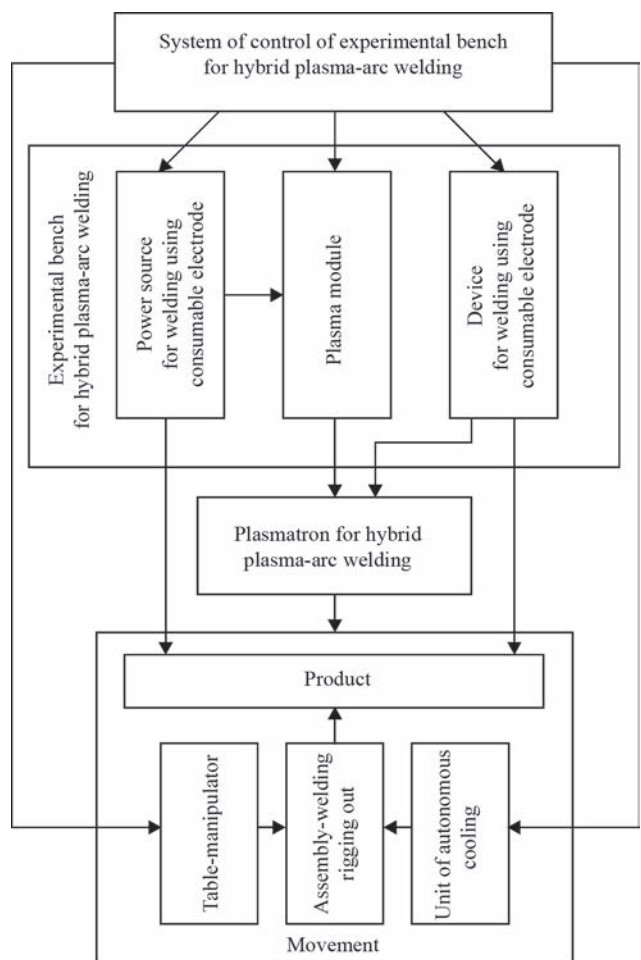


Fig re 2 Block diagram of laboratory complex of Plasma-MIG welding

not less than 250 A both on the plasma-arc as well as on the arc of the consumable electrode with DC of 100 % (Figure 4). During its manufacture, the non-consumable electrode was made with a diameter of 10.0 mm with an axial hole of 5.0 mm to exclude the possibility of contact of the electrode wire of 1.6 mm diameter with the inner wall of the electrode. The diameter of the channel of the plasma-forming nozzle was selected to be equal to 10.0 mm on the grounds of approximation to the dimensions of the working plane of the nonconsumable electrode.



Fig re 3 Appearance of laboratory complex of Plasma-MIG welding

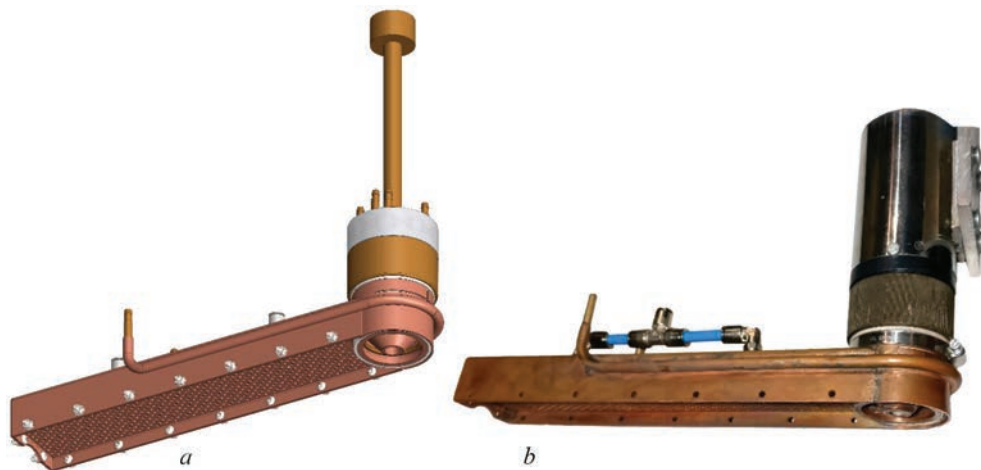


Fig re 4 3D-model (a) and appearance (b) of integrated plasmatron

As specimens for experiments, the plates of aluminium 5083 and 1561 alloys with the dimensions $(400-320) \times (200-100) \times \delta$ mm ($\delta = 5.8$ and 10 mm) were used. The specimens were butt-welded, also surfacing welds were produced on their surface. For welding the electrode wire ER5356 (of 1.6 mm diameter) was used.

At first, a series of experiments was conducted to verify the results of calculations (Figure 5). It was found that the accuracy of the calculated value of the total height of the weld is in the range of 5–10 %, which is a satisfactory result for technological calculations. Using the modes selected by the calculation method, quality joints of 5083 alloy were produced, having a thickness of 8 and 10 mm (Figure 6). Moreover, the arc of the consumable electrode, which was constricted due to the outer plasma-arc, provided the penetration, which is close to the vapour-gas channel as to its shape without a keyhole formation, which is traditionally necessary for this.

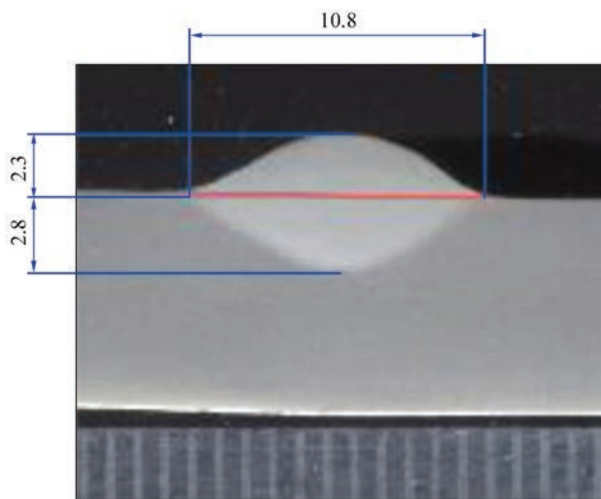


Fig re 5 Cross-section of surfacing weld produced on the plate of 1561 alloy ($\delta = 8$ mm) at a speed of 16.7 mm/s: $I_{MIG} = 200$ A, $U_{MIG} = 20$ V, $I_{PL} = 176$ A, $U_{PL} = 30$ V

After that, the comparative experiments on pulsed-arc welding using consumable electrode (MIG) and hybrid Plasma-MIG welding were performed (Figure 7). Here, the criterion for selecting the mode was the quality of weld formation at equal process speeds. The experiments showed a decrease in input energy by 20–25 % and a similar decrease in the width of the weld (in the example, shown in Figure 7, a, b — from 13.8 to 10.7 mm). At the same time, the integrated input energy of Plasma-MIG welding E_{Σ} was determined as the sum of input energies of the components of E_{MIG} and E_{PL} . Also, the experiments on Plasma-MIG welding at different speeds were carried out (for example, Figure 7, b and Figure 7, c), which showed that when the welding speed increases from 10 to 16.7 mm/s, the welds on the back side are narrowed approximately twice (for example, from 8 to 4 mm), and at the top their width remains almost unchanged. This is facilitated by a reduction in the input energy of E_{Σ} by ~10 % (from 530 to 480 J/mm).

To study the mutual influence of the arcs on the process of Plasma-MIG welding, a filming of the

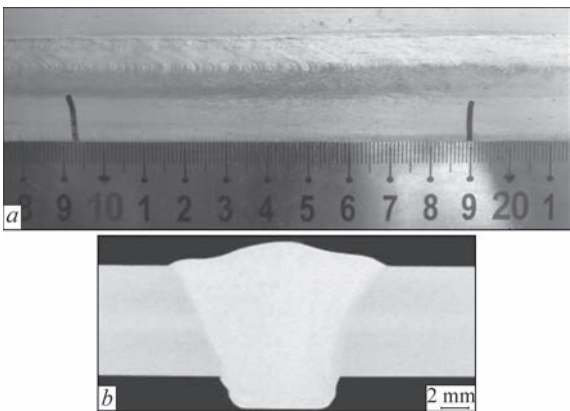


Fig re 6 Appearance (a) and cross-section (b) of butt joint of 5083 alloy ($\delta = 8$ mm), produced by Plasma-MIG welding at a speed of 6.67 mm/s: $I_{MIG} = 142$ A, $U_{MIG} = 20$ V, $I_{PL} = 182$ A, $U_{PL} = 30$ V, $E_{\Sigma} \approx 1230$ J/mm

transfer of an electrode metal drop with the help of a high-speed video camera (minimum exposure time was 4 μ s) was used. This made it possible to establish that the plasma-arc constricts the arc of the consumable electrode and prevents splattering of the metal from the welding pool. The degree of constriction of the arc of the consumable electrode is directly proportional to the current of the plasma-arc. Moreover, the plasma-arc provides a concomitant heating of the weld metal, which increases the penetration depth of the arc of the consumable electrode, and also improves the formation of the upper bead. In addition, the plasma-arc heats the free end of the electrode wire and increases the uniformity of heating of the droplet that is formed in it, in comparison with the heating of a conventional arc of the consumable electrode (Figure 8). In turn, the arc of the consumable electrode contributes to the expansion of the plasma-arc. This expansion is directly proportional to the value of the arc current of the consumable electrode.

One of the important points of arc welding of aluminium alloys is the danger of burnout alloying elements of the wire and the base metal [15]. Thus, during pulsed MIG welding in argon at an increased current, the temperature of the electrode metal droplets grows (up to the temperatures of 2100–2600 K), which leads to an intensive burnout of magnesium in them (content of magnesium is 2–3 times decreased and more) [16]. Due to burnout magnesium, in the electrode metal droplets pores can be formed, which in the process of mass transfer get into the welding pool and can result in porosity of the welds. During Plasma-MIG welding, such burnout of alloying elements may be to some extent associated with the mutual influence of arcs.

This assumption was tested as follows. To obtain the investigated droplets, an instantaneous stop

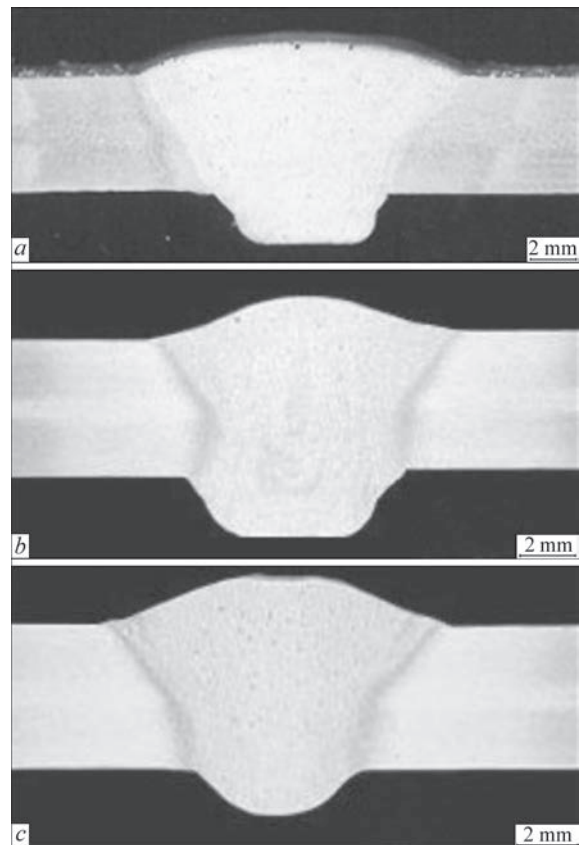


Fig re 7 Cross-sections of butt joints of 1561 alloy ($\delta = 5$ mm): *a* — MIG welding: $V = 10$ mm/s, $I_{\text{MIG}} = 253$ A, $U_{\text{MIG}} = 26$ V, $E_{\text{MIG}} \approx 660$ J/mm; *b* — Plasma-MIG welding: $V = 10$ mm/s, $I_{\text{MIG}} = 165$ A, $U_{\text{MIG}} = 17.4$ V, $I_{\text{PL}} = 100$ A, $U_{\text{PL}} = 24.6$ V, $E_{\Sigma} \approx 530$ J/mm; *c* — Plasma-MIG welding: $V = 16.7$ mm/s, $I_{\text{MIG}} = 154$ A, $U_{\text{MIG}} = 18.2$ V, $I_{\text{PL}} = 178$ A, $U_{\text{PL}} = 29.2$ V, $E_{\Sigma} \approx 480$ J/mm

of welding was performed, which allowed the droplets to be completely formed at the free end of the electrode wire ER5356 with a diameter of 1.6 mm. To average the obtained results, 6–8 such drops were collected, which were separately investigated, applying the metallographic method (determination of porosity), and also after mechanical conglomeration — by the method of optical spectroscopy (determination

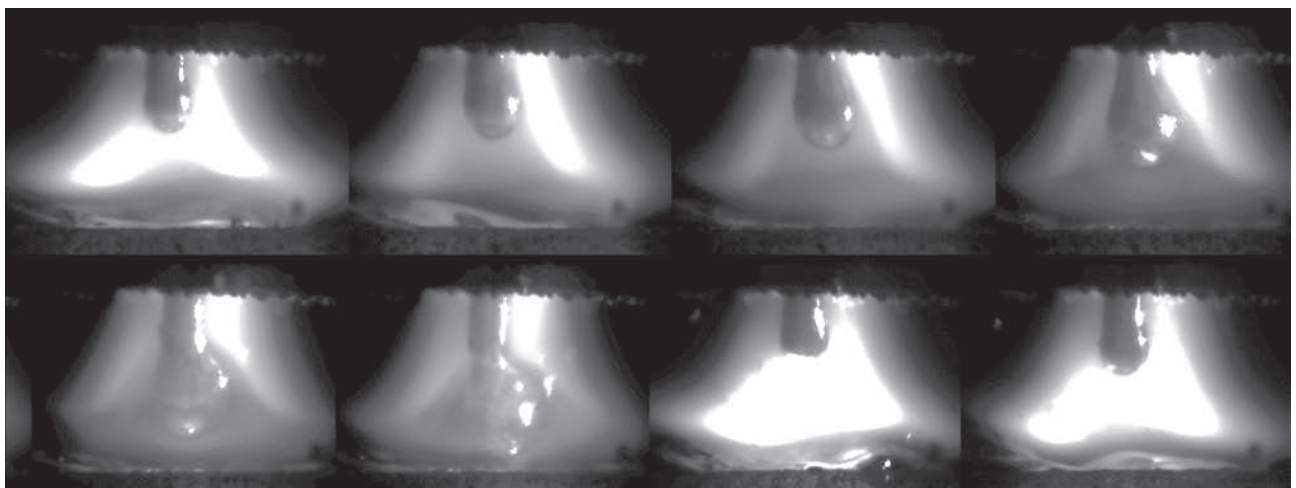


Fig re 8 Successive high-speed video image of metal drop transfer during Plasma-MIG welding at a speed of 7.4 m/min, feeding wire of 1.6 mm diameter ($I_{\text{MIG}} = 165$ A, $U_{\text{MIG}} = 100$ A, time of drop transfer is about 20 ms)

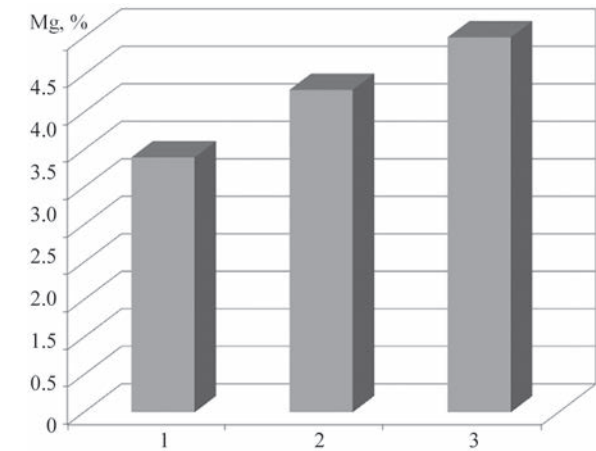


Fig re 9 Averaged content of magnesium (wt.%) in metal: 1 — droplets which were formed during MIG process; 2 — droplets which were formed during Plasma-MIG process; 3 — electrode metal (ER5356)

of magnesium content). To compare the obtained results, the droplets of electrode metal obtained both by Plasma-MIG welding ($P_{\Sigma} \approx 6600$ W) and by pulsed MIG welding ($P_{MIG} \approx 6580$ W) were investigated. It was found that the porosity of the droplets obtained by pulsed MIG welding is higher than the porosity of the droplets obtained by Plasma-MIG welding. According to the results of spectral investigations, the content of magnesium in the conglomerate droplets of the electrode metal was determined (Figure 9).

In the course of investigations, cross macro- and micro-sections of welded joints were made, their metallographic analysis was performed (ISO10042:2018), and mechanical tests on static tension were performed (ISO 4136:2012). Also, the residual stress-strain state (SSS) of the welded specimens was determined [17].

The strength values of the specimens of welded joints during static tensile tests were determined by averaging the data obtained on three specimens with a removed root bead and on three specimens with a removed root bead and an upper weld reinforcement for the cases of pulsed MIG and Plasma-MIG welding. For the base metal, the data were averaged on two specimens of each of the alloys. As is seen from Table 4, the strength of the joints produced by Plasma-MIG welding is 80–90 % of the strength of the base metal, while the strength of the joints produced by pulsed MIG welding is 75–80 % of the strength of the base metal.

SSS of the specimens with the sizes of 320×205×5 mm of 1561 alloy with a longitudinal butt weld produced by pulsed MIG and Plasma-MIG welding were measured by the method described in [17]. The values of longitudinal f_1-f_3 and transverse $\Delta_1-\Delta_2$ deflections (respectively, at the beginning and at the end of the joint) were measured along the axes of the specimens. To provide comparability of the results, the modes were selected having similar values of input energy ($E \approx 630$ J/mm). Welding modes and geometric characteristics of the investigated specimens are presented in Table 5, and their cross-sections are similar to those shown in Figure 7, *a, b*.

Measurements of the component σ_x of the flat stress state were performed in three transverse weld cross-sections S_1-S_3 on the facial side of the plate (from the left edge $S_1 = 166$, $S_2 = 148$, $S_3 = 156$ mm), and in one weld transverse cross-section (from the same edge $S_5 = 168$ mm) — on the back side. Measurements of the longitudinal component σ_x of the flat stress state were performed along the axis along

Tb le 4 Values of strength σ_t at static tension of joints of 1561 and 5083 alloys ($\delta = 5.0$ mm), welded at a speed of 10 mm/s

Welding process/alloy	σ_t , MPa			
	specimens with removed root bead		specimens with removed root and upper beads	
	On separate specimens	Averaged values	On separate specimens	Averaged values
Pulsed-MIG welding/1561	330	335	290	286
	334		283	
	340		284	
Plasma-MIG welding/1561	348	345	308	306
	345		307	
	342		302	
Base metal/1561	—	—	380	377
			374	
Pulsed-MIG welding/5083	282	287	257	254
	292		252	
	287		254	
Plasma-MIG welding/ 5083	305	302	280	286
	303		285	
	299		292	
Base metal/5083	—	—	315	320
			325	

Table 5 Modes of pulsed MIG and Plasma-MIG welding at a speed of 10 mm/s and values of deflections of welded plates of 1561 alloy ($\delta = 5.0$ mm) (electrode wire ER5356 with a diameter of 1.6 mm)

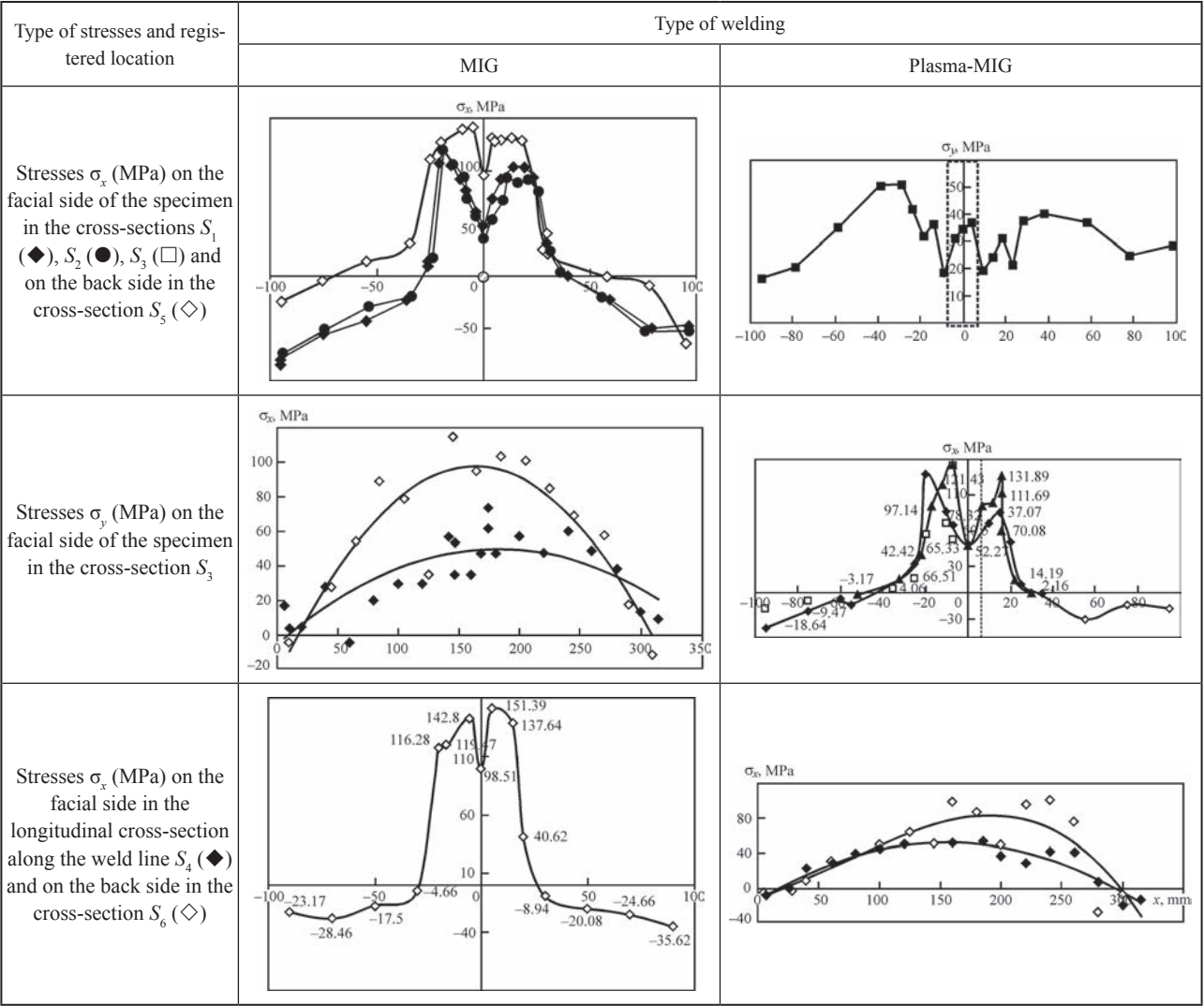
Type of welding											
MIG					Plasma-MIG						
I_{MIG}, A	U_{MIG}, V	$E_{MIG}, J/mm$	$f_1/f_2/f_3, mm$	Δ_1/Δ_2	I_{MIG}, A	U_{MIG}, V	I_{PL}, A	U_{PL}, V	$E_{\Sigma}, J/mm$	$f_1/f_2/f_3, mm$	Δ_1/Δ_2
240	26.5	636	1.0/1.5/1.2	1.5/1.5	150	25.5	100	24.6	629	-0.3/-0.5/-0.4	-0.5/-0.5

the welds: from the facial side in the cross-section S_4 , on the back side — in the cross-section S_6 of the weld. Duplication of σ_x measurements on the facial and back side of the plate were performed to provide reliability of the results. The values of the transverse component σ_y were recorded only on the facial side in the cross-section S_3 .

Analysis of the specimen produced by pulsed MIG welding (Table 5, Figure 6, *a*) showed the presence of longitudinal deflections f_1 – f_3 in the range of values of 1.0–1.5 mm, directed away from the facial surface. The values of the transverse deflections Δ_1 – Δ_2 are stable along the length of the

welded joint and are 1.5 mm. The peculiarities of these changes in the shape of the specimen are determined by the shape of the weld penetration (Figure 6, *a*), which is characterized by the discrepancy between the line of applying shrinkage shortening and the neutral cross-sectional axis. The result of this discrepancy is the appearance of a bending moment that causes deformation of the plate in the longitudinal direction. The stability of the values Δ along the length of the plate is associated with its geometric characteristics that provide a uniform heat removal from the surface during the welding thermodeformational cycle.

Table 6 Distribution of residual welding stresses on the facial and back sides of the plates 1561 ($\delta = 5.0$ mm), welded by pulsed MIG and Plasma-MIG methods



In the case of pulsed MIG welding in the center of the weld on the facial and back surfaces of the plate there is a local reduction in tensile stresses σ_x to +45–+50 and 100 MPa, respectively (Table 6, MIG). The peak values σ_x on the facial and back surfaces of the plate take place in the fusion zone and reach 100 and 140 MPa, respectively. The reactive compressive stresses σ_x on the facial and back surfaces reach the maximum values on the longitudinal edges of the plate –50– –80 and –25– –60 MPa, respectively. Such a form of the diagram of compressive stresses σ_x is associated with a small width of the plate, at which the stresses in the cross-section do not reach zero values. When comparing the diagrams σ_x on both sides of the plate, it can be seen that there is a significant bending component of stresses, which confirms the obtained shape of the specimen deformation.

Estimation of the transverse component of tensile stresses σ_y showed that its level is much lower than the level of stresses σ_x and does not exceed 40–50 MPa, and the sign of stresses is not changed along the measured cross-section (Table 6, MIG). Moreover, there is a local decrease in σ_y on the fusion line, and the peak values of stresses correspond to the zones of cross-section at a distance of 30–40 mm from the center of the weld.

The distribution of residual longitudinal stresses in the welded plate along the weld line confirms the results obtained for the transverse cross-section S_1 (Table 6, MIG). The diagrams of σ_x on both sides of the plate are characterized by a difference in peak values, which determines the significant bending component of the stress-strain state of the plate and confirms the nature of its change of shape.

Analysis of the performed Plasma-MIG welding of the specimen (Table 5, Figure 7, *b*) showed the presence of longitudinal deflections f_1 – f_3 with the values of –0.3– –0.5 mm, directed towards the facial surface. The values of transverse deflections Δ_1 – Δ_2 are stable along the length of the welded joint and are also at the level of 0.5 mm. The peculiarities of this change of shape are determined by the shape of the weld (Figure 7, *b*), which is characterized by the practical coincidence of the line of applying the shrinkage shortening and the neutral axis of the weld cross-section. Comparison of the shapes of the welds in Figure 7, *a* and Figure 7, *b* shows that the cross-sectional area of the weld in Plasma-MIG welding is by ~30 % smaller than in pulsed MIG welding. The plate produced by Plasma-MIG welding is characterized by smaller longitudinal shrinkage shortenings of the weld metal and, accordingly, a lower value of the bending moment than the specimen after pulsed MIG welding. This fact explains the decrease (up to three times) in

the value of deformation in the longitudinal direction of the plate produced by Plasma-MIG welding. Moreover, the stability and low values associated with the shape of the weld Δ is characterized by a more uniform (as compared to pulsed MIG welding) penetration through the thickness of the plate, as well as geometric characteristics of the specimen, which provide a stable heat removal from the surfaces during the welding thermodeformational cycle.

The distribution of residual longitudinal stresses σ_x in the transverse cross-sections of the welded plate after Plasma-MIG welding is presented in Table 6 (Plasma-MIG). In the center of the weld on the facial and back surfaces of the plate there is a local decrease in tensile stresses up to 45–50 and 100 MPa, respectively. The peak values σ_x on the facial and back surfaces take are located in the fusion zone and reach 140 and 150 MPa, respectively. Reactive compressive stresses σ_x on the facial and back surfaces reach maximum values of –20– –40 MPa on the longitudinal edges of the plate. This shape of the diagram σ_x like in the case of pulsed MIG welding, is associated with a small width of the plate, at which the compressive stresses in the transverse cross-section do not reach zero values. When comparing the diagrams σ_x on both sides of the plate, it can be seen that, in contrast to pulsed MIG welding, the bending stress component in the reactive zone of the diagram is insignificant, which determines a lower value of the specimen deformation.

The distribution of residual longitudinal stresses σ_x in the welded plate along the weld line confirms the results obtained for the transverse cross-section S_1 (Table 6, Plasma-MIG). The diagrams σ_x on both sides of the plate produced by Plasma-MIG welding are characterized by a smaller difference in peak values than in pulsed MIG welding, which determines the bending component of the stress-strain state of the plate and confirms the characteristics of its change of shape (Table 5).

In the course of the carried out work, a number of technological experiments with Plasma-MIG welding was performed, which showed that with an increase in the thickness of butt-welded plates, the efficiency of using this method increases. This is associated with the lack of need to perform preparation of edges to be joined during welding plates with a thickness of $\delta \leq 8$ mm and a small angle (15°) of the development for $\delta = 10$ mm, as well as lower electrode wire consumption as compared to MIG welding. If during welding of plates with a thickness of $\delta = 5$ mm, this reduction in wire consumption is 10–15 %, then at $\delta = 8$ mm it is 20–25 %, and at $\delta = 10$ mm it is up to 30 %, which is predetermined first of all by eliminating or minimizing preparation of edges.

Analysis of the parameters of pulsed MIG welding and hybrid Plasma-MIG welding of plates from the considered aluminium alloys, as well as sizes of the produced welds, showed that the use of Plasma-MIG welding allows reducing the weld width by 20–25 %. Moreover, the amount of input energy is reduced to 25 %, which has a positive effect on strength values of the welded joint.

The mutual influence of the plasma-arc and the arc of the consumable electrode during Plasma-MIG welding is mainly expressed in the fact that the former compresses the latter, preventing spattering of the electrode metal and providing a concomitant heating of the welded edges. This allows the constricted arc of the consumable electrode to weld a much greater thickness of the metal than a traditional open arc. In addition, the plasma-arc helps to eliminate undercuts and create a smoother transition from the upper bead to the base metal. An increase in voltage on the arc of the nonconsumable electrode predicted in [12] with an increase in the consumption of plasma-forming gas (from 5 to 25 l/min) was confirmed in practice and amounted to about 1–2 V, which is not a quite significant index, but in general has a positive effect on weld formation.

The study of electrode metal droplets formed during Plasma-MIG welding showed an improvement in the results as compared to traditional MIG welding. It can be assumed that a decrease in the total volume of voids (porosity) in the droplets obtained during Plasma-MIG welding is caused by reducing the diameter of the arc column of the consumable electrode, which occurs under the influence of the plasma-arc, as well as improving the conditions of arc breakdown in the area of droplets transfer. The latter, unlike the process of a pulsed MIG welding, allows the active spot of the arc to be more uniformly distributed along the perimeter of the droplet under the conditions of a lower heat input. All these factors promote the reduction of boiling of the liquid drop, evolution of hydrogen and reducing the evaporation of easily boiling magnesium. As a result, the content of magnesium is increased by 15–25 %, growing from 60–70 % in the MIG process to 80–85 % in the Plasma-MIG process.

When analyzing the residual stress state of the plates welded by pulsed MIG and Plasma-MIG methods, it is possible to note some discrepancy between the level of tensile stresses and the values of deflections. Thus, the peak values of tensile stresses σ_x for these welding methods, in contrast to the values of deflections, are quite close, as well as the values of the bending component of stresses in the active zone (in the center of the weld). This fact can be explained by a low longitudinal rigidity of the studied welded plates,

as well as by the peculiarities of stress-strain states, which are set by pulsed MIG and Plasma-MIG welding. The diagrams σ_x in the reactive stress zone go to the free longitudinal edges. The stresses at the edges of the plate during Plasma-MIG welding are significantly lower than during pulsed MIG welding, which reduces the longitudinal deflections and, accordingly, increases the level of tensile stresses σ_x . Thus, the level of stresses σ_x in the bent plate after pulsed MIG welding can be compared with the level σ_x in a flat plate after Plasma-MIG welding. These observations to some extent coincide with the conclusions given in [18, 19]. It can be concluded that when comparing the stress states of the plates with equal values of deflections made by Plasma-MIG and pulsed MIG welding, the values σ_x in the latter will be higher.

Conclusions

1. To improve the mechanical properties and reduce the values of stress-strain state of welded joints of alloyed aluminium alloys, technological methods of hybrid Plasma-MIG welding were proposed, which as compared to the traditional MIG process allow reducing the electrode wire consumption by 10–30 %, input energy by up to 25 %, residual deformations by 2–3 times, residual stresses by ~ 20 % according to the absolute value and reducing the burnout of such alloying element as Mg by 15–20 %.

2. It was established that a constricted plasma-arc of reverse polarity, which has a power exceeded by 20–30 %, reduces the size of the arc of the consumable electrode, deepens it into the weld metal, allows obtaining a vapour-gas channel of the specimen without a keyhole formation, improves weld formation and reduces the tendency to formation of inner pores and lacks of fusion.

3. It was established that during hybrid Plasma-MIG welding of aluminium 1561 and 5083 alloys of up to 10 mm thickness at the speeds of 30–60 m/h the integrated input energy is $E_{\Sigma} = 500\text{--}1000$ J/mm, which has a positive effect on the composition and structure of the weld, providing the strength of the joints at the level of 80–90 % of the base metal, unlike the strength of 75–80 % during pulsed MIG welding.

The work was performed within the framework of the following projects:

- No.2019A050508006 «Investigation of the stress-strain state of symmetric butt welds in automatic hybrid welding «Plasma-MIG»;

- No.2018GDASCX-0803 «Research and development of laser and plasma technologies for hybrid welding and cutting», Guangzhou, China;

• No.2017GDASCX-0411 «Capacity-Building of Innovation-Driven Development for Special Fund Projects», Guangdong Academy of Sciences (China);

• No.2018A050506058 «Research and application of hybrid laser and arc welding technology with high power on high-strength steel for shipbuilding», Guangzhou, China.

1. Korzhyk, V., Khaskin, V., Perepychay, A. et al. (2020) Forecasting the results of hybrid laser-plasma cutting of carbon steel. *Eastern-European J. of Enterprise Technologies*, 1/2(104), 6–15.
2. Adrianus Christinus Henricus Jozef Liei'kens, Wilhelmus Gerardus Essers (1971) *Method of and device for plasma-arc welding*. U.S. Philips Corporation. Pat. 3,612,807 US, Int. Cl. B23k9/00.
3. Ton, H. (1975) Physical properties of the plasma-MIG welding arc. *J. of Physics D: Applied Physics*, 8, 922–933.
4. Matthes, K.-J., Kusch, M. (2000) *Plasma-MIG-Schweißen. Praktike*, 5, 182–188.
5. (2007) Hybrid welding: An alternative to SAW. *Welding J.*, 86, 42–45.
6. Shchitsyn, Yu.D., Tytkin, Yu.M. (1986) Consumable electrode plasma welding of aluminium alloys. *Svaroch. Proizvodstvo*, 5, 1–2 [in Russian].
7. Shchitsyn, Yu.D., Shchitsyn, V.Yu., Herold, H. et al. (2003) Plasma welding of aluminium alloys. *Ibid.*, 5, 36–42 [in Russian].
8. Bai, Yan, Gao, Hong-Ming, Qiu, Ling (2010) Droplet transition for plasma-MIG welding on aluminium alloys. *Transact. Nonferrous Met. Soc. China*, 20, 2234–2239.
9. Tiago Vieira da Cunha, Jair Carlos Dutra (2007) Processo Plasma-MIG — Contribuição do Arco Plasma na Capacidade de Fusão do Arame. *Soldagem Insp. São Paulo*, 12(2), 89–96.
10. Grinyuk, A.A., Korzhik, V.N., Shevchenko, V.E. et al. (2016) Hybrid technologies of welding aluminium alloys based on consumable electrode arc and constricted arc. *The Paton Welding J.*, 5, 98–103.
11. Hee-Keun, Lee, Kwang-San, Chun, Sang-Hyeon, Park, Chung-Yun, Kang (2015) Control of surface defects on plasma-MIG hybrid welds in cryogenic aluminium alloys. *Int. J. Nav. Archit. Ocean Eng.*, 7, 770–783.
12. Sydorets, V., Korzhyk, V., Khaskin, V. et al. (2017) On the thermal and electrical characteristics of the hybrid plasma-MIG welding process. *Mat. Sci. Forum*, 860, 63–71.
13. Goldak, J.A., Akhlaghi, M. (2005) *Computational welding mechanics*. O., USA.
14. Bofang, Zhu. (2018) *The Finite Element Method: Fundamentals and Applications in Civil, Hydraulic, Mechanical and Aeronautical Engineering*. John Wiley & Sons Singapore Pte. Ltd.
15. Khaskin, V.Yu., Korzhyk, V.M., Peleshenko, S.Y., Wu, Boyi (2015) Evaporation of alloying elements in the material to be welded using laser radiation. *Pervyi Nezavisimiy Nauchny Vestnik*, 3, 108–114.
16. Wang, J., Nishimura, H., Katayama, S., Mizutani, M. (2011) Evaporation phenomena of magnesium from droplet at welding wire tip in pulsed MIG arc welding of aluminium alloys. *Sci. Technol. Weld. Join.*, 16, 418–425.
17. Lobanov, L.M., Pivtorak, V.A., Savitsky, V.V., Tkachuk, G.I. (2006) Procedure for determination of residual stresses in welded joints and structural elements using electron speckle-interferometry. *The Paton Welding J.*, 1, 24–29.
18. Korzhik, V.N., Pashchin, N.A., Mikhoduj, O.L. et al. (2017) Comparative evaluation of methods of arc and hybrid plasma-arc welding of aluminium alloy 1561 using consumable electrode. *Ibid.*, 4, 32–37.
19. Korzhyk, V.N., Kvasnytskyi, V.V., Khaskin, V.Yu. (2017) Influence of rigid restraint on formation of residual stress-strain state of plate butt joints from 1561 alloy in MIG, PAW and hybrid PAW-MIG welding. *American Scientific J.*, 17(1), 14–29.

Received 11.06.2020

XIX INTERNATIONAL INDUSTRIAL FORUM - 2020
INTERNATIONAL TRADE FAIRS

November 24-27

ORGANIZER:
International Exhibition Centre

General Information Partner:
Ukrainian Exhibition Centre

Exclusive Media Partner:
Ukrainian Exhibition Centre

Technical Partner:
RusExpoMedia

International Exhibition Centre
15 Brovarskyi Ave., Kyiv, Ukraine
"Livoberezhna" underground station
☎ +38 044 201 11 55, 201 11 56, 201 11 58
e-mail: alex@iec-expo.com.ua
www.iec-expo.com.ua
www.tech-expo.com.ua

XII International Trade Fair
KYIV TECHNICAL FAIRS

INTERNATIONAL EXHIBITION CENTRE
15 Brovarskyi Ave., Kyiv, Ukraine
☎ +38 044 201 11 55, 201 11 56, 201 11 58
e-mail: alex@iec-expo.com.ua
www.iec-expo.com.ua
www.tech-expo.com.ua

November 24–27' 2020

General Information Partner:
Ukrainian Exhibition Centre

Exclusive Media Partner:
Ukrainian Exhibition Centre

Technical Partner:
RusExpoMedia

wire
Düsseldorf

join the best: 07 - 11 December 2020

Düsseldorf, Germany

EFFECT OF HEAT TREATMENT ON THE STRUCTURE AND MECHANICAL PROPERTIES OF SHEET ALUMINIUM ALLOY V1341 AND ITS WELDED JOINTS PRODUCED BY TIG WELDING

T.M. Labur, M.R. Yavorska and V.A. Koval

E.O. Paton Electric Welding Institute of the NAS of Ukraine

11 Kazymyr Malevych Str., 03150, Kyiv, Ukraine. E-mail: office@paton.kiev.ua

The paper gives the results of studying the effect of various heat treatment operations on the structure and mechanical properties of the base metal and welded joints of sheet aluminium alloy of V1341 grade 1.2 mm thick, produced by manual nonconsumable electrode argon-arc welding. The dependence is established between the structural state of the metal of welded joints of this alloy on the kind of heat treatment that affects the level of strength and ductility. A significant effect of improvement of the structure and mechanical properties is achieved, when conducting complete heat treatment, which includes quenching and artificial ageing of the alloy and its joints. Compared to artificial ageing modes, this kind of heat treatment allows producing a stable metal structure, characterized by smaller dimensions of phase precipitates and inclusions that promotes increase of the strength level, under the condition of preservation of the ductility values. 8 Ref., 2 Tables, 4 Figures.

Keywords: aluminium alloy, manual nonconsumable electrode argon-arc welding, filler wire, welded joints, heat treatment, structure, mechanical properties, investigations

V1341 alloy of Al–Mg–Si–Cu–Fe alloying system belongs to the class of aluminium alloys, which are sensitive to process heating. High-temperature heating of this alloy in welding changes the base metal structure, violating its uniformity, and lowers its strength. Characteristic structural zones, such as the weld, fusion zone and HAZ, are formed. This is affected by the temperature conditions of heating in individual regions, and the features of the local structural transformations depend on the processes of diffusion of alloying elements and impurities, present in this alloy composition. The volumes of precipitation or dissolution of phases which form here, are determined by the duration of temperature gradient staying in the base metal regions relative to the weld axis, i.e. welding speed. The operation of the joint heat treatment is conducted to improve their structure and properties [1–3]. This is due to the need to ensure in manufacture of complex-shaped stamped elements the appropriate level of mechanical properties of aviation parts and components — suspended tanks, containers and other products. Such blanks are joined predominantly by manual argon-arc welding. It should be noted that the kind of heat treatment is selected, depending on welded structure purpose, as well as operating requirements to the products, exposed to complex conditions of alternating loads in service [4].

Heat treatment kinds include the following operations: quenching, natural or artificial ageing. Their temperature-time modes allow regulating the structure state by reproducing the respective phase transformations and achieving certain morphology of the structural components, the dimensions and density of which promote an increase of the strength level.

The process of metal quenching (solid solution treatment) envisages appearance of an equilibrium state in the structure at a high temperature of heating ($0.85\text{--}0.90 T_m$). In this case, the alloying elements and excess phases, included into the alloy composition, dissolve completely or partially. The time of metal soaking at the appropriate temperature, together with cooling to room temperature, ensure the conditions of solid solution oversaturation by alloying elements and point defects up to the appropriate concentrations, characteristic for the selected quenching temperature [3]. Dispersed dimensions of the structural components can be fixed at abrupt cooling of the alloy from the quenching temperature. Precipitates of Guinier–Preston (GP) zones are the first to form. They are in metastable equilibrium with the solid solution that promotes improvement of the alloy mechanical properties. It is known [2] that the degree of strengthening of V1341 alloy during ageing is directly related to the volume fraction of Mg_2Si phase, which goes into the solid solution at heating.

Metal staying under atmospheric conditions after quenching («natural ageing») promotes slow development of phase transformations, realization of which in the future stabilizes the structural state and ensures a certain level of mechanical properties. The structure becomes completely stable after 10–15 days.

Maximum values of strength and yield limit characteristics of aluminium alloys are usually achieved at application of artificial ageing operation [1]. If such an operation is performed one hour after quenching, then a slight lowering of the above-mentioned strength characteristics and increase of the ductility value are observed in the metal. Increase of the time interval between performance of the operations of quenching and artificial ageing does not allow achieving the required level of alloying element concentration, and, hence, of the respective mechanical properties. Therefore, the objective of this work is determination of the effectiveness of the mentioned heat treatment operations, based on studying the structure and mechanical properties of V1341 alloy in the condition of natural ageing (T) and of its welded joints, made by manual nonconsumable electrode welding.

Investigation procedure. Sheet blanks of V1341T alloy 1.2 mm thick were treated by the traditional preparation procedure before welding. The blank end face was cleaned mechanically by a scraper to not less than 0.1 mm depth. Manual arc welding of butt welds was performed along the rolling direction of sheet semi-finished products by different polarity current of a sinusoidal shape, using Fronius Company equipment. The joint was produced using 1.2 mm filler wire of Sv1217 grade, which ensures a high coefficient of structural strength of the joints [6].

Weld quality was controlled [7] by appearance of the technological reinforcement and X-ray examination results (GOST 7512–89), obtained in RAP-150/300 unit. Weld metal density was determined in «Densitometer» instrument. Control results allowed selection of optimum welding modes, at which no coarse defects form, of the type of cracks, lacks of penetration, pores, etc. As shown by analysis of welded butt joints, the highest quality welds were produced in the following mode: $I_w = 54\text{--}56\text{ A}$, $U_a = 11.0\text{--}12.4\text{ V}$.

Heat treatment of test samples of V1341 alloy base metal and its welded joints were conducted by technology variants, the most widely accepted in production, namely, by artificial ageing in the following mode: $T = 190 \pm 5\text{ }^\circ\text{C}$ for 12 h, as well as by performance of complete heat treatment, which included the quenching operation ($T = 525 \pm 5\text{ }^\circ\text{C}$ for 30 min) with cooling in water of room temperature for fixation of dispersed dimensions of the solid solution. Further artificial ageing was performed by the above mode. Part of the joint samples was studied in as-welded state.

Quantitative assessment of the nature of the change of strength and ductility values of the base metal and

welded joints of V1341 alloy, depending on the studied heat treatment modes, were determined in an all-purpose TsD-4 machine with 2t scale by the results of mechanical standard testing under the conditions of tension. Flat samples of XIII type (GOST 6996–66) were used, in order to establish the strength values of the base metal and the joints. Welded joint samples had process reinforcement on the face surface of the butt joint and the weld root. Sample loading at testing was uniform over its entire working part, in keeping with the requirements of GOST 1497–84. Deformability of the base metal and its welded joints was analyzed, using a technological characteristic — bend angle (α), which was achieved under the conditions of three-point bending with application of loading from the weld root side after its scraping.

For optimization of the modes of welding V1341 alloy and assessment of the effect of heat treatment of its welded joints, their macrostructural features were studied on sections, cut out transversely to the weld axis, after chemical etching of the samples in the respective solution. The microstructural features of the base metal and different regions of the welds and HAZ were revealed by electrolytical polishing of the welds in the following solution: 930 ml CH_3COOH + 70 ml HClO_4 .

Investigation results. Results of studying the microstructural features of V1341 alloy base metal at different heat treatment operations are given in Figure 1. In keeping with the data of metallographic analysis, it was found that the alloy microstructure in the «quenching + artificial ageing» state consists of saturated solid solution, phase precipitates and coarse inclusions of insoluble intermetallics (Figure 1, a). In keeping with the state diagram of Al–Mg–Si–Cu–Fe system, both binary phases (Mg_2Si , FeAl_3 , Mg_5Al_8), and ternary phases — SiCuAl_2 , CuFeAl_5 , CuMnAl_2 , FeSiAl_5 , FeMg_3Si_6 , can be in equilibrium with the solid solution. After artificial ageing, an increase of the quantity of phase precipitates on the grain boundaries is observed in the structure (Figure 1, b). The extent of insoluble intermetallic phases is also increased due to their combination, that causes an increase of base metal strength level (Table 1). Metastable equilibrium relative to the solid solution results in improvement during artificial ageing of all the mechanical properties of V1341T alloy, including the ductility values. Performance of complete heat treatment which includes «quenching + artificial ageing» leads to formation of structural components with smaller geometrical dimensions (Figure 1, c). In keeping with the data of [2], presence of a small quantity of copper additives (0.3 %) in the alloy, promotes limitation of precipitates of Guinier–Preston (GP) zones in the alloy structure.

Let us consider the effect of V1341 alloy structural state after different kinds of heat treatment on the nature of the change of mechanical properties (Table 1). Analysis of the obtained results shows that the strength and yield limit of the alloy in the «quench-



Fig re 1 Microstructure ($\times 320$) of base metal of V1341 alloy in the state after quenching and natural ageing (a), after artificial ageing (b) and after complete heat treatment (quenching and artificial ageing) (c)

Tb le 1 Effect of the kinds of heat treatment on mechanical properties of base metal of V1341 alloy

State	σ_y , MPa	$\sigma_{0.2}$, MPa	δ , %	α , deg
Quenching + natural ageing	<u>250.1–250.8</u> 250.5	<u>187.0–188.41</u> 187.6	<u>18.7–19.0</u> 18.9	180
Artificial ageing	<u>333.8–337.3</u> 335.7	<u>310.1–316.4</u> 313.3	<u>8.5–10.0</u> 9.5	180
Quenching + artificial ageing	<u>320.1–332.1</u> 332.1	<u>281.8–282.2</u> 282.0	<u>10.4–11.4</u> 10.7	<u>136–180</u> 158

ing + natural ageing» state (T) are equal to 250.5 and 187.6 MPa, respectively. The relative elongation here is 18.9 %, and bend angle is 180°.

After performance of the operation of the alloy artificial ageing, an increase of the strength level and yield limit up to the values of 335.7 and 313.3 MPa is observed, but the relative elongation value decreases to 9.5 %. Deformability (bend angle) of the metal does not change (180°).

In the case of conducting the complete cycle of heat treatment (quenching + artificial ageing) a slight lowering (to 321.1 and 282.2 MPa) of the level of strength and yield is observed in the alloy. The relative elongation value is equal to 10.7 %, and the bend angle decreases to 158°. The nature of the change of base metal mechanical properties can be related to the features of decomposition of oversaturated solid solution under the certain conditions of inclusion precipitation along the grains boundaries, as well as of highly dispersed hardening of the metal, which ensure the required complex of mechanical values of this alloy [8].

Metallographic analysis of the macrostructure of V1341T alloy joints in different zones: weld, zone of its fusion with the base metal and HAZ (Figure 2) showed that the welds are characterized by high quality, as the structure in the weld bulk is uniform and consists of fine dendrites, while coarse defects are absent. In the near-weld zone in as-welded joints we can see three regions of different degree of etching that reflects the impact of the welding thermal cycle on the metal structure. After artificial ageing of welded joint samples, this zone has a lighter colour of the surface along its entire length, which is in contrast with the weld surface.

Performance of quenching and artificial ageing (complete cycle of the joint heat treatment) leads to greater colour contrast of the HAZ metal that is indicative of the change of structural component parameters (grain size, interlayers between them, phase inclusions, etc.) in these regions under the impact of process heating.

Performance of the process of arc welding of V1341 alloy changes the microstructural pattern in the joint zone, compared to base metal structure (Figure 3). The

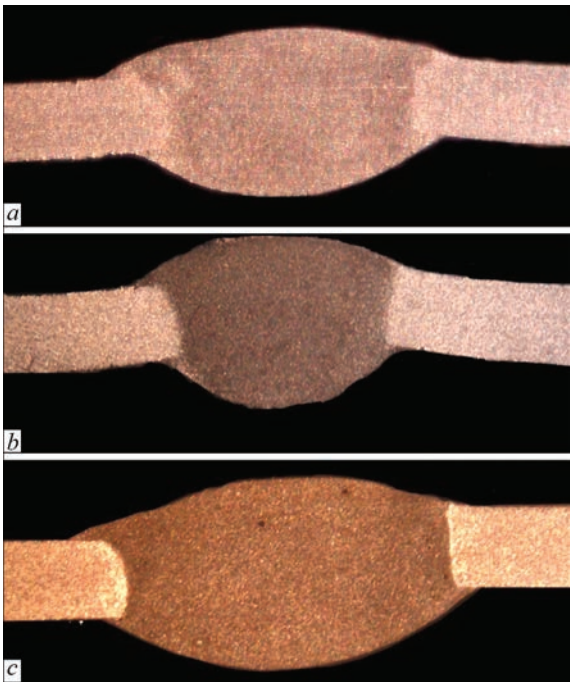


Fig re 2 Macrostructure ($\times 20$) of welded joints of V1341 alloy of Al–Mg–Cu–Si alloying system after welding (a), artificial ageing (b) and complete heat treatment cycle (c)

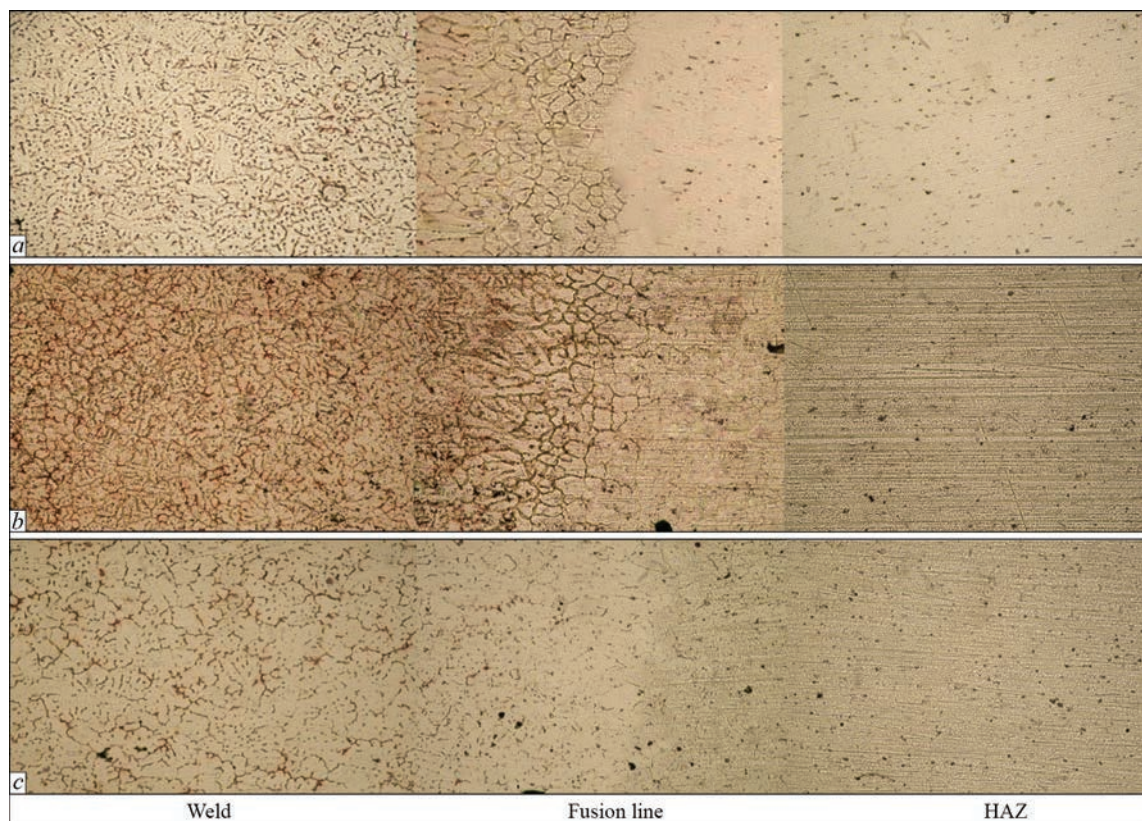


Fig re 3 Microstructure ($\times 320$) of welded joints of V1341T alloy produced by manual process after welding (a), artificial ageing (b) and complete heat treatment (c)

nature of precipitation or dissolution of phases, which form here in different base metal regions relative to weld axis, and their volumes are due to the temperature gradient in the weld, fusion zone and HAZ. Their analysis is indicative of the fact that the impact of the welding thermal cycle results in decomposition of oversaturated solid solution. It is accompanied by dissolution of the earlier formed strengthening phases, precipitation of new phases and coagulation of inclusions of insoluble intermetallic phases. Metal boundary areas are enriched in alloying elements, and the bulk is depleted in them.

Weld structure has a characteristic phase arrangement and consists of fine dendrites. No coarse defects or discontinuities were observed in the weld bulk. In keeping with the data of weld microstructure analysis, the crystallites differ by the shape and direction. They have a typical cellular-dendritic structure characteristic for the cast state of the metal (Figure 3, a). A considerable quantity of metastable phases uniformly arranged over the cross-section, is observed between the crystallites. This is due to the complex nature of alloying, i.e. presence of various main alloying elements and impurities. They differ by their size and shape. Thin eutectic interlayers form along the crystallite boundaries. Enlargement of intermetallic phases due to their combining is also observed.

Near the fusion line, where the first stage of solidification occurs, the structure is predominantly fine-crystalline. The processes of heat removal and solidification

overcooling, which proceed in the weld pool during metal cooling and its solidification, promote formation of the zone of columnar crystallites, which are oriented predominantly in the direction of the action of melting isotherm vector. Presence of partially-melted grain boundaries is observed from the base metal side.

Weld microstructure on the boundary of its fusion with the base metal, is characterized by the presence of partially-melted grain boundaries, which formed under the conditions of heating in welding. It is accompanied by thickening of the boundaries, as a result of contact melting of the grains between each other and Mg_2Si eutectic phase, which is located along the grain boundaries, under the welding conditions. Structure coarsening is observed in the HAZ metal, which is due to increase of the grain dimensions and coagulation of insoluble phase inclusions.

Decomposition of oversaturated solid solution takes place in the fusion zone from the base metal side under the conditions of welding thermal cycle. It is accompanied by the processes of simultaneous precipitation and dissolution of earlier formed strengthening phases, as well as coagulation of insoluble intermetallic phases, which penetrate into the alloy structure at the stage of metallurgical production [3]. Interaction of near-boundary intermetallic inclusions with the solid solution leads to appearance of liquid interlayers of low-melting eutectic along the grain boundaries. Structural transformations, complete or partial lower-

Table 2 Mechanical properties of welded joints of V1341T alloy ($\delta = 1.2$ mm) after manual argon-arc welding and different kinds of heat treatment

Welded joint state after performance of	σ_y , MPa	$\sigma_{0.2}$, MPa	δ , %	α , deg	$K = \sigma_y^{33} / \sigma_y^{BM}$
Welding	<u>208.2–208.0</u> 208.7	<u>131.6–147.8</u> 147.5	<u>4.6–5.4</u> 5.1	<u>45–66</u> 56	0.83
Artificial ageing	<u>248.4–274.0</u> 257.6	<u>198.3–231.7</u> 215.5	<u>1.4–2.8</u> 1.9	<u>20–46</u> 30	0.77
Quenching and artificial ageing	<u>297.0–301.9</u> 299.6	<u>213.8–265.5</u> 241.5	<u>6.4–7.1</u> 6.9	<u>20–50</u> 32	0.93

ing of the effect of strengthening after natural ageing, local annealing and hardening of individual regions of this joint zone take place in the HAZ under the impact of the welding thermal cycle.

After artificial ageing of welded joint samples, a change is observed in the weld structure, which is the result of decomposition of the solid solution, precipitation of additional phases and their dispersion hardening (Figure 3, *b*). It leads to increase of phase density, and their volume fraction that is accompanied by thickening of the boundaries of weld crystallites and grains in the HAZ, as a result of their possible contact melting between each other and Mg_2Si eutectic phase, as it is located near their boundaries. Coarsening of the grains and coagulation of insoluble phase inclusions occur in the HAZ metal that is characteristic for all the aluminium alloys after arc welding [5].

Conducting a complete heat treatment cycle leads to formation of a more uniform nature of distribution of phase precipitates from the matrix (Figure 3, *c*). Here, the shape and the dimensions of the phases change both near the weld crystallites and base metal grains. They are more dispersed. This is due to the fast fixing of the structural components after quenching, the shape and dispersed sizes of which are preserved at further artificial ageing. In addition, a thickening of the boundaries of the crystallites and grains is observed, in particular, in the zone of weld fusion with the base metal, but the thickness dimensions are smaller than in the structure after artificial ageing.

The results of testing samples of welded joints from V1341T alloy under the conditions of uniaxial tension and three-point bending show that the level of mechanical properties directly depends on the arrangement of the structural components, as a result of structural transformations, running in the metal during welding and heat treatment (Table 2).

Compared to base metal values in a similar heat-treated state, the level of mechanical characteristics of the joints is somewhat lower. Their strength factor in as-welded samples, which were tested with a bead and technological reinforcement of the weld, amounts to 0.83 % on average, relative to base metal strength level, and is equal to 208.7 MPa on average. The yield limit value is on the level of 147.5 MPa. Ductility values are as follows: relative elongation 5.1 %, bend angle — 56°. Failure of samples of such

joints occurs in the section of base metal HAZ at the distance of 4–5 mm from the fusion line (Figure 4, *a*).

Increase of the values of strength and yield level up to 257.6 and 215.5 MPa, respectively, is observed in the welded joints after artificial ageing. The strength factor of the joints can reach 0.77 on average. Relative elongation value is equal to 1.9 % that is almost 2–3 times less than that of the base metal in a similar state. The value of bend angle of the joints is 30° on average. Fracture of such welded joints occurs both along the line of fusion of the weld with the base metal, and in the HAZ at 5 mm distance from the boundary (Figure 4, *b*). The first can be caused by metal overheating during performance of manual welding; the second — by a considerable quantity of phases, which precipitate from the solid solution under the conditions of artificial ageing, as well as coagulation of coarse particles of the intermetallic phases. Together they form in the zone of weld fusion with the base metal a continuous net around the grains (Figure 3, *b*). Its presence causes an abrupt lowering of the ductility values (Table 2). The noted fact should be taken into account during selection of the operations of heat treatment of welded joints from V1341T alloy.

After the complete heat treatment cycle (quenching + artificial ageing) the strength of welded joints is equal to almost 300 MPa, and the yield limit is 265.5 MPa. The strength factor of such joints is equal to 0.93 of that of the base metal. The value of relative elongation, although it is two times smaller than in the base metal, still remains on the level of 6.9 %. Bend angle is 32°. The nature of fracture of the samples is the same as in the previous case, i.e. nonuniform (Figure 4, *c*). Some samples break along the fusion line, and others — in the regions of base metal in the HAZ, where annealing of welded joint metal occurs during the thermal cycle of welding. The established fact can also be related both to base metal quality, and to the stability of manual welding performance.

Thus, different kinds of heat treatment ambiguously affect the state of the metal of V1341T alloy welded joints. The greatest effect is produced by the heat treatment technology, which includes quenching and artificial ageing of the alloy joints. Its mode allows obtaining the structure of the metal, with which the strength level is increased compared to modes of only the artificial ageing. This is due to the dimensions of phase precipitates and their density in the metal that

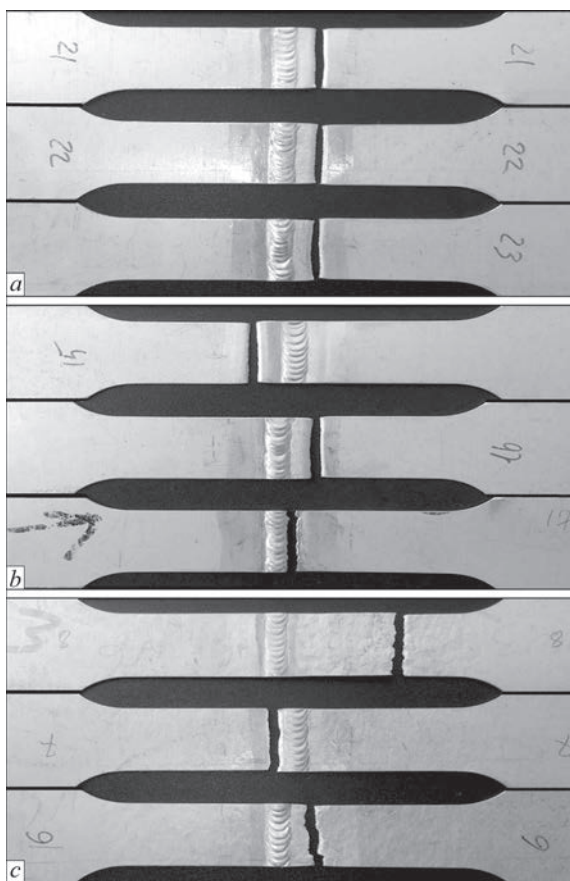


Fig re 4 Nature of fracture of welded joints of V1341T alloy, produced by manual nonconsumable electrode argon-arc welding, depending on the kind of heat treatment: *a* — after welding; *b* — after artificial ageing; *c* — after complete heat treatment cycle

affects the stress level in the structure. Presence of finer phases, with a uniform nature of arrangement in the bulk near the weld crystallites and base metal grains, promotes uniform deformation and does not cause stress localization on their boundaries. Thus, the complete heat treatment cycle is an effective means of improvement of the structure and mechanical properties of V1341T alloy and its welded joints, including the ductility values: relative elongation and bend angle.

Conclusions

1. Results of investigation of the structure of V1341 alloy 1.2 mm thick show that the metal sensitivity to the kinds of heat treatment determines the level of its mechanical properties.

2. It is found that sound weld formation occurs at application of filler wire of Sv1217 grade during manual nonconsumable electrode welding of V1341T alloy. The level of their strength and yield values after welding is equal to 208.7 and 147.5 MPa, respectively. Relative elongation value is 5.1 %. The strength factor is equal to 0.83 relative to base metal values in the state of quenching and natural ageing.

3. Performance of artificial ageing of samples of V1341T alloy welded joints increases the level of strength and yield limit of the joints by 60–70 MPa on average, and they are equal to 257.6 and 215.5 MPa, respectively. Relative elongation value is 1.9 % that is almost 5 times smaller than that of the base metal in a similar state. The value of bend angle of the welded joints is equal to 30° on average. This is related to a large quantity of phases, precipitating along the grain boundaries under the artificial ageing conditions, as well as enlargement (coagulation) of coarse particles of insoluble intermetallic phases. Together, they form a continuous net around the grains and lower the ductility values. Fracture of welded joint samples occurs both on the line of weld fusion with the base metal, and in the HAZ at 5 mm distance from it.

4. Performance of a complete cycle of heat treatment of V1341T alloy welded joints promotes an increase of the strength level by 80–90 MPa, compared to as-welded state. It is on average equal to 299.6 MPa. The yield limit value is 241.5 MPa. Values of ductility characteristics (relative elongation and bend angle) are equal to 6.9 % and 32 %, respectively.

5. It is found that in order to ensure the appropriate level of mechanical properties of welded joints of V1341T alloy in structures under production conditions it is rational to apply the complete cycle of heat treatment, which includes quenching and artificial aging. Its modes do not lead to the conditions, under which coarse changes of the structure and embrittlement of the metal take place, particularly in the zone of the weld fusion with the base metal.

1. Ishchenko, A.Ya., Labur, T.M. (2013) *Welding of modern structures from aluminium alloys*. Kiev, Naukova Dumka [in Russian].
2. Klochkov, G.G., Grushko, O.E., Popov, V.I. et al. (2001) Structure, technological properties and weldability of V1341T alloy sheets of Al–Mg–Cu system. *Aviats. Materialy i Tekhnologii*, **1**, 3–8 [in Russian].
3. Fridlyander, I.N., Grushko, O.E., Sheveleva, L.M. (2004) Properties of sheets from advanced alloy V1341. *Metallovedenie i Termich. Obrab. Metallov*, **2**, 3–6 [in Russian].
4. Krivov, G.A. (1997) *Technology of aircraft construction*. Kiev, KVITs [in Russian].
5. Rabkin, D.M., Lozovskaya, A.V., Sklabinskaya, I.E. (1992) *Metals science of welding of aluminium and its alloys*. Kiev, Naukova Dumka [in Russian].
6. Koval, V.A., Labur, T.M., Yavorska, T.R. (2020) Properties of joints of V1341T grade alloy under the conditions of TIG welding. *The Paton Welding J.*, **2**, 35–40.
7. DSTU ENISO 10042:2015 (ENISO 10042:2005, IDT; ISO 10042:2005, IDT): Welding-arc-welded joints in aluminium and its alloys. Quality levels for imperfections [in Ukrainian].
8. Shamraj, V.F., Gumennikov, A.N., Ovchinnikov, V.V. et al. (2008) Mechanical and corrosion properties of cold-rolled sheets of Al–Mn system alloy. *Metallovedenie i Termich. Obrab. Metallov*, **3**, 28–30 [in Russian].

Received 08.07.2020

COATINGS BASED ON Fe–Al INTERMETALLICS PRODUCED BY THE METHODS OF PLASMA AND SUPERSONIC PLASMA GAS-AIR SPRAYING

Yu.S. Borysov, A.L. Borysova, N.V. Vigilyanska, O.P. Gryshchenko and M.V. Kolomytsev

E.O. Paton Electric Welding Institute of the NAS of Ukraine

11 Kazymyr Malevych Str., 03150, Kyiv, Ukraine. E-mail: office@paton.kiev.ua

The results of investigations of the structure and phase composition of thermal coatings based on Fe–Al intermetallics are presented. Fe–Al intermetallics were selected as a material of protective coatings due to their high heat and corrosion resistance and cost effectiveness as compared to many modern heat-resistant materials. As spraying materials, the powders of mechanical mixtures of Fe and Al as well as powders produced by the method of mechanochemical synthesis of Fe–Al intermetallics by the treatment of mixtures of powders Fe and Al in a high-energy ball mill were used. The content of powder components corresponds to the intermetallics Fe_3Al , FeAl and Fe_2Al_3 . For spraying, the alloyed powders were also used having the composition corresponding to the intermetallic Fe_3Al . To increase the mechanical and physicochemical properties of the intermetallic, as alloying elements Ti, Mg, Cr, Zr, and La were also used. The coating was produced by the methods of plasma and supersonic plasma gas-air spraying. It was found that in plasma coatings with FeAl-powders, in addition to the initial phase (Fe_3Al , FeAl and Fe_2Al_3), Fe and Al oxides are also present, due to which microhardness of the coatings increases by about 1300 MPa relative to the initial powders. The microhardness of the plasma coating of the alloying powder Fe–TiAl, 2 times increases relatively to the initial powder due to the formation of the intermetallic phase FeTi in the coating. During spraying of mechanical mixtures, due to a low probability of contact interaction of Fe and Al particles during flight and rapid cooling of melts particles on the surface of the base, the synthesis of intermetallics does not have a time to develop and in the coatings no intermetallic phases are revealed. In the coatings produced by supersonic plasma gas-air spraying, the main phase is $\alpha\text{-Fe(Al)}$ -solid solution, which is the result of a high rate of melt hardening. 14 Ref., 4 Tables, 8 Figures.

Key words: Fe–Al intermetallic, powders, mechanochemical synthesis, mechanical mixture, plasma spraying, supersonic plasma gas-air spraying, coating, structure, microhardness

Iron aluminides are among the most widely studied intermetallics due to their cheapness, low specific weight, good wear resistance, convenience in mechanical treatment and resistance to oxidation and corrosion [1, 2]. These advantages resulted in determination of areas of their potential application, including heating elements, furnace fittings, heat exchanger pipes, sintered porous «gas–metal» filters, parts of car valve systems, components of installations operating with salt melts [3, 4]. Producing powders of Fe–Al intermetallics by using the method of mechanochemical synthesis (MChS) allows expanding the areas of practical application of these materials by applying a wide range of heat- and corrosion-resistant coatings from intermetallic Fe–Al-alloys produced by thermal spraying (TS) [5]. To provide the process of TS coatings based on Fe–Al intermetallics, MChS technologies were developed, which allow producing composition powders for this purpose Fe_xAl_y [5, 6], as well as composite powders based on Fe–Al intermetallics [7, 8]. Coatings are produced by the methods of plas-

ma [9], detonation [6, 10] and high-velocity oxy-fuel spraying [7, 8]. In the case of spraying powders of mechanical mixtures of iron and aluminium, the formation of intermetallics of the Fe–Al system occurs during heat treatment of coatings at a temperature of $\geq 650^\circ\text{C}$ [11].

The aim of the work was to compare the formation of coatings by spraying mechanical mixtures of iron and aluminium powders and Fe–Al aluminides powders produced by the MChS method. On the other hand, the structure and properties of the coatings produced in terms of their application by the methods of plasma (PS) and supersonic plasma gas-air (SPGAS) spraying were compared, which differ in the conditions of heating the sprayed particles, their acceleration and interaction with a plasma jet.

Materials and procedures for investigations. To select the compositions of coatings from FeAl-alloys, a materials science analysis of the phase equilibrium diagrams of the systems with the participation of Fe and Al was performed [12]. The analysis was made in

Yu.S. Borysov — <https://orcid.org/0000-0002-6019-8464>, A.L. Borysova — <https://orcid.org/0000-0002-7376-3370>,

N.V. Vigilyanska — <https://orcid.org/0000-0001-8576-2095>, O.P. Gryshchenko — <https://orcid.org/0000-0003-2640-8656>,

M.V. Kolomytsev — <https://orcid.org/0000-0003-0602-5615>

© Yu.S. Borysov, A.L. Borysova, N.V. Vigilyanska, O.P. Gryshchenko and M.V. Kolomytsev, 2020

Tb le 1 Characteristics of powders of Fe–Al system used for plasma and supersonic plasma gas-air spraying

Powder	Method of producing	Phase composition	Microhardness H_{μ} , MPa
86Fe + 14Al (wt.%)	Mechanical mixing	Fe, Al	Fe–1500±230; Al–330±50
Fe ₃ Al	MChS	Fe ₃ Al	3590±1010
67Fe + 33Al (wt.%)	Mechanical mixing	Fe, Al	Fe–1500±230; Al–330±50
FeAl	MChS	FeAl, FeAl ₂	2790±820
45Fe + 55Al (wt.%)	Mechanical mixing	Fe, Al	Fe–1500±230; Al–330±50
Fe ₂ Al ₅	MChS	Al, Fe, Fe ₂ Al ₅	3890±840
86Fe + 14(Al1,5Cr1Zr) (wt.%)	Mechanical mixing	Fe, solid solution of Cr and Zr in Al	Fe – 1500±230 AlCrZr – 355±50
	MChS	Solid solution of Cr and Zr in Fe ₃ Al	3840±800
86Fe + 14(Al5Mg) (wt.%)	Mechanical mixing	Fe, solid solution of Mg in Al	Fe–1500±230; AlMg–490±80
	MChS	Solid solution of Mg in Fe ₃ Al	4630±950
86Fe + 14(Al5MgLa) (wt.%)	Mechanical mixing	Fe, solid solution of Mg and La in Al	Fe–1500±230; AlMgLa–580±120
	MChS	Solid solution of Mg and La in Fe ₃ Al	5580±840
61Fe + 39(62,5Ti37,5Al) (wt.%)	Mechanical mixing	of Fe, TiAl	Fe–1500±230; TiAl–440±140
	MChS	Solid solution of Al in FeTi (Fe _{1-x} TiAl _x)	3400±1290

order to select the alloying elements that improve the properties of the intermetallics of the Fe–Al system. According to the results of this analysis, to investigate the structure, microhardness and phase composition of thermal coatings, intermetallic powders were selected (Fe₃Al, FeAl and Fe₂Al₅) and powders of Fe₃Al intermetallics, alloyed with lanthanum, magnesium, chromium, zirconium and titanium, which were produced by the method of MChS [13], as well as mechanical mixtures of powders intended to produce intermetallics of the chosen composition. As the basis to produce alloyed powders, intermetallic Fe₃Al was chosen, since at such a ratio of components it is possible to produce a single-phase product in the MChS process without additional heat treatment [14].

Mechanical mixing of powders was performed in a ball mill for 15 h, the MChS process was performed in a planetary mill «Activator 2SL» during 5 h [13]. Table 1 presents the characteristics of the produced powders, which were used for spraying. The fraction of the sprayed powders was 40–80 μm.

Plasma spraying was performed in the installation UPU-8M, supersonic plasma gas-air spraying was carried out in the installation Kyiv-S. A set of characteristics of the conditions of atmospheric plasma

spraying in the subsonic and supersonic mode of plasma jet leakage, used for coating, is the following:

- subsonic: plasma-forming gas — Ar/N₂, $T_{pl} \sim 10000$ K, $W_{pl} \sim 600$ m/s, $W_h \sim 100\text{--}130$ m/s, $\tau_h \sim 1.5$ ms;
- supersonic: plasma-forming gas-air, $T_{pl} \sim 6000$ K, $W_{pl} \sim 2500$ m/s, $W_h \sim 300\text{--}350$ m/s, $\tau_h \sim 0.5$ ms.

The operating parameters of the spraying processes are given in Table 2.

X-ray diffraction phase analysis (XRD) of the coatings was performed by using the diffractometer DRON-3 in CuK_α radiation with a graphite monochromator at a step displacement of 0.1 deg. and an exposure time at each point of 4 s, followed by a computer processing of the obtained digital data.

The microstructure of the coatings was examined in an optical microscope Neophot 32, and the microhardness of the coatings was determined in a microhardness tester PMT-3.

Results of investigations. As a result of metallographic analysis of plasma coatings (Figure 1) from a mechanical mixture of powders 86Fe + 14Al, 67Fe + 33Al, 45Fe + 55Al and from MChS-powders Fe₃Al, FeAl and Fe₂Al₅, it was found that in

Tb le 2 Parameters of PS and SPGAS processes

Method of spraying	Parameters of spraying process					Heat input	
	Arc current, A	Arc voltage, V	Consumption of plasma-forming gas, m ³ /h	Spraying distance, mm	Powder consumption, kg/h	To plasma, kW·h/m ³	To powder, kW·h/kg
PS	500	40	25	120	3	13.3	6.7
SPGAS	280	380	450	120	6	3.9	17.7

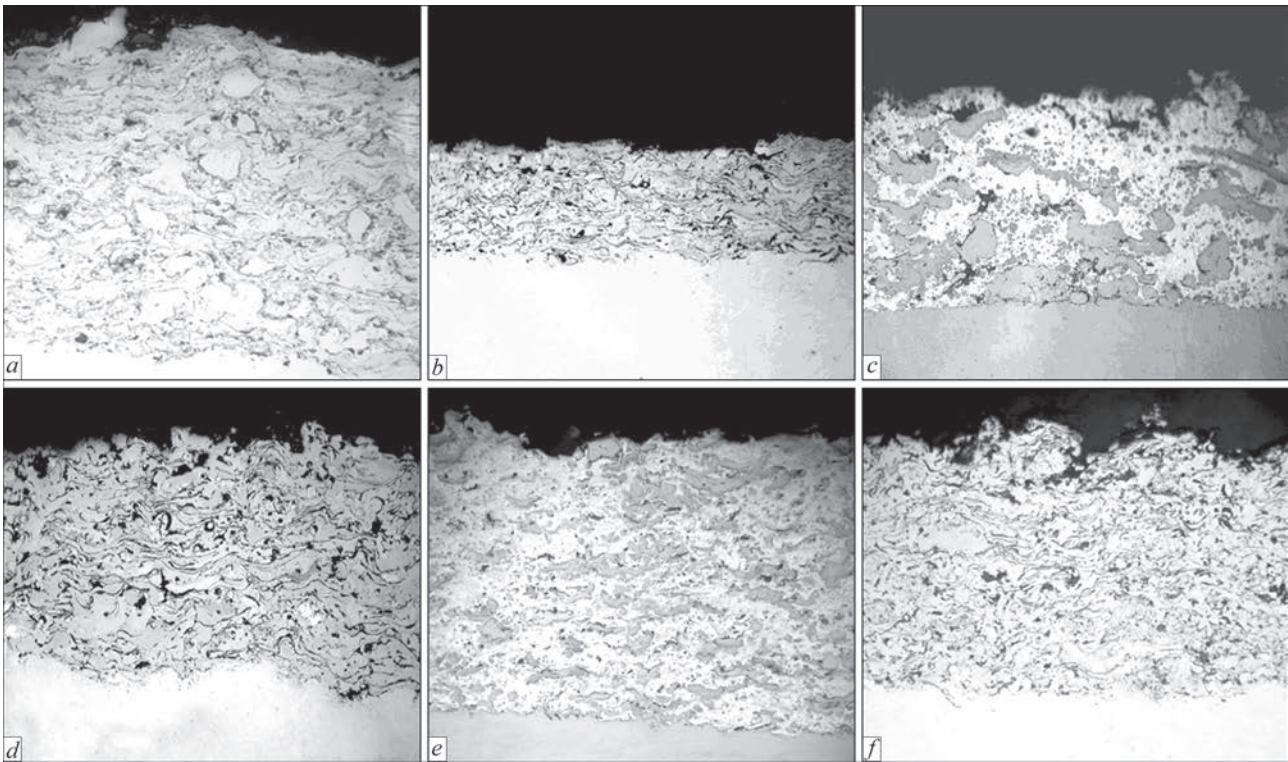


Fig re 1 Microstructure (×200) of plasma coatings: from mechanical mixtures 86Fe + 14Al (*a*), 67Fe + 33Al (*c*), 45Fe + 55Al (*e*); of Fe₃Al intermetallic powders (*b*), FeAl (*d*) and Fe₂Al₅ (*f*)

the case of spraying coatings from a mechanical mixture, the structure of the coatings is coarse-grained, in which it is easy to distinguish iron and aluminium both in the form of separate particles (Figure 1, *a*) and in the form of iron inclusions in aluminium matrix (Figure 1, *c*, *d*). When using intermetallic powders, in all cases a dense lamellar structure is formed (Figure 1, *b*, *d*, *f*).

X-ray diffraction phase analysis (Figure 2) showed that during spraying of mechanical mixtures due to

a low probability of contact interaction of iron and aluminium particles during flight and a rapid cooling of melt particles on the base surface during the formation of the coating layer, the synthesis of intermetallics does not have a time to develop in the coatings also or intermetallic phases are not detected at all (as, for example, in a mixture intended to produce Fe₃Al, Figure 1, *a*, Table 3), or they appear in the form of traces (as in the case of spraying mixtures intended to produce FeAl and Fe₂Al₅, Figure 2, *c*, *d*, Table 3), and

Tb le 3 Characteristics of PS and SPGAS-coatings from powders produced by mechanical mixing and MChS method

Powder		Coating		
Composition	Method of producing	Method of spraying	H_{μ} , MPa	XRD
86Fe + 14Al (wt.%)	Mechanical mixing	PS	Based on Fe–2800±810 Based on Al–540±150	Fe, Al, traces of Al ₂ O ₃ (Figure 2, <i>a</i>)
Fe ₃ Al	MChS	PS	3630±1240	Fe ₃ Al, FeAl, traces of Al ₂ O ₃ (Figure 2, <i>b</i>)
		SPGAS	5090±620	Solid solution of Al in Fe, FeAl, Fe _x Al ₂ O ₄ (Figure 4, <i>a</i>)
67Fe + 33Al (wt.%)	Mechanical mixing	PS	Based on Fe–2470±640 Based on Al–460±90	Fe, Al, traces of FeAl (Figure 2, <i>c</i>)
FeAl	MChS	PS	4150±900	Fe, FeAl, Fe ₃ O ₄ , Fe ₂ O ₃ , Al ₃ Fe ₅ O ₁₂ (Figure 2, <i>d</i>)
		SPGAS	4330±1040	Solid solution of Al in Fe, FeAl, FeO, Al ₂ O ₃ , Fe _x Al ₂ O ₄ (Figure 4, <i>b</i>)
45Fe + 55Al (wt.%)	Mechanical mixing	PS	Based on Fe–2450±800 Based on Al–580±100	Al, Fe, traces of FeAl (Figure 2, <i>e</i>)
Fe ₂ Al ₅	MChS	PS	5200±1250	FeAl, Fe, FeAl ₂ O ₄ , Fe ₂ Al ₅ , Al (traces) (Figure 2, <i>f</i>)
		SPGAS	5360±850	Solid solution of Al in α-Fe, FeAl, Fe ₃ Al, Fe _x Al ₂ O ₄ , Al ₂ O ₃ (Figure 4, <i>c</i>)

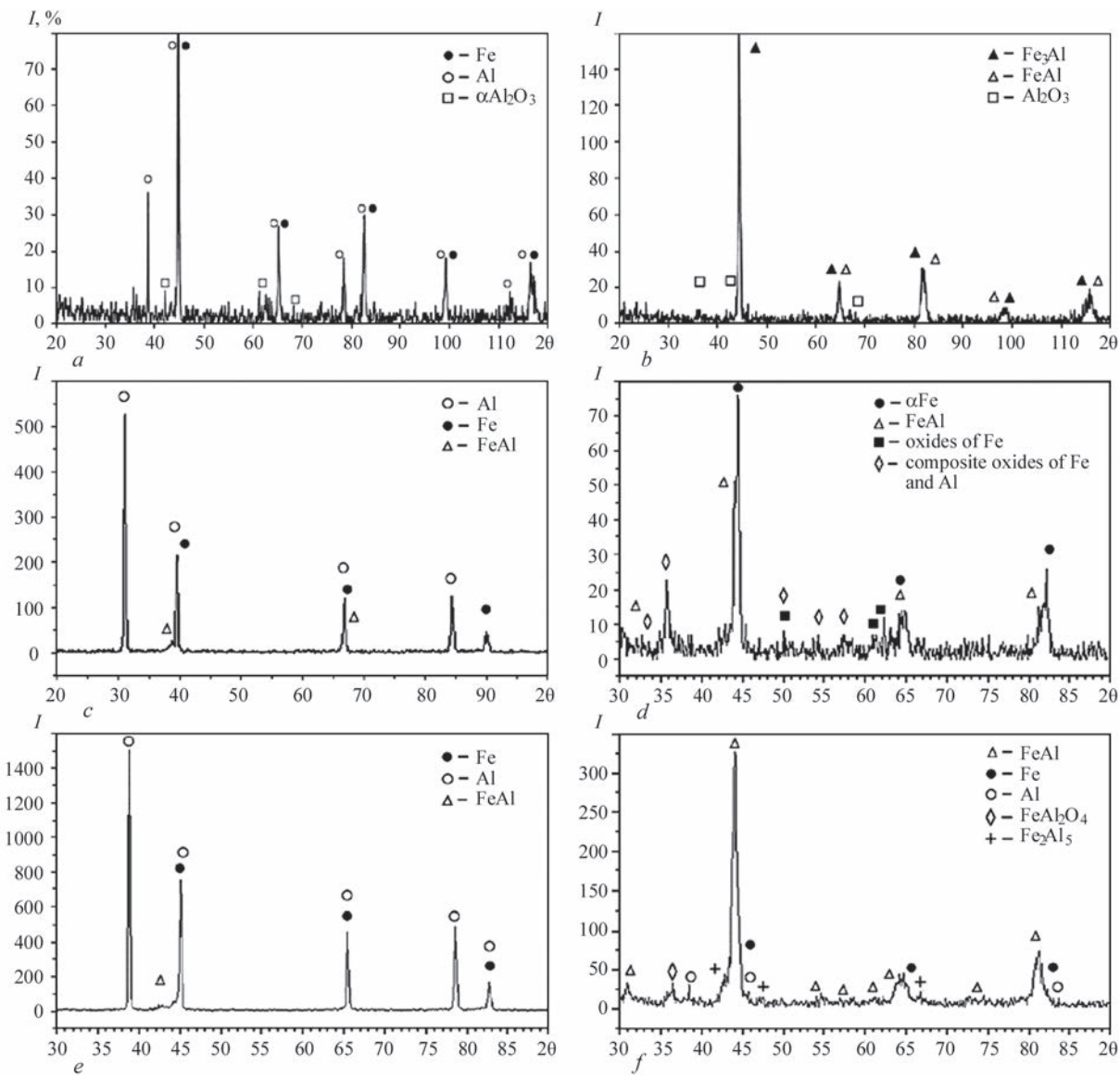


Fig re 2 X-ray patterns of plasma coatings: from mechanical mixtures 86Fe + 14Al (a), 67Fe + 33Al (c), 45Fe + 55Al (e); from intermetallic Fe₃Al powders (b), FeAl (d) and Fe₂Al₅ (f)

phases that do not meet those expected according to the calculation.

During deposition of coatings of intermetallic powders, their phase composition, as a rule, does not completely coincide with the composition of the initial powders, which is associated with the active de-

velopment of the process of particles oxidation during their flight. Oxides are present in all coatings. In the coating Fe₃Al, Al₂O₃ aluminide is present; in the FeAl coating, iron oxides Fe₃O₄, Fe₂O₃ and a composite oxide Al₃Fe₅O₁₂; in the coating Fe₂Al₅, oxide FeAl₂O₄ are present.

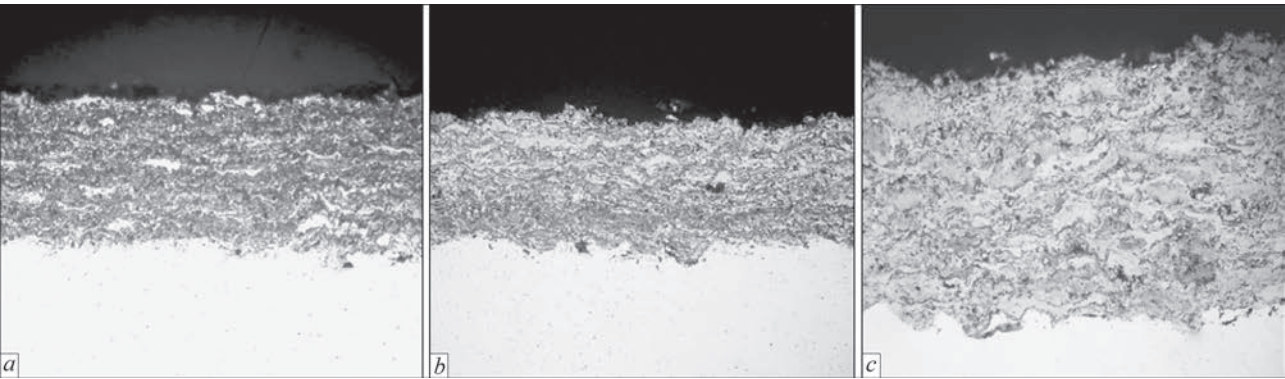


Fig re 3 Microstructure (×200) of SPGAS-coatings produced with the use of MChS powders: a — Fe₃Al; b — FeAl; c — Fe₂Al₅

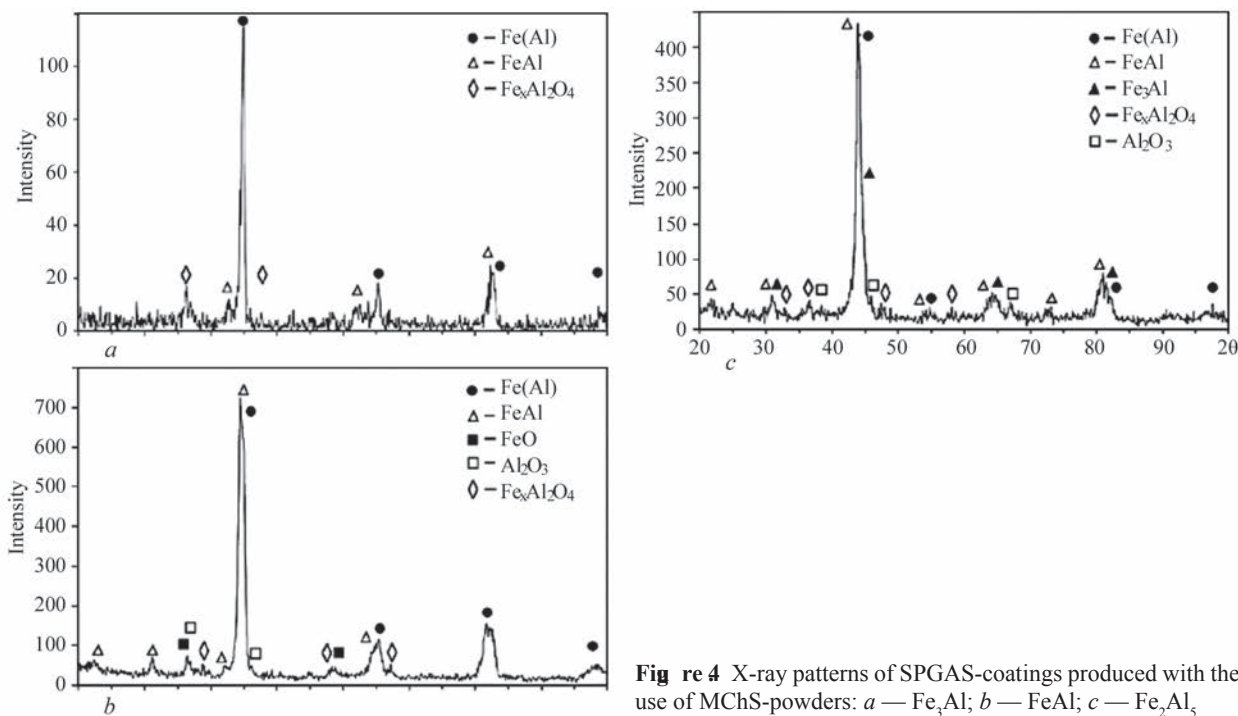


Fig re 4 X-ray patterns of SPGAS-coatings produced with the use of MChS-powders: *a* — Fe₃Al; *b* — FeAl; *c* — Fe₂Al₅

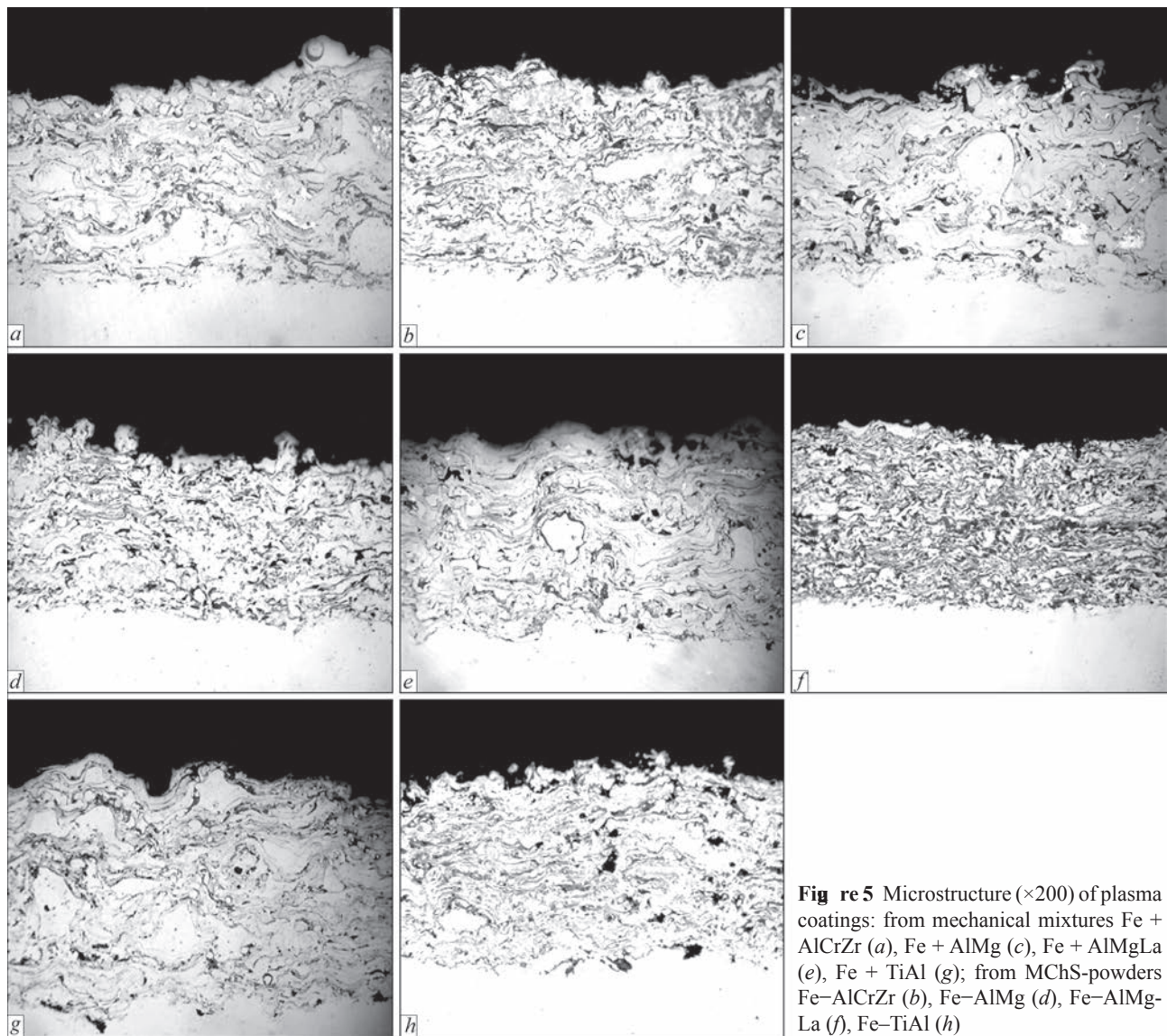


Fig re 5 Microstructure (×200) of plasma coatings: from mechanical mixtures Fe + AlCrZr (*a*), Fe + AlMg (*c*), Fe + AlMgLa (*e*), Fe + TiAl (*g*); from MChS-powders Fe-AlCrZr (*b*), Fe-AlMg (*d*), Fe-AlMg-La (*f*), Fe-TiAl (*h*)

As a result of metallographic analysis of SP-GAS-coatings (Figure 3) it was found that during spraying of MChS-powders Fe_3Al , FeAl and Fe_2Al_5 , a dense structure is formed with the presence of oxide lamellae (content of oxide component in the coatings Fe_3Al , FeAl and Fe_2Al_5 amounts to 50, 25 and 20 vol.%, respectively).

X-ray diffraction phase analysis (Figure 4) found that the phase composition of the SPGAS-coating from the powders Fe_3Al , FeAl and Fe_2Al_5 , as in the case of plasma spraying, does not coincide with the composition of the initial powders, but this difference bears different nature because of the different composition of the plasma jet, its velocity and temperature and the conditions of formation of the

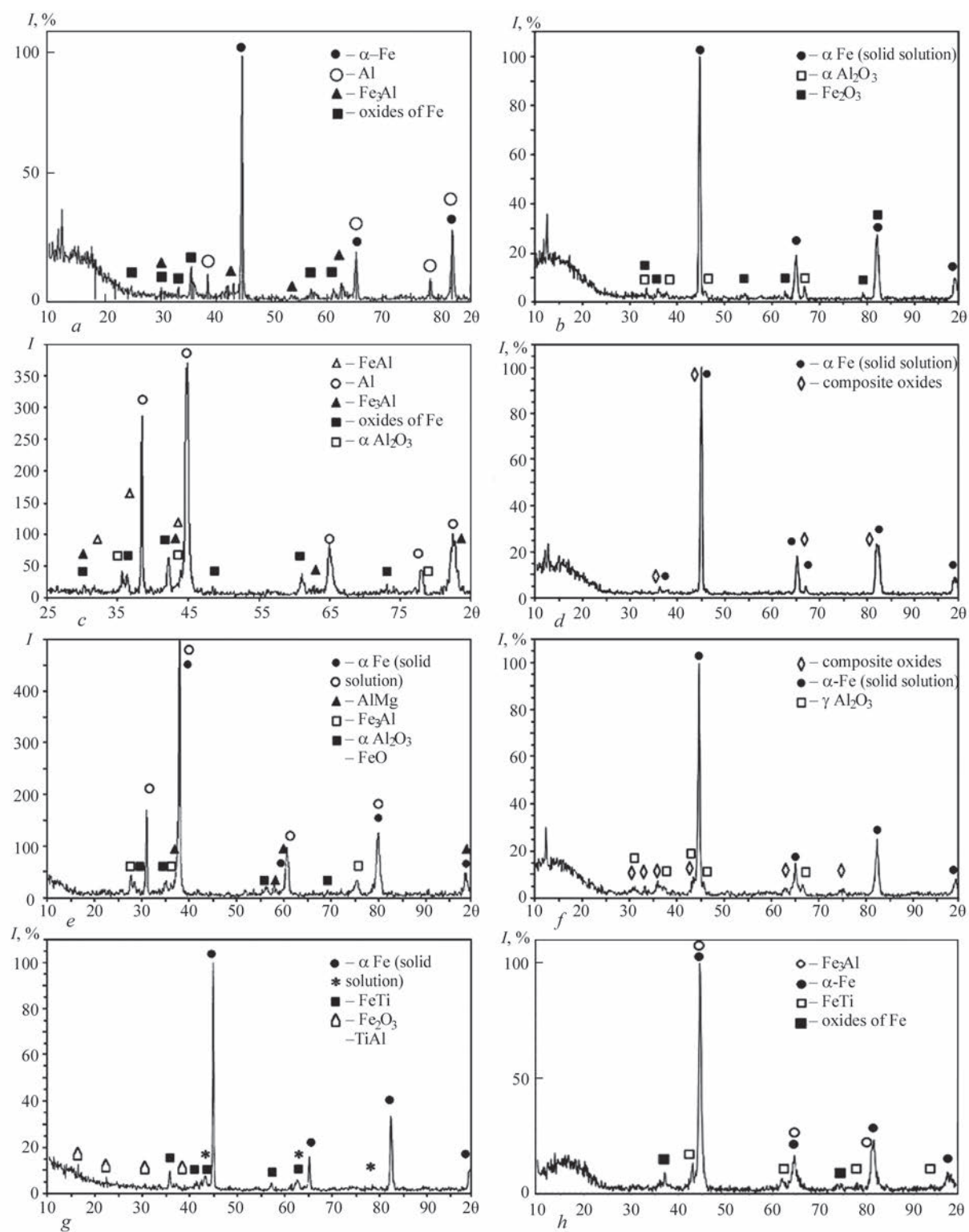


Fig re 6 X-ray patterns of plasma coatings: from mechanical mixtures Fe + AlCrZr (a), Fe + AlMg (c), Fe + AlMgLa (f), Fe + TiAl (g); from MChS-powders Fe–AlCrZr (b), Fe–AlMg (d), Fe–AlMgLa (f), Fe–TiAl (h)

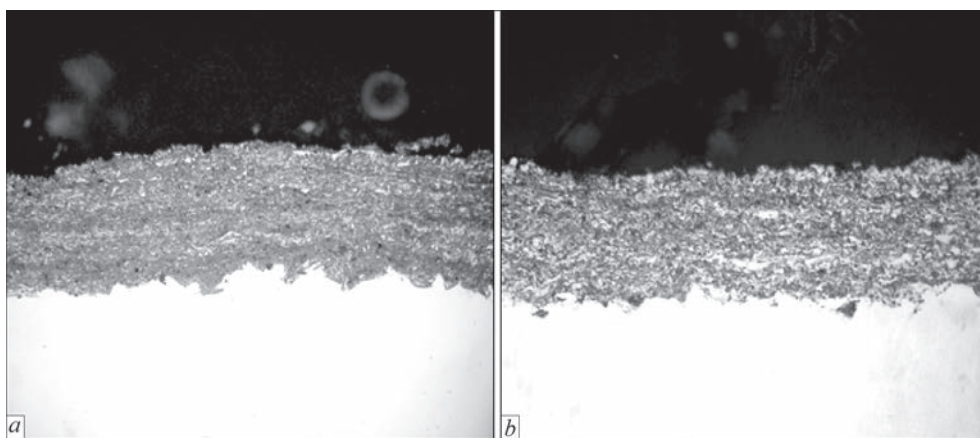


Fig re 7 Microstructure of SPGAS-coatings from alloyed powders: *a* — Fe-AlCrZr; *b* — Fe-AlMg

coating layer. In all cases, in the coatings a solid solution of aluminium in iron and the intermetallic phase FeAl are formed. In the coating Fe_2Al_5 , the intermetallic phase Fe_3Al was also detected. In all coatings, a composite oxide $\text{Fe}_x\text{Al}_2\text{O}_4$ is present, and in the FeAl coating iron oxide FeO, aluminium oxide Al_2O_3 , and in the coating Fe_2Al_3 aluminium oxide Al_2O_3 are present.

Measuring the microhardness of PS- and SPGAS-coatings showed that its value is higher in the coatings with MChS powder Fe_2Al_3 , as compared to the coatings with MChS powders Fe_3Al and FeAl (Table 3), which is agreed with the literature data, according to which the hardness of all intermetallic phases decreases with increasing iron content.

Figure 5 shows the microstructure of plasma coatings from the powders alloyed with Fe aluminides, produced by mechanical mixing and from MChS-powders using Al-alloys of AlCrZr, AlMg, AlMgLa, as well as titanium aluminide.

In the microstructure of plasma coatings produced in the case of spraying mechanical mixtures of powders Fe + AlCrZr, Fe + AlMg, Fe + AlMgLa and Fe + TiAl, separate particles of iron and particles based on aluminium are observed (Figure 5, *a, c, e*); in the case of spraying the coating from the mechanical mixture

Fe + TiAl, no particles of titanium aluminide are observed in the coating (Figure 5, *g*).

When using powders of the systems Fe + AlCrZr, Fe + AlMg and Fe + AlMgLa produced by the MChS method, a dense lamellar structure is formed (Figure 5, *b, d, f*), and in the case of Fe-TiAl powder, spalling elements are observed (5–6 vol.%) (Figure 5, *h*), which indicates the presence of brittle phase inclusions in this coating.

The results of XRD of plasma coatings from alloyed powders (Figure 6, Table 3) showed that in the case of spraying mechanical mixtures of iron with aluminium alloys, as in the case of mixtures of iron with aluminium, the reaction of intermetallic phases formation does not develop noticeably. In the coatings, except for the expected phase of intermetallic Fe_3Al (for Fe-AlCrZr, Fe-AlMg and Fe-AlMgLa compositions) or $\text{Fe}_{1-x}\text{TiAl}_x$ (for Fe-TiAl composition), solid solutions based on iron, aluminium, oxides of aluminium and iron were found.

The coatings from powders produced by MChS method from a mixture of iron with aluminium alloys AlCrZr, AlMg and AlMgLa, contained a large amount of oxides (up to 30 vol.%). Moreover, in addition to oxides of aluminium and iron, composite oxides were also detected, for example, MgFeAlO_4 . Probably

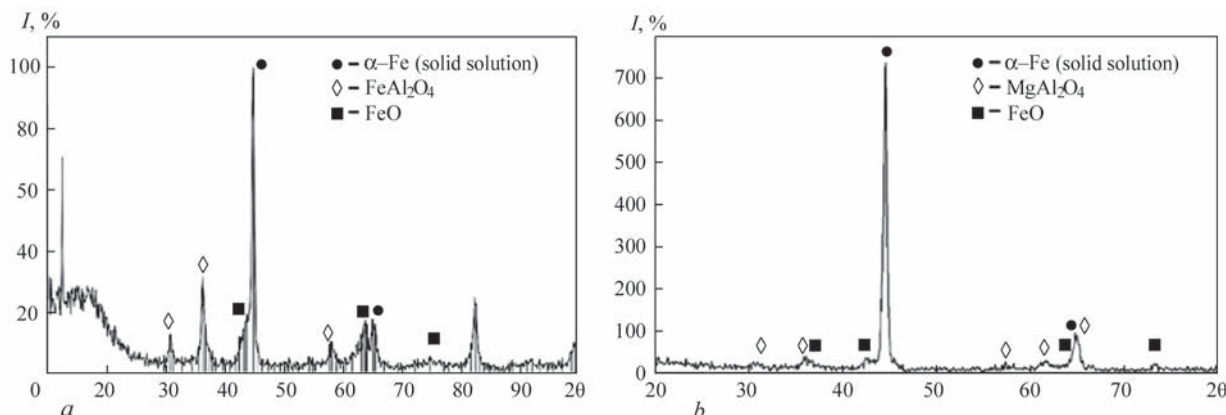


Fig re 8 X-ray patterns of SPGAS-coatings: *a* — Fe-AlCrZr; *b* — Fe-AlMg

Table 4 Characteristics of PS and SPGAS-coatings of powders alloyed by iron aluminides produced by mechanical mixing and MChS method with the use of Fe- and Al-alloys

Powder		Coating		
Composition	Method of producing	Method of spraying	H_{μ} , MPa	XRD
86Fe + 14(Al1.5Cr1Zr) (wt.%)	Mechanical mixing	PS	Based on Fe – 3080±400 Based on Al – 620±100	α -Fe, Al, Fe ₃ Al, Fe ₃ O ₄ , FeO, Fe ₂ O ₃ (Figure 6, a)
Fe–AlCrZr	MChS	PS	3830±630	Solid solution of Cr and Zr in Fe; γ -Al ₂ O ₃ , Fe ₂ O ₃ (Figure 6, b)
		SPGAS	6180±740	Solid solution based on α -Fe, FeAl ₂ O ₄ , FeO, traces of Al ₉ Cr ₄ , AlCr ₂ , Cr ₂ Zr, AlZr ₂ (Figure 8, a)
86Fe + 14(Al5Mg) (wt.%)	Mechanical mixing	PS	Based on Fe – 2800±460 Based on Al – 630±90	FeAl, Al, Fe ₃ Al, α -Al ₂ O ₃ , Fe ₂ O ₃ (Figure 6, c)
Fe–AlMg	MChS	PS	3280±450	Solid solution of Al in α -Fe, MgAl ₂ O ₄ , MgFeAlO ₄ (Figure 6, d)
		SPGAS	4460±740	Solid solution based on α -Fe, MgAl ₂ O ₄ , FeO, traces of Al ₂ Mg, MgO, MgO ₂ (Figure 8, b)
86Fe + 14(Al5MgLa) (wt.%)	Mechanical mixing	PS	Based on Fe – 3080±400 Based on Al – 630±90	Solid solution of Mg in Al, α -Fe, Fe ₃ Al, α -Al ₂ O ₃ , FeO (Figure 6, e)
Fe–AlMgLa	MChS	PS	5040±780	Solid solution of Al and La in α -Fe, Fe ₃ O ₄ , Fe ₂ O ₃ , γ -Al ₂ O ₃ , MgFeAl ₂ O ₄ (Figure 6, f)
61Fe+39(TiAl) (wt.%)	Mechanical mixing	PS	3670±870	α -Fe, FeTi, TiAl, Fe ₂ O ₃ (Figure 6, g)
F–TiAl	MChS	PS	6910±1640	Fe ₃ Al, Fe, FeTi, Fe ₂ O ₃ , Fe ₃ O ₄ , FeO (Figure 6, h)

by this fact it is possible to explain the detection of phases based on FeAl and solid solutions of Al in Fe in the structure of the coating instead of the expected intermetallic based on Fe₃Al, containing alloying elements. Only in the coating of the system Fe–TiAl, Fe₃Al is the main phase. In addition to this phase, the coating contains FeTi and iron oxides.

Analysis of the microstructure of SPGAS-coatings (Figure 7) showed that during spraying of alloyed powders of the systems Fe–AlCrZr and Fe–AlMg produced by the MChS method, a dense lamellar structure is formed, in which the content of the oxide component is 60–65 and 30–35 vol.%, respectively.

Using X-ray diffraction phase analysis (Figure 8, Table 3) it was found that during SPGAS-spraying of powders Fe–AlCrZr and Fe–AlMg, produced by the MChS method, the reaction of intermetallic phases formation does not proceed, and in the coating solid solution based on iron, iron oxide FeO and composite oxides FeAl₂O₄ and MgAl₂O₄ are revealed (Table 3). In addition, in the coating Fe–AlCrZr traces of compounds Al₉Cr₄, AlCr₂, Cr₂Zr and AlZr₂ were detected, and in the coating Fe–AlMg there are traces of AlMg compound and magnesium oxides MgO and MgO₂.

The microhardness of plasma coatings from the powders of alloyed iron aluminides (Table 4) produced by MChS is much higher as compared to the coatings from the mechanical mixture of Fe- and Al-alloys. The maximum value of microhardness (6910 MPa) was marked in the coating from the pow-

der of the system Fe–TiAl produced by MChS due to the formation of FeTi intermetallic in the coating.

Analysis of the microhardness of SPGAS-coatings from the alloyed powders (Table 4) showed that in the coating Fe–AlCrZr it is 1.6 times higher than in the sprayed initial powder (3840 MPa, Table 1), and the microhardness of the coating Fe–AlMg almost does not differ from the microhardness of the initial powder due to the absence or limited development of the contact interaction of Fe and Al in the process of coating deposition. This is explained by the lower degree of oxidation of Fe–AlCrZr coatings (60–65 vol.%) as compared to Fe–AlMg coatings (30–35 vol.%).

Conclusions

The investigation of microstructure, microhardness and phase composition of plasma coatings from Fe–Al-powders produced by the MChS method, showed that in addition to the initial phase (Fe₃Al, FeAl and Fe₂Al₅) in the coatings to a greater or lesser extent oxides of Fe and Al are present, which is reflected on the value of microhardness (Fe₃Al — 3630 MPa, FeAl — 4150 MPa and Fe₂Al₅ — 5200 MPa). When iron alloying elements are introduced into aluminides by using Al-alloys AlCrZr, AlMg and AlMgLa, microhardness of the coatings amounts to 3830, 3280 and 5040 MPa, respectively. Microhardness of the plasma coating Fe–TiAl (6910 MPa) increases 2 times in respect to the initial powder due to the formation of the intermetallic phase FeTi in the coating.

During plasma spraying of mechanical mixtures of iron with aluminium and iron with aluminium alloys, the reaction of intermetallic phases formation does not develop noticeably due to the lack of development of contact interaction of Fe and Al during the process of coating. The main phases in the coatings are the initial components of iron, aluminium and their oxides.

In the coatings produced by the method of supersonic plasma gas-air spraying intermetallic phases were not detected, the main phase is α -Fe (Al)-solid solution, which is obviously the result of a high rate of hardening the melt particles during the formation of intersections on the base surface.

1. Zamanzade, M., Barnoush, A., Motz, C. (2016) A review on the properties of iron aluminide intermetallics. *Crystals*, 6(1), 10.
2. Palm, M., Stein, F., Dehm, G. (2019). Iron aluminides. *Annual Review of Materials Research*, 9, 297–326.
3. Cebulski, J. (2015) Application of FeAl intermetallic phase matrix based alloys in the turbine components of a turbo-charger. *Metalurgija-Sisak then Zagreb*, 5, 154–156.
4. Morris, D. G., Muñoz-Morris, M. A. (2010) Recent developments toward the application of iron aluminides in fossil fuel technologies. *Adv. Engineering Materials*, 13(1–2), 43–47.
5. Cordier-Robert, C., Grosdidier, T., Ji, G., Foct, J. (2006) Moessbauer and X-ray diffraction characterization of Fe-60Al40 coatings prepared by thermal spraying. *Hyperfine Interact.*, 168(1), 951–957.
6. Senderowski, C., Bojar, Z. (2008) Gas detonation spray forming of Fe–Al coatings in the presence of interlayer. *Surf. & Coat. Technol.*, 9, 3538–3548.
7. Xiao, Ch., Chen, W. (2006) Sulfidation resistance of CeO₂-modified HVOF sprayed FeAl coatings at 700 °C. *Surf. & Coat. Technol.*, 9, 3625–3632.
8. Xiang, J., Zhu, X., Chen, G. et al. (2009) Oxidation behavior of Fe40Al-xWC composite coatings obtained by high-velocity oxygen fuel thermal spray. *Transact. of Nonferrous Metals Society of China*, 9, 1545–1550.
9. Yang, D. M., Tian, B. H., Cao, Y. (2011) Microstructures and properties of FeAl coatings prepared by LPPS, APS and HVOF. In: *Proc. of the Int. Thermal Spray Conf., Hamburg, Germany*, 1229–1234.
10. Borisov, Yu.S., Borisova, A.L., Astakhov, E.A. et al. (2017) Detonation coatings of intermetallic powders of Fe–Al system produced using mechanical alloying. *The Paton Welding J.*, 4, 23–29.
11. Chen, Y., Liang, X., Wei, Sh. et al. (2009) Heat treatment induced intermetallic phase transition of arc-sprayed coating prepared by the wires combination of aluminium-cathode and steel-anode. *Appl. Surface Sci.*, 255(9), 8299–8304.
12. Hansen, M., Anderko, K. (1962) *Structure of binary alloys*. Vol. 2. Moscow, Metallurgizdat [in Russian].
13. Borisova, A.L., Timofeeva, I.I., Vasil'kovskaya, M.A. et al. (2015) Structural and phase transformations in Fe–Al intermetallic powders during mechanochemical sintering. *Powder Metallurgy and Metal Ceramics*, 54(8), 490–496.
14. Borisov, Yu.S., Borisova, A.L., Burlachenko, A.N. et al. (2017) Structure and properties of alloyed powders based on Fe₃Al intermetallic for thermal spraying produced using mechanochemical synthesis method. *The Paton Welding J.*, 9, 33–39.

Received 30.06.2020

WORLD TRADE FAIR FOR WELDING ENGINEERING —
JOINING, CUTTING, SURFACING

LET'S JOIN
THE WORLD!

13. – 17. September, 2021

REGISTER NOW!

www.schweissen-schneiden.com

DVS GERMAN WELDING SOCIETY

MESSE ESSEN

SCHWEISSEN & SCHNEIDEN
No. 1 IN THE WORLD

INFLUENCE OF CONTENT OF ALLOYING ELEMENTS AND HEAT TREATMENT ON LIFE CHARACTERISTICS OF HIGH-STRENGTH WHEEL STEELS DURING MANUFACTURE OF RAILROAD WHEELS AND THEIR REPAIR SURFACING

OP. Ostash¹, V.V. Kulyk¹, S.Ya. Shipitsyn², O.A. Haivoronsky³ and R.V. Chepil¹

¹G.V. Karpenko Physical-Mechanical Institute of the NAS of Ukraine.

5 Naukova Str., Lviv, 79060, Lviv, Ukraine

²Physical and Technological Institute of Metals and Alloys of the NAS of Ukraine

34/1 Blvd., Akad. Vernadsky, 03142 Kyiv, Ukraine

³E.O. Paton Electric Welding Institute of the NAS of Ukraine

11 Kazymyr Malevych Str., 03150, Kyiv, Ukraine. E-mail: office@paton.kiev.ua

A new concept of creating steels to provide high resistance of the rolling surface of wheels to wear and damage was proposed, requirements for a set of mechanical characteristics of such steels were developed and chemical composition of steel of a new generation for railroad wheels, as well as heat treatment mode during their repair surfacing were substantiated. 15 Ref., 2 Tables, 4 Figures.

Key words: high-strength railroad wheels, slid flat, shelled tread, wear, operational reliability

Growth in the axial load and speed of railway transport requires the creation of high-strength wheel steels, at the same time providing reliability and long life of railroad wheels. Until recently, reducing wear of their rolling surface was one of the most important tasks in solving this problem, which in the world practice was solved by developing low-alloy carbon steels with an increased carbon content (0.6–0.7 %), hardness ($>HB\ 300$) and tensile strength ($>1000\text{ MPa}$). In particular, in Ukraine, the steel of grade T was proposed to replace the steel of grade 2 [1]. However, the experience in operation of such high-strength wheels showed that on their rolling surface a number of operational damages (slid flats, shelled treads, etc.) grows significantly [2], which results in reducing service life of wheels and the need in expensive reprofiling (machining) of their rim.

Defects on the rolling surface of wheels are caused primarily by initiation and growth of surface and sub-surface cracks as a result of a contact fatigue of the metal, as well as crack formation resulted by changes in structure and phase composition under a thermal impact on the metal during braking and cornering. In general, this is the result of the influence of an increased carbon content in such wheel steels on its susceptibility to martensitic transformation [2]. A similar problem of the negative impact of a high carbon con-

tent exists during repair surfacing of wheels because of cracking in the heat-affected-zone [3]. Therefore, steels for railroad wheels of a new generation must be high-strength at a low carbon content, have a high crack resistance and an increased thermal stability of the structural-phase composition and mechanical properties. As far as the wheels receive mainly cyclic loads, a preference should be given to the characteristics of cyclic crack resistance of wheel steels. As a result, wheel steels with an increased service life should optimally combine high characteristics of strength and cyclic crack and wear resistance and resistance to contact-fatigue damage formation.

The negative effect of reducing carbon content on the strength of wheel steels should be compensated by their additional alloying. However, the use of chromium, molybdenum and nickel can significantly increase the cost of steel. It is more rational to increase the content of silicon and manganese (promotes a solid-solution strengthening and reduces sensitivity to heat and contact fatigue) [4] and microalloy steel with vanadium and nitrogen (promotes dispersion strengthening due to the formation of nitrides and carbonitrides, which hinder the recrystallization process, providing structural strengthening of steel) [5]. Data on the life characteristics of such complex alloyed steels are almost absent in the literature.

O.A. Haivoronskyi — <https://orcid.org/0000-0002-8146-7790>

© O.P. Ostash, V.V. Kulyk, S.Ya. Shipitsyn, O.A. Haivoronskyi and R.V. Chepil, 2020

Table 1 Chemical composition and mechanical characteristics of wheel steels

Variant of steel	C, wt. %	Si, wt. %	Mn, wt. %	[VN]·10 ⁴ , wt. %	$\sigma_{0.2}$, MPa	σ_p , MPa	δ , %	ΔK_{th} , MPa \sqrt{m}	ΔK_{fc} , MPa \sqrt{m}
1	0.60	0.34	0.64	—	670	1010	11.5	7.0	100
2	0.63	0.72	0.32	—	1080	1250	10.5	6.6	65
3	0.63	0.18	0.76	8.1	486	843	16.8	6.5	73
4	0.56	0.22	0.87	11.6	547	756	22.2	—	—
5	0.63	0.13	0.65	15.6	520	789	14.6	—	—
6	0.57	0.27	0.85	22.1	877	592	17.0	6.6	87
7	0.61	0.26	0.65	41.9	520	810	18.7	6.6	83
8	0.58	0.97	0.85	—	735	1051	10	6.0	52
9	0.52	0.67	0.81	28.9	806	1025	17.7	6.0/5.0	80/65
10	0.45	1.44	1.36	18.7	869	1060	15	6.3	59

Note. Variants 1 and 2 — steels of grades 2 and T, respectively [1]; variant 8 — steel of grade K [6]; the rest are test steels.

Materials and procedures. Standard high-strength wheel steels of grades 2 and T (Table 1, variants 1 and 2) and new (with solid-solution or nitride strengthening as well as at the simultaneous combination of solid-solution and nitride strengthening) steels for railroad wheels were studied (Table 1, variants 3–10). The investigations were carried out on the specimens cut out from the wheels manufactured according to the technology of PJSC «INTERPIPE NTZ» from steels of grades 2, T and K (variants 1, 2 and 8), as well as from the experimental castings after thermal and thermomechanical treatments (Table 1, variants 3–7, 9, 10), produced according to the technology of PTIMA of the NAS of Ukraine.

The mass fraction of carbon, sulfur and phosphorus was determined according to the standards of GOST 12344–88, GOST 12345–88, GOST 12347–88; nitrogen — by the method of melting specimens in a flow of helium with a purity of 99.99 % in the analyzer TC-30 of the LECO Company; other elements — using the spectral analysis in the installation «Spectromax» according to GOST 18895–97.

Structural stresses of the II kind (τ_{loc}) were determined by the calculation method, using the established indices of the dislocation structure [3]: $\tau_{loc} = Gb\rho/\pi(1 - \nu)$ where G is the displacement modulus; b is the Burgers vector; ρ is the density of dislocations, ν is the Poisson's ratio, and t is the thickness of the foil.

A short-term strength (yield strength $\sigma_{0.2}$ and tensile strength σ_t) and ductility (relative elongation b) were determined on five-fold cylindrical specimens with a diameter of the working part of 3 or 5 mm at temperatures from 20 to 800 °C.

The characteristics of cyclic crack resistance of steel at a normal tear were determined according to the diagrams of growth rates of fatigue macrocrack — dependences $da/dN - \Delta K_f$ obtained according to the standard procedure (ASTM E647–08) on the compact specimens with a thickness of 8–10 mm at a frequency of 10–15 Hz and the loading cycle asymmetry co-

efficient $R = 0.1$. As the characteristics of cyclic crack resistance of materials, the fatigue threshold $\Delta K_{th} = \Delta K_{10^{-10}}$ and the cyclic fracture toughness $\Delta K_{fc} = \Delta K_{10^{-5}}$ — ranges of the stress intensity factor at the crack growth rate $da/dN = 10^{-10}$ and 10^{-5} m/cycle, respectively, were selected. In some cases, the values of ΔK_{fc} were set on the range ΔK , when fatigue crack begins to grow spontaneously.

The damage tests were performed on the model specimens of a wheel of 8 mm thickness and 40 mm in diameter in contact with a rail of 220 mm long, 8 mm wide and 16 mm high. The wheels were manufactured of the above-described steels, and the rails were cut out from the head of the natural rail with a hardness of HRC 46. The tests were carried out in a specially designed bench [7] under the load on the wheel $P = 1300$ N, which creates stresses in the contact zone of the wheel-rail $p_0 = 750$ MPa, determined by the known Hertz formula.

The rolling surfaces of the wheels were studied under the microscope after $2 \cdot 10^5$ load cycles (25 km on track) at a magnification of 130 times. The images were analyzed using a specially designed computer program and the average number of defects \bar{n} , mm⁻² in field of vision of the microscope was determined depending on their size in different parts of the rolling surface and the damage was evaluated by the ratio of the area of shelled treads formed by pitting formation and delamination (F_d) to the total area of the rolling surface of a wheel (F_0). In the conditions of contact fatigue, the damage resistance ($1/D$) and the wear resistance ($1/W$), which are the inverse values respective to the damage $D = F_d/F_0$ and wear $W = (R_0 - R)/R_0$ of the rolling surface of the model wheel were evaluated, where F_d is the area of defects (pitting and shelled treads), F_0 is the area of rolling surface; R is the radius of the wheel after tests; R_0 is its initial value. The averaged values of the characteristics based on the results of the tests of at least three specimens were given.

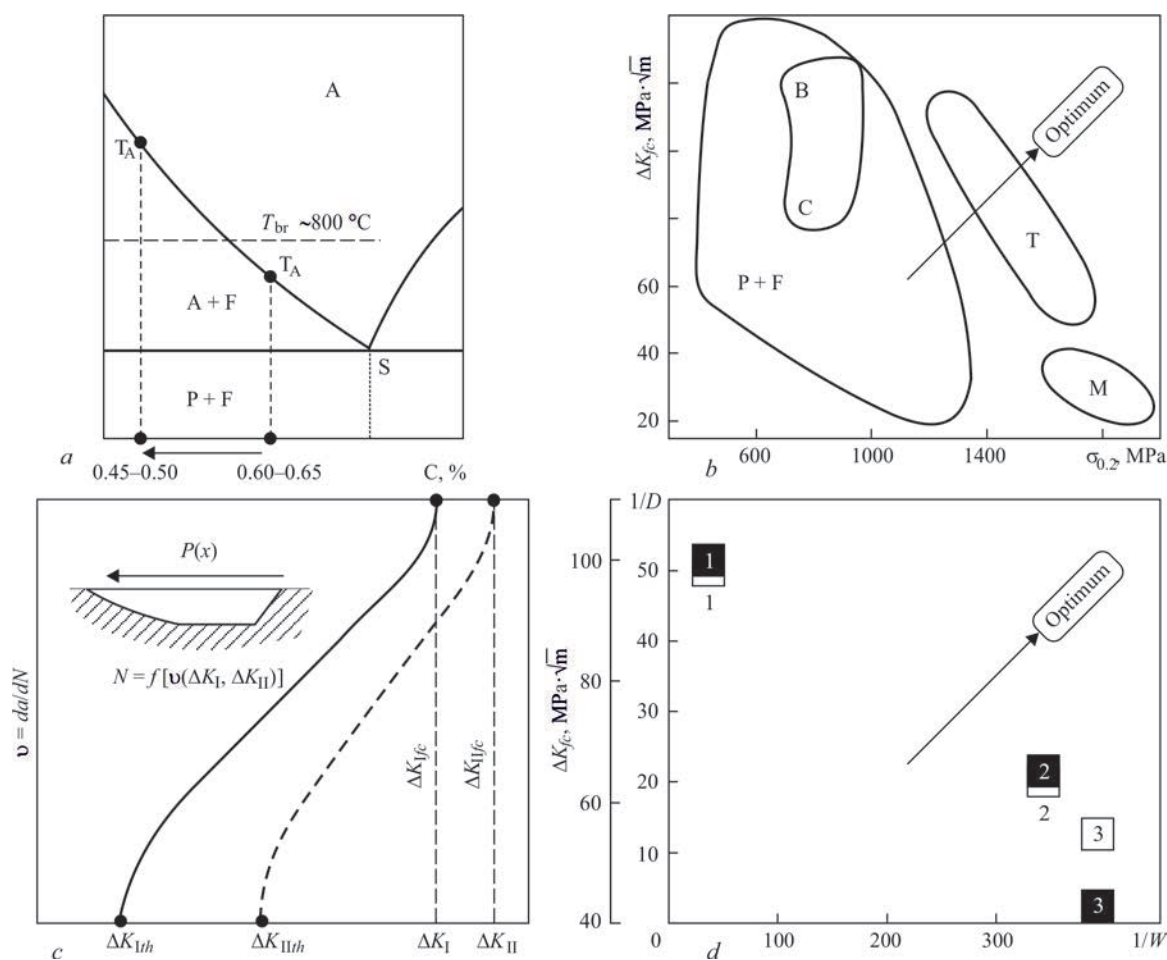


Fig re 1 New concept of creating high-strength wheel steels: T_A — austenitization temperature; T_{br} — temperature in the area of wheel-rail contact during braking; A — austenite, F — ferrite, P — pearlite, B — bainite, M — martensite, T — troostite, S — sorbite; 1 — steel of grade 2, 2 — of grade T, 3 — of grade T_m . Light symbols — diagram ($1/D - 1/W$); dark — ($\Delta K_{Ic} - 1/W$); description a–d see in the text

Results 6 in v stig in s. New concept for the development of high-strength wheel steels. Based on the data of the analysis of operational damages of wheels of type KP-2 and KP-T on all road network of the Ukrzaliznytsia, as well as laboratory investigations of life characteristics of steels of grades 2 and T, it was established that mechanical behavior of these steels under the influence of operational factors depends on the carbon content [2]. The obtained results substantiated the need in changing the concept of selection (development) of steels to increase the long life of high-strength railroad wheels, which should be carried out both according to the criterion of wear (which determines the strength and hardness of steels), as well as on the criterion of arising shelled treads of the rolling surface (which determines the crack resistance of steels). An increased (up to 0.7 %) carbon content in the steel of grade T, causing an increase in wear resistance (hardness), facilitates its susceptibility to martensitic transformation, an increase in residual stresses of the II type and, as a result, a decrease in cyclic crack resistance [2]. It was established that a contact-fatigue damage unambiguously depends on

the cyclic fracture toughness of steel under the conditions of normal tear (ΔK_{Ic}) and transverse displacement (ΔK_{IIc}): it is the largest in the model wheels of the steel, which has the lowest cyclic fracture toughness. At the same time, such an unambiguous dependence is absent when as a determining parameter of crack resistance a fatigue threshold ΔK_{Ith} and ΔK_{IIth} is taken [7, 8].

As a result, a new concept of developing high-strength wheel steels [2] was proposed, which is based on the approaches of structural fracture mechanics (Figure 1). It envisages (Figure 1, a) the need in the maximum possible reduction in carbon content to prevent martensitic transformation during braking and crack formation in repair surfacing. It includes the search on the basis of diagrams of structural strength of wheel steels, which provide an optimal combination of characteristics of their strength and crack resistance, taking into account their structure (Figure 1, b) and the mechanisms of fracture under the conditions of normal tear and transverse displacement (Figure 1, c) to minimize crack formation on the rolling surface of wheels. It regulates the need in providing an opti-

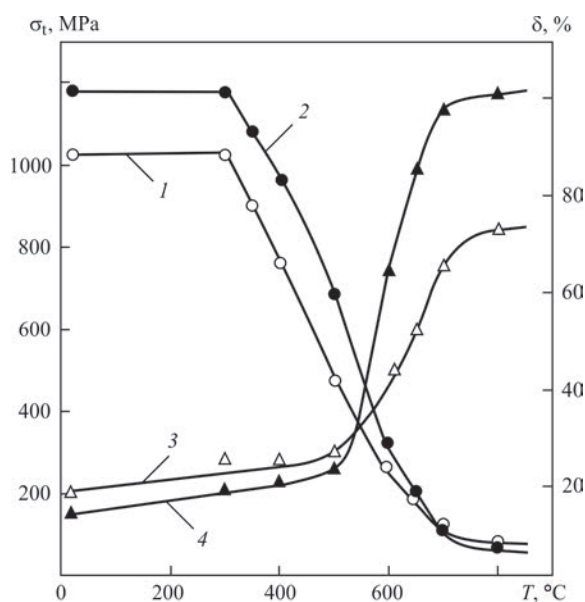


Fig re 2 Temperature dependence of strength (1, 2) and ductility characteristics (3, 4) of steels of grades 2 (1, 3) and T (2, 4)

mal combination of their characteristics of wear resistance and a contact-fatigue damage (Figure 1, *d*). Therefore, as the main characteristic of a service life and reliability of wheel steels the diagram was proposed [9], which demonstrates operational reliability (Figure 1, *d*) — dependence between cyclic fracture toughness (ΔK_{fc}), which determines resistance to formation of operational defects on the rolling surface of wheels ($1/D$), and resistance to wear of the flange and rolling surface of wheels ($1/W$). It is obvious that the desired optimum will be located in the upper right corner of this diagram (Figure 1, *d*).

It was also proposed [2] that the second main characteristic of service life and reliability of wheel steels, which determines their susceptibility to formation of slid flats on the rolling surface of wheels, is the dependence of ductility (relative elongation) at temperatures above 500 °C, in particular, at 700 °C, which

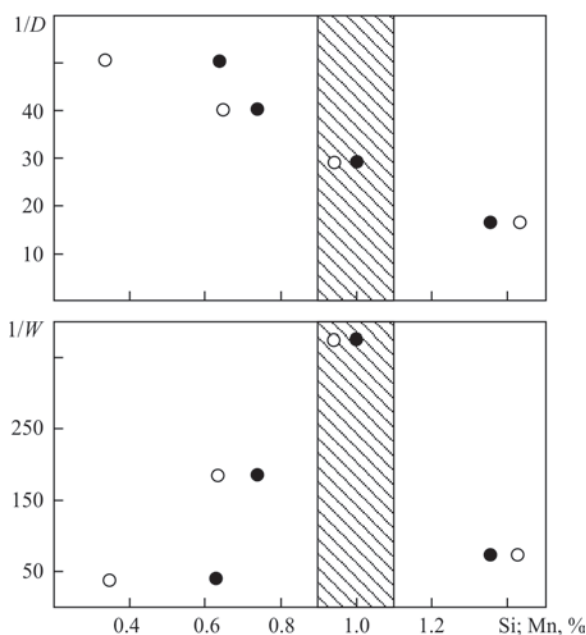


Fig re 4 Dependence of resistance to damage and wear on silicon and manganese content, as well as their recommended content (shaded area)

in this case is informative in contrast to the strength characteristics (Figure 2): the higher the values of δ^{700} , the higher the susceptibility of steel to formation of slid flats [2].

Substantiation of chemical composition of the new high-strength wheel steel. Steel of grade T with a high carbon content (Table 1, variant 2) is introduced for manufacture of high-strength railroad wheels instead of steel of grade 2 (variant 1), it has a high yield and tensile strength, but an elevated high-temperature ductility δ^{700} and a low cyclic toughness of fracture ΔK_{fc} , which causes its high wear resistance at a low damage resistance (Figure 3, *a*) and an increased susceptibility to formation of slid flats (Figure 3, *b*). During microalloying with vanadium and nitrogen, the steels with disper-

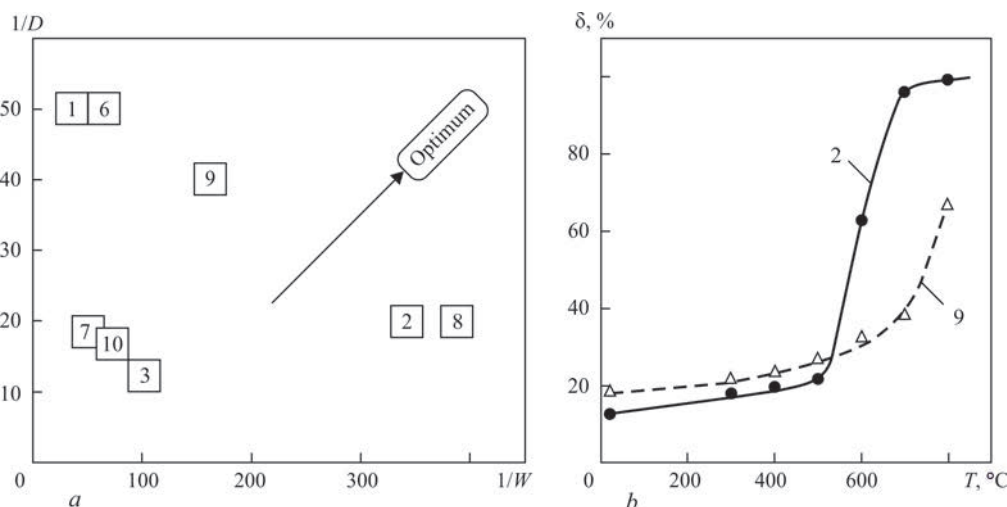


Fig re 3. Diagram of operational reliability (*a*) and temperature dependence of relative elongation (*b*) of steel variants according to Table 1

sion strengthening at a lowered carbon content (up to 0.56 %) and silicon (up to 0.13–0.18 %) show increased values of ΔK_{fc} (Table 1, variants 3–7) as compared to standard steel of grade T, but low strength characteristics at a high ductility. Moreover, the optimum of the value $[V \cdot N] = 22.1 \cdot 10^{-4} \%$ was revealed (Table 1, variant 6). This steel has a high resistance to damage, which is at the level set for the steel of grade 2 (Figure 3, *a*), but requires an increased wear resistance [10].

At a solid-solution strengthening when using an increased content of silicon and manganese (Table 1, variant 8), the steel shows a high strength, but the

lowest cyclic fracture toughness ($\Delta K_{fc} = 52 \text{ MPa} \cdot \sqrt{\text{m}}$), which is associated with an excessive stress of the structure at a solid-solution strengthening of ferrite at a relatively high (0.58 %) carbon content [4]. Therefore, the steel has a high resistance to wear and a low resistance to damage, similar to that established for the steel of a high-carbon grade T (Figure 3, *a*).

The use of complex strengthening (Table 1, variant 9), namely dispersion and solid-solution one at a low (0.52 %) carbon content, proved to be more effective [11, 12]. Such steel is characterized both by a high yield and also tensile strength, ductility and cyclic fracture toughness. As a result, we obtained the

Tb le 2 Conditions and parameters of heat treatment of steel 65G

Mode	Scheme and parameters of heat treatment	
1		Temperature of austenitisation $T_A = 850 \text{ }^\circ\text{C}$; Rate of cooling in the range of 600–500 $^\circ\text{C}$; $w_{6/5} = 5 \text{ }^\circ\text{C/s}$
2		$T_A = 850 \text{ }^\circ\text{C}$; $w_{6/5} = 5 \text{ }^\circ\text{C/s}$; $T_1 = 250 \text{ }^\circ\text{C}$, $\tau_1 = 10 \text{ min}$
3		$T_A = 850 \text{ }^\circ\text{C}$; $w_{6/5} = 5 \text{ }^\circ\text{C/s}$; $T_1 = 300 \text{ }^\circ\text{C}$, $\tau_1 = 1 \text{ min}$
4		$T_A = 850 \text{ }^\circ\text{C}$; $w_{6/5} = 5 \text{ }^\circ\text{C/s}$; $T_1 = 250 \text{ }^\circ\text{C}$, $\tau_1 = 10 \text{ min}$; $T_2 = 100 \text{ }^\circ\text{C}$, $\tau_2 = 2 \text{ h}$
5		$T_A = 850 \text{ }^\circ\text{C}$; $w_{6/5} = 5 \text{ }^\circ\text{C/s}$; $T_1 = 300 \text{ }^\circ\text{C}$, $\tau_1 = 1 \text{ min}$; $T_2 = 100 \text{ }^\circ\text{C}$, $\tau_2 = 2 \text{ h}$
6		$T_A = 850 \text{ }^\circ\text{C}$; $w_{6/5} = 5 \text{ }^\circ\text{C/s}$; $T_2 = 180 \text{ }^\circ\text{C}$, $\tau_2 = 2 \text{ h}$
7		$T_A = 850 \text{ }^\circ\text{C}$; $w_{6/5} = 5 \text{ }^\circ\text{C/s}$; $T_2 = 100 \text{ }^\circ\text{C}$, $\tau_2 = 2 \text{ h}$

best combination of damage and wear resistance, as close as possible to the optimum (Figure 3, *a*). At the same time, it has a significantly lower susceptibility to formation of slid flats as compared to standard steel of grade T (Figure 3, *b*). The complex alloying with a further reduction in carbon content (up to 0.45 %) at a sufficiently high content of silicon and manganese (1.36–1.44 %) led to a high strength, low cyclic fracture toughness of steel (Table 1, variant 10), as well as a worse operational reliability as compared to the steel of variant 9 (Figure 3, *a*).

Let us note, that in all investigated steels the value of fatigue threshold $\Delta K_{th} = 6.0\text{--}7.0 \text{ MPa}\cdot\sqrt{\text{m}}$ (Table 1) is almost constant, i.e. it can be concluded that this parameter is not decisive during optimization of life characteristics of high-strength wheel steels.

Based on the analysis of the obtained results of the influence of chemical composition on life characteristics of steels (Table 1 and Figure 4) and the literature analysis [4], a new high-strength steel (tensile strength of 1050–1100 MPa) of the following chemical composition was recommended (wt.%): 0.45–0.50 C; 0.90–1.10 Si; 0.90–1.10 Mn; 0.14–0.16 V; 0.016–0.018 N at an austenitization temperature of 860–880 °C and a tempering temperature of 500–550 °C.

Optimization of heat treatment parameters in repair surfacing. During a long-term operation, the railroad wheels wear out, and on their rolling surface defects of various types appear. Therefore, they are machined and the profile is restored by electric arc surfacing [3]. However, after that, in the heat-affected-zone of the wheel, depending on the carbon content in steel and the cooling rate, a martensitic structure is formed, which is prone to brittle fracture by a facilitated initiation and growth of cracks. This requires the search for effective modes of surfacing and cooling of restored wheels to provide a structural strength of metal in the heat-affected-zone, in particular, increased crack resistance in the high-strength state [13, 14]. To optimize the parameters of the process of cooling wheels after repair surfacing according to the technology developed at the PWI, the influence of different heat treatment conditions (Table 2) on the properties of steel 65G, used as a model wheel steel, was investigated [14].

According to the traditional scheme of Q-n-P treatment [14] (Table 2, modes 2 and 3) as compared to the initial state, an increase in the fatigue threshold ΔK_{th} (by 27 %) and the cyclic fracture toughness ΔK_{fc} (by 27–43 %) was fixed depending on the content of residual austenite. According to the modified scheme (modes 4 and 5), the value ΔK_{th} grows by 38–47 %, and ΔK_{fc} — by 48–66 %. According to the characteris-

tics of cyclic crack resistance, the best result is shown by treatment according to the mode 7 [15], which allows forming a mixed structure in HAZ of upper and lower bainite (~ 66 %) and martensite (~ 34 %) at 2–3 h holding, interrupting the cooling of the steel at 100 °C, i.e. at the temperature between the points of start (M_s) and finish (M_f) of the martensitic transformation. This causes almost 2 times increase in both the fatigue threshold ΔK_{th} as well as the cyclic fracture toughness ΔK_{fc} . Based on the results of electron microscopic investigations, it was established [13] that during this treatment in the metal some changes occurred at the substructural level: the density of dislocations ρ decreased approximately by 1.5 times. The comparison of local stresses of the II type τ_{loc} in the structural components of this metal showed that after such an isothermal holding, in the upper bainite the local stresses and strains decreased by 1.4 times; in the lower bainite by 1.5 times; in martensite by 1.3–1.4 times.

Conclusions

1. To improve the resistance of the rolling surface of high-strength (> 1000 MPa) all-rolled railroad wheels to damage and wear, as well as their reparability by surfacing, it is necessary to use steels with a reduced content of carbon (< 0.50–0.55 %), in which the high-strength state is achieved by both solid-solution (alloying with silicon and manganese) as well as dispersion (microalloying with vanadium and nitrogen) strengthening.

2. Based on the developed concept of creating high-strength (> 1000 MPa) wheel steels, a new complex-alloyed steel with a solid-solution (0.90–1.10 % of Si and 0.90–1.10 % of Mn and dispersion ($[V\cdot N] = (20\text{--}25)\cdot 10^{-4}$ %) strengthening at a lowered (to 0.45–0.50 %) carbon content was proposed, which is superior to the standard steel of grade 2 (0.58–0.62 % C) as to its resistance to wear and damage and reparability by surfacing.

3. Increasing the cyclic crack resistance of the metal in the heat-affected-zone of repair surfacing of high-strength railroad wheels is achieved by the formation of a mixed structure of the upper and lower bainite (~66 %) and martensite (~34 %) at 2–3 h holding at a temperature of 100 °C, interrupting cooling of the steel between the points of beginning (M_s) and finish (M_f) of the martensitic transformation.

1. (2016) DSTU GOST 10791-2016. *All-rolled wheels. Specifications* [in Ukrainian].
2. Ostash, O.P., Anofriev, V.H., Andreiko I.M. et al. (2011) On the concept of selection of steels for high-strength railroad wheels. *Materials Sci.*, 48(6), 697–703.

3. Haivorons'kyi, O.A., Poznyakov, V.D., Markashova, L.I. et al. (2015) Structure and mechanical properties of the heat-affected zone of restored railway wheels. *Ibid.*, 51(4), 563–569.
4. Kulyk, V.V., Ostash, O.P., Vira, V.V. (2019) Influence of the elevated contents of silicon and manganese on the operating characteristics of high-strength wheel steel. *Ibid.*, 55(2), 143–151.
5. Babaskin, Yu.Z., Shipitsyn, S.Ya., Kirchu, I.F. (2005) *Structural and special steels with nitride phase*. Kiev, Naukova Dumka [in Russian].
6. Babachenko, O.I., Kuzmichov, V.M., Knysh, A.V., Besednov, S.V. et al. (2013) *Steel for all-rolled wheels*. Ukraine, Pat. 101757, Publ. 25.04.2013, Bull. 8 [in Ukrainian].
7. Ostash, O.P., Kulyk, V.V., Lenkovskiy, T.M. et al. (2018) Relationships between the fatigue crack growth resistance characteristics of a steel and the tread surface damage of railway wheel. *Archives of Materials Sci. and Engineering*, 90(2), 49–55.
8. Kulyk, V.V., Lenkovskiy, T.M., Ostash, O.P. (2017) Mode I and mode II cyclic crack resistance of wheel steel. *Strength of Materials*, 49(2), 256–262.
9. Ostash, O.P., Andreiko I.M., Kulyk, V.V. (2014) *Method of estimation of wheel steels serviceability*. Ukraine, Pat. 106836, Publ. 10.10.2014, Bull. 19 [in Ukrainian].
10. Kulyk, V.V., Shipitsyn, S.Ya., Ostash, O.P. et al. (2018) The joint effect of vanadium and nitrogen on the mechanical behavior of railroad wheels steel. *J. of Achievements in Materials and Manufacturing Engineering*, 89(2), 56–63.
11. Shipitsyn, S.Ya., Ostash, O.P., Kulyk, V.V. et al. (2018) New steel for railway wheels with an increased service life. *Metall i Litio Ukrainy*, 300–301(5–6), 52–61 [in Russian].
12. Kulyk, V.V., Shipitsyn, S.Ya., Ostash, O.P. et al. (2019) Mechanical behavior of wheel steels with solid solution and precipitation hardening. *Archives of Materials Sci. and Engineering*, 95(2), 49–54.
13. Ostash, O.P., Kulyk, V.V., Poznyakov, V.D. et al. (2017) Fatigue crack growth resistance of welded joints simulating the weld-repaired railway wheels metal. *Ibid.*, 86(2), 49–55.
14. Ostash, O.P., Kulyk, V.V., Poznyakov, V.D. et al. (2019) Influence of the modes of heat treatment on the strength and cyclic crack-growth resistance of 65G steel. *Materials Sci.*, 54(6), 776–782.
15. Ostash, O.P., Haivoronskyi, O.A., Poznyakov, V.D., Kulyk, V.V. (2016) *Method of heat treatment of high-strength low-alloyed carbon steels*. Ukraine Pat. on utility model 105440, Publ. 25.03.2016, Bull. 6 [in Ukraine].

Received 07.07.2020

SUBSCRIPTION



«The Paton Welding Journal» is Published Monthly Since 2000 in English, ISSN 0957-798X, doi.org/10.15407/tpwj.

«The Paton Welding Journal» is Cover-to-Cover Translation of «Avtomaticheskaya Svarka» Journal Published Since 1948.

12 issues per year, back issues available.

\$384, subscriptions for the printed (hard copy) version, air postage and packaging included.

\$312, subscriptions for the electronic version (sending issues of Journal in pdf format or providing access to IP addresses).

Institutions with current subscriptions on printed version can purchase online access to the electronic versions of any back issues that they have not subscribed to. Issues of the Journal (more than two years old) are available at a substantially reduced price.

The archives for 2009–2017 are free of charge on [www://patonpublishinghouse.com/eng/journals/tpwj](http://patonpublishinghouse.com/eng/journals/tpwj)

ADVERTISING

in «The Paton Welding Journal»

External cover, fully-colored:

First page of cover
(200×200 mm) — \$700
Second page of cover
(200×290 mm) — \$550
Third page of cover
(200×290 mm) — \$500
Fourth page of cover
(200×290 mm) — \$600

Internal cover, fully-colored:

First/second/third/fourth page
(200×290 mm) — \$400

Internal insert:

(200×290 mm) — \$340
(400×290 mm) — \$500

• Article in the form of advertising is 50 % of the cost of advertising area

• When the sum of advertising contracts exceeds \$1001, a flexible system of discounts is envisaged

• Size of Journal after cutting is 200×290 mm

Address

11 Kazimir Malevich Str. (former Bozhenko Str.), 03150, Kyiv, Ukraine

Tel.: (38044) 200 60 16, 200 82 77

Fax: (38044) 200 82 77, 200 81 45

E-mail: journal@paton.kiev.ua

[www://patonpublishinghouse.com/eng/journals/tpwj](http://patonpublishinghouse.com/eng/journals/tpwj)